LUDWIG-MAXIMILIANS-UNIVERSITÄT MÜNCHEN
TECHNISCHE UNIVERSITÄT MÜNCHEN
MAX-PLANCK-INSTITUT FÜR QUANTENOPTIK


# Digital quantum simulation of lattice gauge theory

October 2017 Julian Bender

LUDWIG-MAXIMILIANS-UNIVERSITÄT MÜNCHEN
TECHNISCHE UNIVERSITÄT MÜNCHEN
MAX-PLANCK-INSTITUT FÜR QUANTENOPTIK


# Digital quantum simulation of lattice gauge theory

First reviewer: Prof. Dr. Ignacio Cirac

Second reviewer: Dr. Erez Zohar

Thesis submitted
in partial fulfillment of the requirements
for the degree of

**Master of Science**

within the programme
Theoretical and Mathematical Physics

Munich, October 2017 Julian Bender

# Abstract

In the present work, a digital quantum simulation scheme is proposed for the construction of lattice gauge theories in 3+1 dimensions, including dynamical fermions. All interactions are obtained as a stroboscopic sequence of two-body interactions with an auxiliary system, therefore allowing implementations with ultracold atoms using atomic scattering as a resource for interactions. Compared to previous proposals, the four-body interactions arising in models with 2+1 dimensions and higher, are obtained without the use of perturbation theory, resulting in stronger interactions. The algorithm is applicable to generic gauge theories, with gauge groups being either compact Lie groups or finite groups. To back up the validity of this approach, bounds on the error due to the trotterized time evolution are presented.

Furthermore, using ultracold atoms in optical lattices, an implementation of a lattice gauge theory with a non-abelian gauge group, the dihedral group $D_6$, is described employing the aforementioned simulation scheme. We show how the different parts of the Hamiltonian of this lattice gauge theory can be mapped to a Hamiltonian accessible in ultracold atom experiments. This extends current quantum simulation proposals of non-abelian gauge theories with dynamical matter to more than 1+1 dimensions, thus, paving the way towards the quantum simulation of non-abelian gauge theories in regimes otherwise inaccessible to any numerical methods.

# Contents

# 1 Introduction

The physics of the microscopic scale is governed by the laws of quantum mechanics. Although they are mathematically well understood, solving the dynamical equations for a system consisting of many particles is a very difficult task as the Hilbert space dimension grows exponentially with the system size. One approach to this problem - first proposed by Feynman in 1982 [1] - is to build a highly controllable system obeying the laws of quantum mechanics itself and therefore simulating the system in a much more efficient way compared with classical simulations [2].

Various platforms can serve as quantum simulators, reaching from atomic systems such as ultracold atoms [3–5] and trapped ions [6,7] to solid-state devices such as quantum dots [8,9] and superconducting qubits [10, 11].

According to the simulation scheme, quantum simulators can be divided into analog and digital simulators. The former relies on an analogous quantum system whose Hamiltonian can be exactly or approximately mapped into the Hamiltonian of the system to be simulated. The latter, however, is based on a highly controllable quantum system which can be manipulated to an extent that its dynamics can obey different Hamiltonians for different time intervals. The quantum operation for a single time step is called a quantum gate. The time evolution of the system is then approximated by a stroboscopic sequence of quantum gates given by Trotter's formula $e^{-itH} = \lim_{N\to\infty}(\prod_j e^{-itH_j/N})^N$ [12]. If the set of these gates is universal we refer to the quantum simulator as a quantum computer [13].

From the experimental point of view, a quantum computer - outperforming classical computers - is still a long-term goal. Nevertheless, great progress has been made over the last decades in the manipulation of microscopic quantum systems as those mentioned above. This has led to the fact that, when such systems are tailored to a specific problem, they can serve as quantum simulators which are capable of unveiling interesting physics. Some prominent examples are the realization of the Bose-Hubbard model [14], the Tonks-Girardeau gas [15] or topologically non-trivial models like the Haldane model [16].

The implemented Hamiltonians mainly originate from condensed matter physics, including the aforementioned ones. Quantum simulations of high energy physics are equally possible but more demanding, since additional constraints have to be taken care of. A particular active field in that regard is the quantum simulation of gauge theories.

The concept of gauge invariance lies at the core of fundamental physics. The standard model

of particle physics - describing electromagnetic, weak and strong interactions - is built upon this principle [17]. We distinguish abelian gauge theories, e.g. quantum electrodynamics (QED) with gauge group $U(1)$, and non-abelian ones like quantum chromodynamics (QCD) with gauge group $SU(3)$ describing the strong interactions. Local gauge invariance requires introducing additional degrees of freedom, the gauge fields, which are the force carriers of the theory. If the force's coupling is small enough, perturbative expansions allow calculations up to arbitrary accuracy. Since the coupling in quantum field theories depends on the scale (*running coupling*) [18], there are regimes where this assumption does not hold. This concerns in particular the low-energy sector of QCD, where the quarks are subject to *confinement* [19] which prevents the existence of free quarks. If we are in such a non-perturbative regime where the coupling is too strong for perturbation theory, only very few methods can produce meaningful results.

The most common approach is lattice gauge theory [19, 20]. The idea is to discretize space (and sometimes time as well) to construct a framework in which numerical tools can be applied - with Monte Carlo methods being the most prominent ones [21]. In spite of their success, there are limitations which are inherent to Monte-Carlo simulations of lattice gauge theory. A major one is the *sign problem*, which prevents investigations in fermionic systems with a finite chemical potential [22]. As a consequence, corresponding phases in quantum field theories still remain relatively unexplored, e.g. the quark-gluon plasma or the color-superconducting phase of QCD [23, 24]. Another drawback of these simulations is that they take place in euclidean spacetime, i.e. the time coordinate is rotated from real to imaginary time. This obviously makes real-time dynamics inaccessible and thereby e.g. preventing the study of non-equilibrium properties of quantum field theories [25]. Quantum simulation of lattice gauge theories [26, 27] could overcome these obstacles and provide new insights into these questions. However, as mentioned earlier, special care has to be taken of the symmetries present in lattice gauge theories but naturally not present in a typical candidate system for a quantum simulator like ultracold atoms or trapped ions. The two symmetries are Lorentz symmetry and local gauge invariance.

In the context of ultracold atoms, the former can be achieved by putting the atoms on a lattice. It is known that in the continuum limit fermionic lattices can give rise to both spin and linear dispersion relations typical for relativistic theories [28,29]. This is not uncommon in condensed matter systems with graphene being the most prominent example [30]. There, around certain energy levels, the so called Dirac points, the system is described by the Lorentz invariant Dirac equation. On the other hand, local gauge invariance can either be obtained as a low-energy

effective symmetry [31, 32] or by an exact mapping to an internal symmetry, like e.g. hyperfine angular momentum conservation [33, 34].

Quantum simulations of lattice gauge theory have been proposed using various quantum devices, such as ultracold atoms in optical lattices, trapped ions or superconducting qubits. The simulated models can be distinguished by different features, for example, the gauge group (abelian and non-abelian), the matter content (dynamical or static) or the simulation scheme (analog or digital) [31–55]. Ultracold atom experiments are starting to realize simple proposals, with one experiment being set up to study the Schwinger model, (1+1) dimensional quantum electrodynamics [56]. Using trapped ions, a digital quantum simulation of a lattice gauge theory was already implemented in 2016 [57], allowing the observation of real-time dynamics in the Schwinger model.

Compared to other quantum devices, ultracold atoms do not rely on Jordan-Wigner transformations (mapping a spin-1/2 chain to a chain of spinless fermions [58]) to realize fermionic degrees of freedom since they arise naturally by using a fermionic atomic species. Thus, they are not restricted to one dimension and are suitable candidates to study lattice gauge theories in higher dimensions (higher-dimensional versions of Jordan-Wigner transformations exist but would require nonlocal interactions [59]). As the dimension is a crucial parameter and might change the qualitative behavior of the theory, three-dimensional schemes for quantum simulations are desirable. Another important step is the implementation of lattice gauge theories with non-abelian gauge groups in more than 1+1 dimensions including dynamical fermionic matter since numerically inaccessible regimes of quantum field theories (e.g. in QCD) are precisely of that nature.

This thesis aims at tackling these problems. Using ultracold atoms in optical lattices, a digital algorithm, based on the concept of stators [60], is proposed to enable quantum simulations of lattice gauge theories in three dimensions. By mediating the four-body interactions of the magnetic Hamiltonian via an auxiliary degree of freedom, we can avoid fourth order perturbation theory as compared to previous proposals. Moreover, an implementation of a lattice gauge theory with a non-abelian gauge group, the dihedral group $D_6$, in 2+1 and 3+1 dimensions is suggested.

In the first chapter, the basic ingredients for quantum simulations with ultracold atoms in optical lattices are presented, in particular scattering theory required as a resource to implement interactions. Secondly, a background in lattice gauge theory will be provided, with an emphasis on the Hamiltonian formulation used later on in the quantum simulation. The third chapter is

devoted to the digital algorithm enabling quantum simulations of lattice gauge theories including fermionic matter in three dimensions. Since the digital quantum simulation scheme is an approximated one, the validity of this approach will be backed up by giving exact bounds on the trotterization error in lattice gauge theories. The fifth and last chapter will discuss an implementation of a lattice gauge theory with a dihedral gauge group, presenting a novel idea to realize non-abelian gauge groups with ultracold atoms which takes advantage of the semidirect product structure of the gauge group.

# 2 Ultracold atoms in optical lattices

Over the last decades experimental techniques to control atomic systems have been developed to an extent that allows to manipulate and observe quantum systems in regimes that were not accessible before. This has in particular led to the emergence of a new field, the field of ultracold atoms [3,5,61]. Neutral atoms are trapped and cooled down to almost absolute zero temperature, revealing their quantum mechanical behavior. The groundbreaking achievement of creating a Bose-Einstein condensate [62] of bosonic atoms allowed the study of collective phenomena in the quantum degenerate regime. One direction of research in the field is aiming at simulating many-body systems - from condensed matter physics as well as from high energy physics - by emulating the corresponding dynamics with ultracold atoms. Various quantum simulations have already been successfully performed [14–16, 57]. In this chapter we review the main ingredients to perform a quantum simulation with ultracold atoms. We present the trapping of ultracold atoms in optical lattices and their physics in periodic potentials arising from that. Also scattering as a source of interactions will be addressed.

## 2.1 Optical lattices

In this section we shall discuss how off-resonant lasers are used to trap neutral atoms and naturally create optical potentials resembling a lattice. The following formalism will be semi-classical, i.e. the laser field will be treated classically. This is justified since the influence of the atom on the laser field can be neglected. The trapping mechanism will be explained by considering a single atom in the laser field. For simplicity we assume the atom to be a two-level system with a ground state $|g\rangle$ and an excited state $|e\rangle$ (see figure 1). The Hamiltonian of the atom has the form

$$H_A = \frac{\mathbf{p}^2}{2m} + \omega_e \left|e\right\rangle \left\langle e\right| \tag{1}$$

where the first term corresponds to the kinetic energy and the second one to the internal energy levels. The laser is generating a classical electrical field of the form (assuming a time-independent amplitude)

$$\mathbf{E}(\mathbf{x}, t) = \mathbf{E}(\mathbf{x})e^{-i\omega t} + \mathbf{E}^*(\mathbf{x})e^{i\omega t} \tag{2}$$

The laser induces a dipole moment $\mathbf{d}$ in the atom creating an interaction of the form

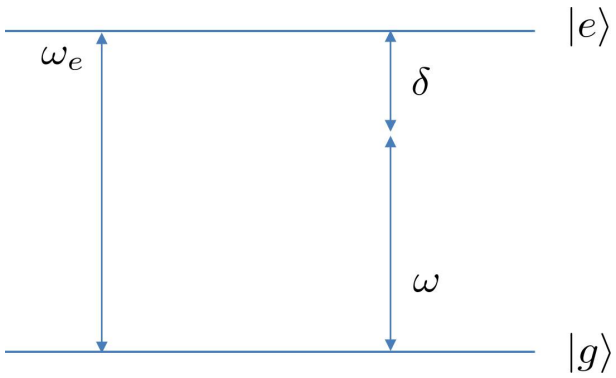


Figure 1: The two energy levels of the atom, $|e\rangle$ and $|g\rangle$, are coupled non-resonantly with a laser of frequency $\omega$. The difference to the frequency $\omega_e$ of the level separation is called the detuning $\delta$

$$H_{dip} = -\mathbf{d} \cdot \mathbf{E}(\mathbf{x}, t) \tag{3}$$

under the condition that the dipole approximation holds which requires a sufficiently low strength of the laser field and that the field is varying slowly compared to the atomic size. The atom has a vanishing dipole moment if it is in an energy eigenstate, so $\langle e|\mathbf{d}|e\rangle = \langle g|\mathbf{d}|g\rangle = 0$. Thus, we can write the dipole moment operator as

$$\mathbf{d} = \mathbf{d}_{eg} |e\rangle \langle g| + \mathbf{d}^*_{eg} |g\rangle \langle e| \tag{4}$$

with $\mathbf{d}_{eg} := \langle e|\mathbf{d}|g\rangle$. After transforming to the rotating frame of the laser - determined by the unitary transformation $U(t) = |g\rangle \langle g| + e^{-i\omega t} |e\rangle \langle e|$ - we perform a rotating wave approximation, neglecting highly oscillating terms. The resulting Hamiltonian - including $H_A$ - is of the form:

$$H = \frac{\mathbf{p}^2}{2m} + \delta |e\rangle \langle e| - \left( \frac{\Omega(\mathbf{x})}{2} |e\rangle \langle g| + h.c. \right) \tag{5}$$

with $\delta \equiv \omega_e - \omega$ the detuning and the Rabi frequency $\Omega(\mathbf{x})$ defined as

$$\Omega(\mathbf{x}) = 2\mathbf{d}_{eg} \cdot \mathbf{E}(\mathbf{x}) \tag{6}$$

The laser frequency $\omega$ is chosen to be off-resonant so that transitions from the ground state to the excited state are very unlikely. However, virtual second-order processes to the excited level and back are possible. This allows to apply adiabatic elimination for the excited state which

results in an effective Hamiltonian for the ground state of the form

$$H = \frac{\mathbf{p}^2}{2m} + V_{op}(\mathbf{x}) \tag{7}$$

with the optical potential

$$V_{op}(\mathbf{x}) = -\frac{|\Omega(\mathbf{x})|^2}{4\delta} \tag{8}$$

By choosing the detuning sufficiently large and applying adiabatic elimination we basically traced out the Hilbert space of the internal levels and got in return an optical potential for the ground state. The Hilbert space of the atoms can therefore be considered to act only in configuration space. The large detuning has the additional advantage that we can neglect spontaneous emission of the excited state whose lifetime we implicitly assumed to be infinite. Moreover, we see that the optical potential is proportional to $|\mathbf{E}(\mathbf{x})|^2$ and thus the intensity of the laser. This opens up the possibility to design the desired potential by choosing an appropriate configuration of the lasers.

## 2.2 Periodic potentials

The desired structure for the optical potential is typically a lattice. This section will therefore be devoted to the physics of an atom moving in a periodic potential. The starting point of the discussion is the corresponding Schrdinger equation

$$\left[\frac{p^2}{2m} + V(\mathbf{r})\right]\psi(\mathbf{r}) = E\psi(\mathbf{r}) \tag{9}$$

with $V$ being periodic, i.e. $V(\mathbf{r}) = V(\mathbf{r} + \mathbf{d})$ where $\mathbf{d}$ can be any lattice vector. The solution to it is given by Bloch's theorem [63]. It states that the space of solutions is spanned by a basis of wave functions, labeled by $n$, which are all of the form

$$\psi_{\mathbf{k}}^{(n)}(\mathbf{r}) = e^{i\mathbf{k}\mathbf{r}}u(\mathbf{r}) \tag{10}$$

where $u$ has the same periodicity as the potential $V$. The wave functions $\psi_{\mathbf{k}}^{(n)}$ are called Bloch waves and their energy levels $E_{\mathbf{k}}^{(n)}$ Bloch bands. All Bloch waves are spread out over the whole lattice. However, one can choose another basis, the Wannier basis, whose wave functions are localized. They are related to the Bloch waves by a Fourier transform:

$$w_n(\mathbf{r}-\mathbf{r}_i) = \frac{1}{\sqrt{M}} \sum_{\mathbf{k}} e^{-i\mathbf{k}\mathbf{r}_i} \psi_{\mathbf{k}}^{(n)}(\mathbf{r}) \tag{11}$$

where $M$ is a normalization constant and $\mathbf{r}_i$ denoted the lattice site where the atom is localized. The Wannier basis can be used to express a Hamiltonian in second quantized form using operators acting only on lattice sites. Ultracold atom experiments are nowadays able to cool atoms down to temperatures where only the lowest Bloch band has to be considered. They typically reach microkelvin temperatures ($\mu K$), using a combination of several techniques. In the first step the atoms are usually trapped and pre-cooled by lasers in a magneto-optical trap. To get to the lowest temperatures accessible at the moment, evaporative cooling is applied in a second step [64]. Thus, defining the lowest Bloch band as $\phi_{\mathbf{i}}(\mathbf{r}) \equiv w_0(\mathbf{r}-\mathbf{r}_i)$, a bosonic wave function $\Phi(\mathbf{r})$ in second quantization can be expanded in terms of single particle annihilation operators $a_{\mathbf{i}}$

$$\Phi(\mathbf{r}) = \sum_{\mathbf{i}} a_{\mathbf{i}} \phi_{\mathbf{i}}(\mathbf{r}) \tag{12}$$

The annihilation operators $a_{\mathbf{i}}$ corresponding to the bosonic species obey the commutation relations

$$[a_{\mathbf{i}}, a_{\mathbf{j}}^{\dagger}] = \delta_{ij} \tag{13}$$

However, the same expansion is possible for a fermionic wave function. The only difference are the fermionic annihilation operators $c_{\mathbf{i}}$ which obey the anticommutation relations

$$\{c_{\mathbf{i}}, c_{\mathbf{j}}^{\dagger}\} = \delta_{ij} \tag{14}$$

## 2.3 Scattering of ultracold atoms

In the classical sense one may think of scattering events as rather chaotic processes which are not well suited to mediate a specific interaction as required for quantum simulations. However, in the ultracold regime things are much different due to the quantum behavior of the particles. We consider two asymptotically free particles in their center of mass frame interacting through a spherically symmetric potential $V(r)$ [65]. An incoming particle from the z-direction can be described after sufficiently large times after the scattering process in the asymptotic form

$$\Psi \simeq e^{ikz} + f(\theta)\frac{e^{ikr}}{r} \tag{15}$$

where the factor $f(\theta)$ in front of the spherical wave is the scattering amplitude. It can be expressed in terms of Legendre polynomials characterized by different values $l$ of angular momentum (partial wave expansion) [65]:

$$f(\theta) = \frac{1}{2ik}\sum_{l=0}^{\infty}(2l+1)f_l(k)P_l(\cos\theta) \tag{16}$$

where $P_l$ is a Legendre polynomial and $f_l(k)$ the partial wave amplitude. In the low-energy limit $f_l(k)$ scales as

$$f_l \approx k^{2l} \tag{17}$$

Hence, all amplitudes are negligible apart from $l = 0$, the s-wave scattering term. The ultracold regime is defined by this approximation, i.e. if the lowest partial wave governs the scattering. One has to be a bit careful here since the lowest accessible partial wave is not always the s-wave. For bosons and unidentical fermions this holds true, for identical fermions, however, it is the p-wave with $l = 1$ due to Pauli's exclusion principle [5]. Focusing on the s-wave channel since we will not deal with scattering of identical fermions, we can characterize the scattering process by a single quantity, the *scattering length* a. It is defined as

$$a = -\lim_{k\to 0}\frac{f_0(k)}{k} \tag{18}$$

The total scattering cross section

$$\sigma = \int \mathrm{d}\Omega |f(\theta)|^2 \tag{19}$$

takes then the form

$$\sigma = 4\pi a^2 \tag{20}$$

Another valid approximation we can make in this regime concerns the form of the scattering potential. Since the de-Broglie wavelength $\lambda_{DB} = \sqrt{\frac{2\pi}{k_B T}}$ is much larger than the effective range of the potential, it can be described by the pseudopotential [5, 66]:

$$V(\mathbf{x}-\mathbf{x}') = \frac{2\pi a}{m}\delta(\mathbf{x}-\mathbf{x}') \equiv \frac{g}{2}\delta(\mathbf{x}-\mathbf{x}') \tag{21}$$

So far only two-body processes were considered. This has to do with the diluteness of ultracold atomic gases. Typical densities $n$ of atoms are $10^{12}$ to $10^{15} cm^{-3}$. In these regimes three-body interactions are negligible. Another consequence is that the interparticle distance $n^{-1/3}$ (of the order of micrometers $\mu m$) is larger than the scattering length (of the order of nanometers $nm$ [5]). This allows the assumption that the atoms occupy the ground state of the gas. This regime is therefore called the *weak interaction regime*.

## 2.4 Second quantization and the Bose-Hubbard model

With the previous sections at hand we can formulate the Hamiltonian of a single species in second quantized form. We start from the Hamiltonian density with the pseudopotential already inserted:

$$\mathcal{H} = \Phi^\dagger(\mathbf{x})\left(-\frac{\nabla^2}{2m} + V_{op}(\mathbf{x}) + V_T(\mathbf{x})\right)\Phi(\mathbf{x}) + \frac{g}{2}\phi^\dagger(\mathbf{x})\phi^\dagger(\mathbf{x})\phi(\mathbf{x})\phi(\mathbf{x}) \tag{22}$$

where $V_T$ is an external trapping potential. In the next step the wave functions are expanded in terms of Wannier functions according to eq. (12). Defining the overlap integrals

$$\epsilon_n = \int d^3x\, \phi_n^*(\mathbf{x})\left(-\frac{\nabla^2}{2m} + V_{op}(\mathbf{x}) + V_T(\mathbf{x})\right)\phi_n(\mathbf{x}) \tag{23}$$

$$J_{mn} = \int d^3x\, \phi_m^*(\mathbf{x})\left(-\frac{\nabla^2}{2m} + V_{op}(\mathbf{x}) + V_T(\mathbf{x})\right)\phi_n(\mathbf{x}) \tag{24}$$

$$U_{mnkl} = g\int d^3x\, \phi_m^*(\mathbf{x})\phi_n^*(\mathbf{x})\phi_k(\mathbf{x})\phi_l(\mathbf{x}) \tag{25}$$

we can write the Hamiltonian in its most general form

$$H = \sum_n \epsilon_n a_n^\dagger a_n + \sum_{m,n} J_{mn} a_m^\dagger a_n + \sum_{m,n,k,l} U_{mnkl} a_m^\dagger a_n^\dagger a_k a_l \tag{26}$$

where we chose the creation and annihilation to be bosonic for this demonstration because of the following discussion of the Bose-Hubbard model. However, similar Hamiltonian terms may be written for fermionic creation and annihilation operators, as well as for boson-fermion

interactions.

In the following, we will specify the parameters $\epsilon_n, J_{mn}, U_{mnkl}$ to the case of the Bose-Hubbard Hamiltonian, one of the simplest many-body Hamiltonians and the first one that was realized experimentally [14]. The first assumption of the model is that the energies of all lattice sites are the same, i.e. $\epsilon_n = \epsilon$. The Wannier functions are considered to be well localized, i.e. the optical potential is sufficiently deep, but only to an extent that the wave functions of neighboring sites still overlap and are equal throughout the lattice, i.e. $J_{mn} = -J$. For the interaction term these contributions are negligible and only on-site interactions will be present, i.e. $U_{mnkl} = U$. The resulting Hamiltonian is of the form

$$H_{BH} = \epsilon \sum_n a_n^\dagger a_n - J \sum_{<m,n>} a_m^\dagger a_n + U \sum_n \hat{N}_n(\hat{N}_n - 1) \tag{27}$$

where $< m, n >$ indicates the sum over nearest neighbors and $\hat{N}_n = a_n^\dagger a_n$ is the particle number operator at site $n$. The important quantity of the model is the ratio $J/U$ which can be controlled in experiments by varying the depth of the optical potential. As demonstrated in experiment [14], by tuning this ratio a phase transition between the two quantum phases of the Bose-Hubbard model can be induced. If the tunneling is much smaller than the on-site interactions ($J \ll U$), a Mott-insulator ground state appears. This is characterized by the presence of $n$ localized particles per lattice site. It can be described by a product state of the form

$$|\Psi_{Mott}\rangle \sim \prod_i (a_i^\dagger)^n |0\rangle \tag{28}$$

where the $|0\rangle$ state stands for an empty lattice. On the other hand, if the tunneling dominates the on-site interactions ($J \gg U$), the ground state of the system behaves as a superfluid. In this case the atom is delocalized over the whole lattice and can be expressed as

$$|\Psi_{SF}\rangle \sim \left( \sum_i a_i^\dagger \right)^n |0\rangle \tag{29}$$

which in the limit of vanishing on-site interactions ($U = 0$) becomes just a product of coherent states in each lattice site.

## 2.5 Multiple species

The discussion of the previous sections can be generalized by considering multiple species. One possibility to realize this is by taking the internal structure of the atoms into account. We will focus in the following on different atomic hyperfine levels [61, 66–68], in particular on alkali atoms possessing a single electron in the outer energy level. The hyperfine angular momentum is defined as

$$\mathbf{F} = \mathbf{S} + \mathbf{L} + \mathbf{I} \tag{30}$$

where $\mathbf{S}$ denotes the valence electron's spin, $\mathbf{L}$ the electron's orbital angular momentum and $\mathbf{I}$ the nuclear spin. Since the valence electron of an Alkali atom is in an s-orbital, its orbital angular momentum is zero, i.e. $\mathbf{L} = 0$. The hyperfine angular momentum $\mathbf{F}$ fulfills the commutation relations

$$[F_i, F_j] = i\epsilon_{ijk}F_k \tag{31}$$

The states can be characterized by two quantum numbers $F$ and $m_F$, the eigenvalue of the squared angular momentum operator

$$\mathbf{F}^2 \left|F; m_F\right\rangle = F(F+1) \left|F; m_F\right\rangle \tag{32}$$

and the eigenvalue of the z-component

$$F_z \left|F; m_F\right\rangle = m_F \left|F; m_F\right\rangle \tag{33}$$

Labeling the different internal levels by Greek indices and taking into account that different species might experience different optical potential $V_{op}^{\alpha}$, we can express the second quantized Hamiltonian density for multiple species in the form:

$$\begin{aligned}\mathcal{H} = &\sum_{\alpha,\beta} \Phi_\alpha^\dagger(\mathbf{x}) \left( \delta^{\alpha\beta} \left( -\frac{\nabla^2}{2m} + V_{op}^{\alpha}(\mathbf{x}) + V_T(\mathbf{x}) \right) + \Omega^{\alpha\beta}(\mathbf{x}) \right) \Phi_\beta(\mathbf{x}) \\ &+ \sum_{\alpha,\beta,\gamma,\delta} \int d^3x' \Phi_\alpha^\dagger(\mathbf{x}') \Phi_\beta^\dagger(\mathbf{x}) V_{\alpha,\beta,\gamma,\delta}(\mathbf{x}-\mathbf{x}') \Phi_\gamma(\mathbf{x}') \Phi_\delta(\mathbf{x})\end{aligned} \tag{34}$$

where $\Omega^{\alpha\beta}(\mathbf{x})$ accounts for a possible coupling (*Rabi coupling*) between different atomic levels induced by external lasers. The two- body scattering potential for different species $V_{\alpha,\beta,\gamma,\delta}(\mathbf{x} -$

$\mathbf{x}'$) will be discussed now. The first atom shall have angular momentum $F_1$ and the second atom $F_2$. The scattering can occur via different intermediate states depending on the total angular momentum $F_T$. Each one can have a different scattering length resulting in the following scattering potential:

$$V_{\alpha,\beta,\gamma,\delta}(\mathbf{x}-\mathbf{x}') = \frac{2\pi a}{\mu}\delta(\mathbf{x}-\mathbf{x}')\sum_{F_T} a_{F_T}(P_{F_T})_{\alpha,\beta,\gamma,\delta} \tag{35}$$

where $\alpha, \beta, \gamma, \delta$ denote the different in and outgoing states, $P_{F_T}$ the projection operator on the subspace of total angular momentum $F_T$ and $\mu$ the reduced mass of the two species. For later purposes it will be advantageous to express the projection operators $P_{F_T}$ by a function of $\mathbf{F}_1 \cdot \mathbf{F}_2$. This is possible since the total angular momentum depends on the relative orientation of $\mathbf{F}_1$ and $\mathbf{F}_2$. Mathematically speaking, this corresponds to the equation

$$\mathbf{F}_1 \cdot \mathbf{F}_2 = \frac{1}{2}\left(\mathbf{F}_T^2 - \mathbf{F}_1^2 - \mathbf{F}_2^2\right) \tag{36}$$

with $\mathbf{F}_1^2$ and $\mathbf{F}_2^2$ being fixed. If the total angular momentum operator $F_T$ can take $n$ different values, then the projection operator $P_{F_T}$ can be obtained as a polynomial of $\mathbf{F}_1 \cdot \mathbf{F}_2$:

$$P_{F_T} = \sum_{k=0}^{n-1} G_{F_T,k}(\mathbf{F}_1 \cdot \mathbf{F}_2)^k \tag{37}$$

with an appropriate choice of the coefficients $\{G_{F_T,k}\}$. Thus, the scattering potential can be written in terms of $\mathbf{F}_1 \cdot \mathbf{F}_2$:

$$V_{\alpha,\beta,\gamma,\delta}(\mathbf{x}-\mathbf{x}') = \frac{2\pi}{\mu}\delta(\mathbf{x}-\mathbf{x}')\sum_{k=0}^{n-1} g_k((\mathbf{F}_1 \cdot \mathbf{F}_2)^k)_{\alpha,\beta,\gamma,\delta} \tag{38}$$

where the $g_k$ coefficients are simply functions of $G_{F_T,k}$ and $a_{F_T}$. Hence, the corresponding Hamiltonian density takes the form

$$\mathcal{H}_{scat,mul} = \frac{2\pi}{\mu}\sum_{\alpha,\beta,\gamma,\delta}\sum_{k=0}^{n-1} g_k((\mathbf{F}_1 \cdot \mathbf{F}_2)^k)_{\alpha,\beta,\gamma,\delta}\Phi_\alpha^\dagger(\mathbf{x})\Phi_\beta^\dagger(\mathbf{x})\Phi_\gamma(\mathbf{x})\Phi_\delta(\mathbf{x}) \tag{39}$$

To obtain the time evolution of this interaction we have to integrate the Hamiltonian density over space and time. Assuming for simplicity that the wave functions of all internal states of the two atoms have the same spatial overlap $\mathcal{O}(t)$ throughout the interaction, we can write down

the unitary for the scattering process

$$\mathcal{U}_{scat} = e^{-i\frac{2\pi}{\mu}\int \mathcal{O}(t)\mathrm{d}t \sum_{k=0}^{n-1} g_k((\mathbf{F}_1\cdot\mathbf{F}_2)^k)} \tag{40}$$

This scattering process is a key ingredient to perform quantum simulations with ultracold atoms. One can even tailor this interaction by, for example, tuning the overlap in a way that only certain internal levels overlap. To illustrate the process of going from the projection operators $P_{F_T}$ to $\mathbf{F}_1 \cdot \mathbf{F}_2$, we will explicitly calculate all the relevant quantities for the scattering processes which will be discussed in later chapters. In the first one both scattering partner have angular momentum $F = 1$, i.e. $F_1 = F_2 = 1$. Since we will consider unidentical particles the total angular momentum can take the values $F_T = 0, 1, 2$. Hence, we need to express the projection operators $P_0, P_1$ and $P_2$ in terms of $\mathbf{F}_1 \cdot \mathbf{F}_2$ and $(\mathbf{F}_1 \cdot \mathbf{F}_2)^2$. We obtain

$$\begin{aligned} P_0 &= -\frac{1}{3}\left(\mathbb{I} - (\mathbf{F}_1 \cdot \mathbf{F}_2)^2\right) \\ P_1 &= \mathbb{I} - \frac{1}{2}\left(\mathbf{F}_1 \cdot \mathbf{F}_2 + (\mathbf{F}_1 \cdot \mathbf{F}_2)^2\right) \\ P_2 &= \frac{1}{3}\mathbb{I} + \frac{1}{2}\mathbf{F}_1 \cdot \mathbf{F}_2 + \frac{1}{6}(\mathbf{F}_1 \cdot \mathbf{F}_2)^2 \end{aligned} \tag{41}$$

From the above expressions we can read off the coefficients $\{g_k\}$ as a function of the scattering lengths $a_0, a_1$ and $a_2$:

$$\begin{aligned} g_0 &= -\frac{1}{3}a_0 + a_1 + \frac{1}{3}a_2 \\ g_1 &= -\frac{1}{2}a_1 + \frac{1}{2}a_2 \\ g_2 &= \frac{1}{3}a_0 - \frac{1}{2}a_1 + \frac{1}{6}a_2 \end{aligned} \tag{42}$$

The second process required for the implementation later on is the scattering process between two unidentical atoms of angular momentum $F_1 = F_2 = 1/2$. The Projection operators $P_0$ and $P_1$ can be written as

$$\begin{aligned} P_0 &= \frac{1}{4}\mathbb{I} - \mathbf{F}_1 \cdot \mathbf{F}_2 \\ P_1 &= \frac{3}{4}\mathbb{I} + \mathbf{F}_1 \cdot \mathbf{F}_2 \end{aligned} \tag{43}$$

The coefficients $g_0$ and $g_1$ are consequently

$$
\begin{aligned}
g_0 &= \frac{1}{4}a_0 + \frac{3}{4}a_1 \\
g_1 &= -a_0 + a_1
\end{aligned}
\tag{44}
$$

The last scattering process involves an $F_1 = 1$ atom and an $F_2 = 1/2$ atom. The projection operators for the total angular momentum $P_{1/2}$ and $P_{3/2}$ can be expressed as

$$
\begin{aligned}
P_{1/2} &= \frac{1}{3}\mathbb{I} - \frac{2}{3}\mathbf{F}_1 \cdot \mathbf{F}_2 \\
P_{3/2} &= \frac{2}{3}\mathbb{I} + \frac{2}{3}\mathbf{F}_1 \cdot \mathbf{F}_2
\end{aligned}
\tag{45}
$$

The corresponding coefficients $g_0$ and $g_1$ are (depending on the scattering lengths $a_{1/2}$ and $a_{3/2}$):

$$
\begin{aligned}
g_0 &= \frac{1}{2}a_{1/2} + \frac{2}{3}a_{3/2} \\
g_1 &= -\frac{2}{3}a_{1/2} + \frac{2}{3}a_{3/2}
\end{aligned}
\tag{46}
$$

Finally, a comment on the scattering lengths which were assumed to be given. However, there are experimental techniques which allow to tune it via a scattering resonance called *Feshbach resonance* [5, 68, 69]. The underlying idea consists of two coupled scattering channels, one open and the other one closed. Even though the closed channel does not directly contribute to the scattering process, it can influence the scattering length due to its coupling to the open channel. The coupling between the channels is usually tuned with a magnetic field, although there exist optical Feshbach resonances [70]. For a magnetic Feshbach resonance the resonant scattering length can be calculated in terms of the magnetic field and the off-resonant scattering length $a_0$:

$$
a = a_0 \left(1 + \frac{\Delta B}{B - B_0}\right) \tag{47}
$$

where $\Delta B$ denotes the width of the resonance and $B_0$ the position of the resonance.
Realizing Feshbach resonances in experiments requires some effort. First of all, not all atomic species exhibit a Feshbach resonance so that the choice of possible atomic species is reduced. The resonances for the remaining species are different so that it is only possible to tune one scattering length. Moreover, if a specific scattering length is supposed to be implemented, the fluctuations of the magnetic field have to be well-controlled. This may be overcome by the use of optical Feshbach resonances; however, their realization is very challenging and demanding.

# 3 Lattice gauge theories

The principle of gauge invariance states that by locally changing a certain quantity of a theory the observables will remain unchanged. Theories exhibiting this property are called gauge theories. They are particularly relevant for high-energy physics as they explain the dynamics of elementary particles. These theories, such as quantum electrodynamics (QED) or quantum chromodynamics (QCD), are based on vector fields, e.g. the electromagnetic field, that mediate the forces between elementary particles. Gauge invariance is incorporated in a way that certain transformations of the field, called gauge transformations, still give rise to the same measurable quantities like energy or charge. The study of these quantum field theories culminates in the standard model of particle physics, a corner stone of modern physics as it quantizes all fundamental forces except gravity.
However, as most techniques in quantum field theories rely on a perturbative expansions in the coupling, important quantities - especially in the non-perturbative regime - can not be computed due to the running coupling [18]. One approach is therefore to put the quantum field theory on a lattice, thus providing a natural regularization scheme (it can be viewed as introducing a UV-cutoff). This allows to apply numerical methods - mainly Monte-Carlo simulations - what has led to new insights into QCD, e.g. the calculation of the hadronic spectrum or a better understanding of the confinement of quarks.
In this chapter, we shall first review basic concepts of gauge theories in the continuum and use them as an introduction to Wilson's lattice gauge theory, a euclidean formulation involving a discretization of space and time. The major part of this chapter will then be devoted to the Hamiltonian formulation of lattice gauge theories as it will be present throughout the whole thesis.

## 3.1 Gauge theories in the Continuum

The starting point of the discussion is a field theory described by a Lagrangian with a global symmetry, i.e. the system is invariant under an application of the same transformation at each point in space-time. This global symmetry can then be gauged, i.e. it is promoted to a local one. As a consequence of requiring local gauge invariance, the gauge fields will emerge naturally. To elucidate the concept of gauge invariance we will perform the usual gauging procedure following the example of quantum electrodynamics.

Let us consider the Dirac Lagrangian density

$$\mathcal{L}(x) = \bar{\psi}(x)(i\gamma^\mu \partial_\mu - m)\psi(x) \tag{48}$$

where $\psi(x)$ is the free field of the electron, $\bar{\psi}(x)$ its conjugate and $\gamma^\mu$ the Dirac matrices. The global symmetry is characterized by a phase transformation under which the Lagrangian is invariant. With $\alpha \in \mathbb{R}$, it is defined as:

$$\begin{aligned} \psi(x) &\to e^{i\alpha}\psi(x) \\ \bar{\psi}(x) &\to e^{-i\alpha}\bar{\psi}(x) \end{aligned} \tag{49}$$

In contrast to a global phase transformation, a local one - where $\alpha = \alpha(x)$ would depend on spacetime - would change the Lagrangian. The reason for that is the derivative $\partial_\mu$ which would act on the phase factor $e^{i\alpha(x)}$ and create an extra term by means of the product rule. The typical method to remedy that issue is by introducing an additional field $A_\mu$, the gauge field, which compensates for the changes in $\alpha$. It is incorporated into a new kind of derivative, the covariant derivative $D_\mu$, replacing the ordinary derivative $\partial_\mu$. It is defined as:

$$D_\mu = \partial_\mu - ieA_\mu \tag{50}$$

where $e$ is the coupling constant. Its main feature is the restoration of gauge invariance due to the transformation of the additional field $A_\mu$ under gauge transformations:

$$A_\mu \to A_\mu + e^{-1}\partial_\mu \alpha(x) \tag{51}$$

Writing the new Lagrangian density $\mathcal{L}'$ in terms of the old one, one sees that an additional term appears, describing a coupling between the gauge field $A_\mu$ and the conserved current $J^\mu$ associated to the global symmetry by Noether's theorem:

$$\mathcal{L}'(x) = \mathcal{L}(x) + e\bar{\psi}(x)\gamma^\mu\psi(x)A_\mu = \mathcal{L}(x) + eJ^\mu A_\mu \tag{52}$$

This is usually referred to as minimal coupling since the term does not involve higher orders of $A_\mu$. To make the gauge field dynamical a kinetic term is added to the Lagrangian. It has to fulfill Lorentz invariance and gauge-invariance. Moreover, as a kinetic term it needs to be of

second order. The simplest expression taking all that into account is the term

$$\mathcal{L}_{kin,A} = -\frac{1}{4} F_{\mu\nu} F^{\mu\nu} \tag{53}$$

where the factor $-\frac{1}{4}$ is the correct normalization factor when added to $\mathcal{L}'$. The tensor $F_{\mu\nu}$ is the electromagnetic field strength tensor defined as

$$F_{\mu\nu} = \partial_\mu A_\nu - \partial_\nu A_\mu \tag{54}$$

Thus, the complete Lagrangian of quantum electrodynamics takes the form:

$$\mathcal{L}_{QED} = \mathcal{L}(x) + e\bar{\psi}(x)\gamma^\mu \psi(x) A_\mu - \frac{1}{4} F_{\mu\nu} F^{\mu\nu} \tag{55}$$

The above gauging procedure was performed for a local phase transformation corresponding to the gauge group $U(1)$. However, in principle any Lie group can be chosen. The most common generalizations are the Lie groups SU(N). The associated theories are called Yang-Mills theories with quantum chromodynamics (QCD) being the most prominent example, corresponding to the gauge group SU(3). As a consequence of the non-abelian nature of these theories the matter fields form representations under the transformation of the gauge group. Hence, unlike in quantum electrodynamics, the matter spinor will have several "color" components, mixed by gauge transformations. These fields will form a tuple depending on the dimension of the representation. Assuming it to be n-dimensional, i.e.

$$\begin{aligned} V : G &\to GL(n, \mathbb{C}) \\ g &\mapsto V(g) \end{aligned} \tag{56}$$

the multiplet of fields, $\mathbf{\Psi}(x) = (\psi_1(x), \psi_2(x), ..., \psi_n(x))$, transforms as:

$$\mathbf{\Psi}(x) \to V(g)(x)\mathbf{\Psi}(x) \tag{57}$$

Starting again from the Lagrangian $\mathcal{L}(\mathbf{\Psi}, \partial\mathbf{\Psi})$ in eq. (48) which is invariant under global transformations, i.e. the above transformations is fixed for all spacetime points $x$, one can gauge the symmetry in a similar fashion. The ordinary derivative is replaced with the covariant derivative according to eq. (50) with the difference that the gauge field $A_\mu$ will now take values in the Lie algebra $\mathfrak{su}(N)$. It can be expressed in terms of the generators $T^a$ of the Lie algebra:

$$A_\mu = A_\mu^a T^a \tag{58}$$

(summation on the group indices $a$ assumed). Hence, the number of gauge fields is characterized by the dimension of the Lia algebra $\mathfrak{su}(N)$. The kinetic term of the gauge fields is of a similar form compared to QED:

$$\mathcal{L}_{\mathrm{YM}} = -\frac{1}{4} F_{\mu\nu}^a F^{\mu\nu a} = -\frac{1}{2}\mathrm{Tr}(F^2) \tag{59}$$

A novel feature, however, lies in the different form of the field strength tensor:

$$F_{\mu\nu} = \partial_\mu A_\nu - \partial_\nu A_\mu - i[A_\mu, A_\nu] \tag{60}$$

because the extra term at the end gives rise to three and fourth order terms in the Lagrangian resulting in interactions between the gauge fields. This is a crucial difference compared to photons in quantum electrodynamics. It also has the consequence that the equations of motion become nonlinear and thus makes such theories hard to solve.

## 3.2 Euclidean formulation of lattice gauge theories

In this section, Wilson's formulation of lattice gauge theories shall be briefly reviewed [19]. The underlying idea is to put a Yang-Mills theory in $d+1$ dimensions on a lattice and rotate to euclidean spacetime (Wick rotation). The advantage of working in such a framework is that the dynamics of the theory is transformed into an additional spatial dimension. It reduces therefore to a static problem that can be studied by means of classical techniques like the partition function. In order to do so, one has to do the following transformations:

$$\begin{aligned} \int d^{d+1}\mathbf{x}\mathcal{L}(\mathbf{x}) &\to a^{d+1} \sum_{\mathbf{n}\in\mathbb{Z}^{d+1}} \mathcal{L}(a\mathbf{n}) \\ \partial_\mu \psi(a\mathbf{n}) &\to \frac{1}{2a}\left[\psi(a(\mathbf{n}+\hat{\mu})) - \psi(a(\mathbf{n}-\hat{\mu}))\right] \\ t &\to i\tau \end{aligned} \tag{61}$$

After this discretization of spacetime combined with a Wick rotation, we will have the matter degrees of freedom placed on the vertices of the $d+1$ dimensional lattice and the gauge fields will reside on the links. They will no longer be represented by an element of the Lie algebra but an element of the Lie group. The gauge field on the link between vertex $\mathbf{n}$ and vertex $\mathbf{n}+\hat{\mu}$ is

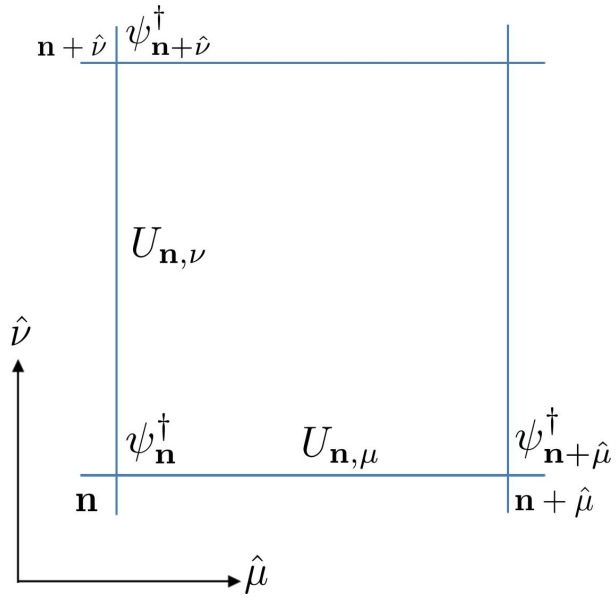


Figure 2: The gauge fields are represented by group elements $U_{\mathbf{n},\mu}$ residing on the links, whereas the matter fields, represented by spinors $\psi_{\mathbf{n}}$, are located on the vertices

denoted as $U_{\mathbf{n},\mu}$ (see Fig.(2) . It can be written in terms of the generators of the Lie algebra:

$$U_{\mathbf{n},\mu} = e^{i\theta^a_{\mathbf{n},\mu}T^a} \tag{62}$$

where $\theta^a_{\mathbf{n},\mu}$ are the parameters corresponding to the group element $U_{\mathbf{n},\mu}$. To obtain gauge invariance for all lattice spacings $a \in \mathbf{R}$ a new action is defined which is invariant under the gauge transformations of $U_{\mathbf{n},\mu}$,

$$U_{\mathbf{n},\mu} \to V(a\mathbf{n})U_{\mathbf{n},\mu}V^\dagger(a(\mathbf{n}+\hat{\mu})) \tag{63}$$

where $V(a\mathbf{n}) \in G$ are group elements varying throughout the whole lattice. Wilson's approach to that problem was based on the observation that oriented products of group elements $U_{\mathbf{n},\mu}$ along closed paths are gauge invariant. It is therefore natural to take the shortest of such paths as a building blocks for the action. Choosing appropriate constants to recover Yang-Mills theory in the continuum limit, one obtains the Wilson action:

$$S_{\text{Wilson}} = -\frac{a^{d-3}}{2g^2}\sum_{\mathbf{x},\mu,\nu}\text{Tr}\left(U_{\mathbf{n},\mu}U_{\mathbf{n}+\hat{\mu},\nu}U^\dagger_{\mathbf{n}+\nu,\mu}U^\dagger_{\mathbf{n},\nu}\right) + H.c. \tag{64}$$

where g is the coupling constant. One can show that this action indeed resembles the action of Yang Mills theory in the limit $a \to 0$ [92]:

$$S_{YM} = -\frac{1}{2} \int d^{d+1}\mathbf{x} \mathrm{Tr}\left(F_{\mu\nu} F^{\mu\nu}\right) \tag{65}$$

## 3.3 Hamiltonian formulation of lattice gauge theories

### 3.3.1 General description

Lattice gauge theories may also be formulated in a Hamiltonian framework exhibiting a continuous time coordinate, first proposed by Kogut and Susskind [28]. The lattice consists of $d$ spatial dimensions, where the matter fields are placed on the vertices and the gauge fields reside on the links. For a detailed description we first pick some compact or finite group G. We label its irreducible representations by j and introduce a Hilbert space spanned by a basis of the form $|jm\rangle$ with m a label for the states within the representation j. The action of a group element on this representation space can be described by a unitary operator $\theta_g$ leaving the representation invariant and acting on the internal states with the matrix $D^j_{nm}(g)$:

$$\theta_g \left|jm\right\rangle = D^j_{nm}(g) \left|jn\right\rangle \tag{66}$$

If we relate the state $|jm\rangle$ to fermionic creation operators $\psi^{\dagger j}_m$ they obey the transformation rule:

$$\theta_g \psi^{\dagger j}_m \theta^\dagger_g = \psi^{\dagger j}_n D^j_{nm}(g) \tag{67}$$

In the case of a compact group we can expand $\theta_g$ in terms of charges $Q_a$:

$$\theta_g = e^{i\phi_a Q_a} \tag{68}$$

with the charges

$$Q_a = \psi^{\dagger j}_m (T^j_a)_{mn} \psi^j_n \tag{69}$$

Here $T^j_a$ is the matrix representation of the $a$-generator. These matter fields $\psi^{\dagger j}_n$ will reside, as mentioned, on the vertices (the $j$ will be omitted in the following as we assume that we will use only one fixed representation $j$, although this does not necessarily have to be the case). They are expressed in second quantized form as they will be allowed to tunnel so that the number

of fermions is only globally conserved but not locally. The states on the vertices are then Fock states building upon the Fock vacuum $|0\rangle$. A natural choice for the Hamiltonian is then (ignoring local gauge invariance for the moment):

$$H = \sum_{\mathbf{x}} M(\mathbf{x})\psi_m^\dagger(\mathbf{x})\psi_m(\mathbf{x}) + \epsilon \sum_{\mathbf{x},k} \psi_m^\dagger(\mathbf{x})\psi_m(\mathbf{x}+\hat{k}) + h.c. \tag{70}$$

where the sum of $\mathbf{x} = a\mathbf{n}$ goes over all $\mathbf{n} \in \mathbb{Z}^d$, $k \in \{1, ..., d\}$ labels the lattice's directions and $\hat{k}$ is the corresponding unit vector.

This naive discretization procedure, however, gives rise to a problem called *fermion doubling* [71, 72]. It has its origin in the different behaviors of the dispersion relation in the continuum and on the lattice. Deducing them from the Dirac equation, one obtains (for simplicity in one dimension)

$$p = \pm\sqrt{E^2 - m^2}, \qquad -\infty < p < \infty \tag{71}$$

for the continuum and

$$\frac{\sin(pa)}{a} = \pm\sqrt{E^2 - m^2}, \qquad -\pi/a < p \leq \pi/a \tag{72}$$

on the lattice. Taking the limit $a \to 0$ of the dispersion relation for the lattice around $p = 0$, one recovers the dispersion relation for the continuum. The problem occurs when considering the corners of the Brillouin zone, e.g. momentum $p = \pi/a$ where - in the massless case - no energy is required to create a particle and the dispersion relation has the same behavior like it has around $p = 0$ (up to an irrelevant minus sign). In the continuum limit this corresponds to a pole in the fermionic propagator on the lattice and one recovers the single-particle Green's function of the continuum. Since there are $2^d$ such momenta in the Brillouin zone of $d$ dimensions, a single fermionic field on the lattice gives rise to $2^d$ fermionic fields in the continuum. Hence, the name *fermion doubling*.

Several methods have been developed to resolve that problem, one of the most prominent being *Wilson fermions* [73] where additional terms are introduced (vanishing in the continuum limit) to remove the zeros in the Brillouin zone. Other techniques are for example Ginsparg-Wilson fermions [74] or domain wall fermions [75]. The focus of this thesis will lie, however, on *Staggered fermion*, invented by Kogut and Susskind [76]. The basic idea is to distribute the spinor components of the fermionic field over the lattice in a way that the effective lattice

spacing for each of the components will be increased. This can be understood as a cutoff for higher momenta and thus removing the undesired zeros in the corners of the Brillouin zone. Neighboring sites with different components will then form the spinor in the continuum limit. One can formulate a Hamiltonian in terms of a single component spinor which incorporates this concept:

$$H = M \sum_{\mathbf{x}} (-1)^{\mathbf{x}} \psi_m^\dagger(\mathbf{x}) \psi_m(\mathbf{x}) + \epsilon \sum_{\mathbf{x},k} e^{i\alpha_k} \psi_m^\dagger(\mathbf{x}) \psi_m(\mathbf{x} + \hat{k}) + h.c. \tag{73}$$

where the phases $\alpha_k$ must be carefully chosen to obtain the correct (Dirac) continuum limit. However, for $U(1)$ gauge theories or theories with a gauge group that contains $U(1)$ as a subgroup, one can set $\alpha_k = 0$ as the later inclusion of gauge fields will allow to gauge these phases away. Note that the component $m$ of $\psi$ refers to the gauge group (as discussed earlier) and not the Lorentz group. The factor $(-1)^{\mathbf{x}}$ assigns a positive mass $M$ to fermions on even sites and negative mass $M$ to odd sites. This can be interpreted as the Dirac Sea: Occupied even sites correspond to particles whereas vacant odd sites correspond to anti-particles. The energetically most favourable configuration is therefore an occupation of all odd sites and vacancies at all even sites. This state, the fermionic vacuum, is called the Dirac state, denoted as $|D\rangle$.
We will now turn the focus on the gauge degrees of freedom located at the links which are characterized by $(\mathbf{x}, k)$. For the Hilbert space on the links, representing the gauge fields, we can choose the group element basis or the representation basis. The group G can act on the group element basis in two ways, corresponding to left and right transformations:

$$\Theta_g |h\rangle = |hg^{-1}\rangle \tag{74}$$

$$\tilde{\Theta}_g |h\rangle = |g^{-1}h\rangle \tag{75}$$

We define an operator $U^j_{mn}$, a matrix of operators in Hilbert space:

$$U^j_{mn} = \int D^j_{mn}(g) \, |g\rangle \langle g| \, \mathrm{d}g \tag{76}$$

It obeys the following transformation rules:

$$\begin{aligned} \Theta_g U^j_{mn} \Theta_g^\dagger &= U^j_{mn'} D^j_{n'n}(g) \\ \tilde{\Theta}_g U^j_{mn} \tilde{\Theta}_g{}^\dagger &= D^j_{mm'}(g) U^j_{m'n} \end{aligned} \tag{77}$$

If G is a compact Lie group, we can expand the matrix operator $U^j$ as:

$$U^j = e^{i\hat{\phi}_a T_a^j} \tag{78}$$

where $\hat{\phi}_a$ are operator-valued group parameters. We may also expand the transformations $\Theta_g$ and $\tilde{\Theta}_g$:

$$\begin{aligned} \Theta_g &= e^{i\phi_a R_a} \\ \tilde{\Theta}_g &= e^{i\phi_a L_a} \end{aligned} \tag{79}$$

where $R_a$ and $L_a$ are right and left generators fulfilling the commutation relations

$$\begin{aligned} [R_a, R_b] &= i f_{abc} R_c \\ [L_a, L_b] &= -i f_{abc} L_c \\ [L_a, R_b] &= 0 \end{aligned} \tag{80}$$

One can think of the group parameters $\hat{\phi}_a$ as the color components of the vector potential. Thus, one may refer to the group element basis as magnetic basis. The conjugate degrees of freedom can be identified with the generators, hence representing the electric field. The corresponding basis is the representation basis, denoted as $|jmn\rangle$. We have two components $m$ and $n$ identifying the components within the representation $j$. The reason for that is the non-abelian nature of the gauge group so that one has to distinguish left and right transformations. $m$ will be chosen as the eigenvalue of the left generators and $n$ for right transformations. The two basis are connected by the relation (also valid for finite groups):

$$\langle g|jmn\rangle = \sqrt{\frac{dim(j)}{|G|}} D_{mn}(g) \tag{81}$$

where $|G|$ is the order of $G$. A singlet state is given by $|000\rangle$. Then, it follows straightforwardly that

$$|jmn\rangle = \sqrt{dim(j)} U^j_{mn} |000\rangle \tag{82}$$

A useful property for calculations carried out later on is the connection between the hermitian conjugate of $U^j$ in Hilbert space and in Matrix space. It has the form:

$$(U^j_{mn})^\dagger = \int dg\, |g\rangle\, \langle g|\, \bar{D}^j_{mn}(g) = \int dg\, |g\rangle\, \langle g|\, D^{j\dagger}_{mn}(g) = (U^{j\dagger})_{mn} \tag{83}$$

Since all matrix elements of $U$ commute, one can treat the matrix elements as numbers and define functions of the matrix $U$. One object that will turn out to be useful later on is the logarithm of $U$ in matrix space:

$$Z_{mn} = -i(log_{mat}(U^j))_{mn} \tag{84}$$

where $log_{mat}$ is understood as the logarithm only in matrix space. As a consequence,

$$(Z^j_{mn})^\dagger = Z^j_{nm} \tag{85}$$

where the hermitian conjugate is taken in Hilbert space. The representation indices $j$ shall be omitted in the following. With these definitions at hand we can define a local gauge transformation which acts on all Hilbert spaces intersecting at a vertex. It depends on a group element which itself can depend on the position.

$$\hat{\Theta}_g(\mathbf{x}) = \tilde{\Theta}_g(\mathbf{x},1)\tilde{\Theta}_g(\mathbf{x},2)\tilde{\Theta}_g(\mathbf{x},3)\Theta^\dagger_g(\mathbf{x}-\hat{1},1)\Theta^\dagger_g(\mathbf{x}-\hat{2},2)\Theta^\dagger_g(\mathbf{x}-\hat{3},3) \tag{86}$$

A state $|\psi\rangle$ is therefore said to be gauge-invariant if

$$\hat{\Theta}_{g(\mathbf{x})}(\mathbf{x})\, |\psi\rangle = |\psi\rangle\,, \qquad \forall \mathbf{x} \tag{87}$$

We can now define the singlet state for the whole lattice, including matter and gauge fields:

$$|0\rangle \equiv |D\rangle \bigotimes_{links} |000\rangle \tag{88}$$

All other gauge invariant states can be obtained by acting with gauge invariant operators on this singlet state. There are four such types of gauge invariant Hamiltonians which shall be discussed in the following.

1. The *Magnetic Hamiltonian*

   As already discussed in the section on Wilson's formulation of lattice gauge theories, one can obtain gauge invariant operators by taking products of $U$-operators along closed paths. The most natural choice is therefore to take this product along a plaquette resulting in the Hamiltonian:

$$H_B = \lambda_B \sum_{\text{plaquettes } p} \text{Tr}\left(U_1(\mathbf{p})U_2(\mathbf{p})U_3^\dagger(\mathbf{p})U_4^\dagger(\mathbf{p})\right) + H.c. \tag{89}$$

This term is often called *magnetic Hamiltonian* as it gives rise to the magnetic interactions in the case of QED ($G = U(1)$).

2. The *Electric Hamiltonian*

$$H_E = \lambda_E \sum_{\mathbf{x},k} h_E(\mathbf{x}, k) \tag{90}$$

with

$$h_E(\mathbf{x}, k) = \sum_{j,m,n} f(j) \left|jmn\right\rangle \left\langle jmn\right| \tag{91}$$

It is diagonal in representation space and thus gauge invariant. The correspondence with the electric field becomes clear for the case of $G = U(1)$ where - if we set $f(j) = j^2$ - the Hamiltonian is just a sum over the electric field of all links. The same holds true for $SU(2)$ where $f(j)$ is replace by the Casimir operators $\mathbf{J}^2$, i.e. $f(j) = j(j+1)$

The two terms above only involve the gauge fields. In the case of compact Lie groups they both add up to the *Kogut-Susskind Hamiltonian*

$$H_{KS} = H_B + H_E\,, \tag{92}$$

a Hamiltonian formulation of a Yang-Mills theory on the lattice.

3. The *fermionic mass Hamiltonian*
To solve the problem of fermion doubling we introduced staggered fermions which give rise to the following Hamiltonian

$$H_M = M \sum_{\mathbf{x}} (-1)^{\mathbf{x}} \psi^\dagger(\mathbf{x})\psi(\mathbf{x}) \tag{93}$$

where the alternating minus comes from the Dirac sea picture: particles on even sites and anti-particles on odd sites.

4. The *gauge-matter Hamiltonian*

The other term coming from the staggered fermion discussion was a hopping term. However, this term would not be locally gauge invariant which is why it needs to be coupled to the gauge field in form of the operator $U$. The resulting interaction is:

$$H_{GM} = \lambda_{GM} \sum_{\mathbf{x},k} \psi_m^\dagger(\mathbf{x}) U_{mn}(\mathbf{x}, k) \psi_n(\mathbf{x} + \hat{k}) + H.c. \tag{94}$$

In the following we want to look at some concrete examples of lattice gauge theories. We will start with one of the most canonical examples, compact QED ($G = U(1)$). Afterwards its truncation $\mathbb{Z}_N$ will be discussed. The same procedure will then be repeated for $O(2)$ and its truncation $D_{2N}$.

### 3.3.2 Compact QED

The Hilbert space of the gauge fields residing on the links is described in terms of the group representation basis which in the case of $U(1)$ can be characterized by an angle $\phi$ and the corresponding operator $\hat{\phi}$. Alternatively, one can use the eigenbasis of its conjugate operator, the angular momentum operator $L$. They fulfill the commutation relation

$$[\hat{\phi}, L] = i \tag{95}$$

One can identify $\hat{\phi}$ as the vector potential and $L$ as the electric field operator. It has an unbounded integer spectrum

$$L\,|m\rangle = m\,|m\rangle \qquad (m \in \mathbb{Z}) \tag{96}$$

where the states $|m\rangle$ have a clear interpretation as electric flux states. The $U$ operators are in this case not matrices as the group is abelian. It takes the form:

$$U = e^{i\hat{\phi}} \tag{97}$$

The $U$ operator is therefore a flux raising operator. With these definitions at hand the Hamiltonian of compact QED can be defined. As already mentioned, the electric Hamiltonian can be expressed in terms of $L$:

$$H_E = \lambda \sum_{\mathbf{x},k} L^2(\mathbf{x},k) \tag{98}$$

The magnetic Hamiltonian has the form:

$$H_B = 2\lambda_B \sum_{\text{plaquettes } p} \cos\left(\hat{\phi}_1(\mathbf{p}) + \hat{\phi}_2(\mathbf{p}) - \hat{\phi}_3(\mathbf{p}) - \hat{\phi}_4(\mathbf{p})\right) \tag{99}$$

The mass Hamiltonian:

$$H_M = M \sum_{\mathbf{x}} (-1)^{\mathbf{x}} \psi^\dagger(\mathbf{x})\psi(\mathbf{x}) \tag{100}$$

and the gauge-matter Hamiltonian:

$$H_{GM} = \lambda_{GM} \sum_{\mathbf{x},k} \psi^\dagger(\mathbf{x}) e^{i\hat{\phi}(\mathbf{x},k)} \psi(\mathbf{x}+\hat{k}) + H.c. \tag{101}$$

### 3.3.3 $\mathbb{Z}_N$

The importance of the gauge group $\mathbb{Z}_N$ comes from its large $N$ limit ($N \to \infty$), where $\mathbb{Z}_N$ converges to $U(1)$. Thus, it can be viewed as a truncation of $U(1)$. So is the Hilbert spaces of the gauge fields on the links not an integer spectrum from $-\infty$ to $\infty$ but truncated such that only $N$ states remain. They are labeled by $|m\rangle$ and we define unitary operators $P$ and $Q$ on them:

$$\begin{aligned} P^N &= Q^N = 1 \\ PQP^\dagger &= e^{i\frac{2\pi}{N}} Q \\ Q\,|m\rangle &= |m+1\rangle \quad \text{(cyclically)} \\ P\,|m\rangle &= e^{i\frac{2\pi}{N}m} \end{aligned} \tag{102}$$

Like in the U(1) case - since the group is abelian - there are single fermionic species, $\psi^\dagger$, on the vertices. We can now define the Hamiltonian of the $\mathbb{Z}_N$ lattice gauge theory.

$$
\begin{aligned}
H_E &= \lambda_E \sum_{\mathbf{x},k} 1 - P(\mathbf{x},k) - P^\dagger(\mathbf{x},k) \\
H_B &= \lambda_B \sum_{\text{plaquettes } p} Q_1(\mathbf{p})Q_2(\mathbf{p})Q_3^\dagger(\mathbf{p})Q_4^\dagger(\mathbf{p}) + H.c. \\
H_M &= M \sum_{\mathbf{x}} (-1)^{\mathbf{x}} \psi^\dagger(\mathbf{x})\psi(\mathbf{x}) \\
H_{GM} &= \lambda_{GM} \sum_{\mathbf{x},k} \psi^\dagger(\mathbf{x})Q(\mathbf{x},k)\psi(\mathbf{x}+\hat{k}) + H.c.
\end{aligned}
\tag{103}
$$

### 3.3.4 $O(2)$

A crucial difference to the previous examples is that the group $O(2)$ is non-abelian. That has a lot of consequences for the corresponding lattice gauge theory since the representations of the group become non-trivial and thus a lot of terms more complicated. Therefore, we will start by discussing the most important group properties and the irreducible representations of $O(2)$.
$O(2)$ is the symmetry group of rotations in a two-dimensional plane and reflections along a certain axis (any axis passing through the center of rotations is possible). We identify pure rotations by an angle R($\theta$) and we identify reflections along the x-axis with S. Any other reflection can be obtained by composing S with some rotation. We can write the group as

$$
G = \{g = (\theta, m) \equiv R(\theta)S^m | \theta \in [0, 2\pi) \,\text{and}\, m \in \{0, 1\}\}
\tag{104}
$$

The structure of the group is defined by the composition rules which are originating from the usual composition rules for rotations R($\theta$) and reflections S:

$$
\begin{aligned}
R(\theta)R(\phi) &= R(\theta + \phi) \\
SR(\theta)S &= R(-\theta)
\end{aligned}
\tag{105}
$$

Thus, the neutral element is $e = R(0)S^0$ and the composition rules for $O(2)$ follow straightforwardly:

$$
R(\theta)S^m R(\phi)S^n = R(\theta + (-1)^m\phi)S^{m+n}
\tag{106}
$$

Written in the group notation $(\theta, m)$:

$$
(\theta, m) \cdot (\phi, n) = (\theta + (-1)^m\phi, m + n)
\tag{107}
$$

where the addition of m and n is understood as modulo 2. The inverse element of $(\theta, m)$ is:

$$(R(\theta)S^m)^{-1} = S^m R(-\theta) = R((-1)^{m+1}\theta)S^m \tag{108}$$

The representation theory is characterized by the three irreducible representations of $O(2)$ shown in the following table:

| | |
|---|---|
| Trivial (dimension 1) | $D^t(\theta, m) = 1$ |
| Sign (dimension 1) | $D^s(\theta, m) = (-1)^m$ |
| k-th (dimension 2) | $D^k(\theta, m) = e^{ik\sigma_z\theta}\sigma_x^m$ |

The operator $U$ is chosen to be in the two-dimensional representation

$$U = e^{i\hat{\theta}\sigma_z}\sigma_x^{\hat{m}} \tag{109}$$

This implies that the fermionic fields located on the vertices will have two color components, denoted by $\psi_1^\dagger$ and $\psi_2^\dagger$. This allows us to write down the pure matter Hamiltonian:

$$H_M = M\sum_{\mathbf{x}}(-1)^{\mathbf{x}}\psi^\dagger(\mathbf{x})\psi(\mathbf{x}) = M\sum_{\mathbf{x}}(-1)^{\mathbf{x}}\left(\psi_1^\dagger(\mathbf{x})\psi_1(\mathbf{x}) + \psi_2^\dagger(\mathbf{x})\psi_2(\mathbf{x})\right) \tag{110}$$

Moreover, we can explicitly give the gauge-matter interactions

$$H_{GM} = \lambda_{GM}\sum_{\mathbf{x},k}\left(\psi_1^\dagger(\mathbf{x}), \quad \psi_2^\dagger(\mathbf{x})\right)e^{i\hat{\theta}\sigma_z}\sigma_x^{\hat{m}}(\mathbf{x}, k)\begin{pmatrix}\psi_1(\mathbf{x})\\ \psi_2(\mathbf{x})\end{pmatrix} + H.c. \tag{111}$$

and the plaquette interactions

$$H_B = \lambda_B\sum_{\text{plaquettes } p}\mathrm{Tr}\left(U_1(\mathbf{p})U_2(\mathbf{p})U_3^\dagger(\mathbf{p})U_4^\dagger(\mathbf{p})\right) + H.c. \tag{112}$$

The last part, the electric Hamiltonian, can easily be given in the representation basis. However, since this form of the Hamiltonian is not very feasible for later purposes we will bring it to another form involving the group representation basis. This will have the additional advantage that the electric Hamiltonian for the dihedral group can easily be obtained as a truncation. The interactions corresponding to the electric Hamiltonian act on the gauge degrees of freedom residing on the links of the lattice. Since they act on every link independently, they are of the

form:

$$H_E = \lambda_E \sum_{\mathbf{x},k} h_E(\mathbf{x}, k) \tag{113}$$

On each link Hilbert space they act diagonally in representation space:

$$h_E(\mathbf{x}, k) = \sum_{j,m,n} f(j) \left|jmn\right\rangle \left\langle jmn\right| \tag{114}$$

where j labels the different irreducible representations. By summing over m and n, the term is automatically gauge-invariant. The coefficients can be chosen arbitrarily which is why we will keep them general in the following discussion. As we will use the group representation basis in our implementation, we transform the electric Hamiltonian accordingly:

$$\begin{aligned} h_E(\mathbf{x}, k) &= \sum_{g,g'} \sum_{j,m,n} f(j) \left|g\right\rangle \left\langle g|jmn\right\rangle \left\langle jmn|g'\right\rangle \left\langle g'\right| \\ &= \sum_{g,g'} \sum_{j,m,n} f(j) \left|g\right\rangle \sqrt{\frac{dim(j)}{|G|}} D^j_{mn}(g) \sqrt{\frac{dim(j)}{|G|}} \overline{D}^j_{mn}(g') \left\langle g'\right| \\ &= \sum_{g,g'} \sum_{j,m,n} \frac{dim(j)}{|G|} f(j) \left|g\right\rangle D^j_{mn}(g) D^{j\dagger}_{nm}(g') \left\langle g'\right| \\ &= \sum_{g,g'} \sum_{j} \frac{dim(j)}{|G|} f(j) \left|g\right\rangle \mathrm{Tr}(D^j(g) D^{j\dagger}(g')) \left\langle g'\right| \end{aligned} \tag{115}$$

To specify this expression for $O(2)$ we need to calculate the trace from above for all irreducible representations.

Trivial representation:

$$\mathrm{Tr}(D^t(g) D^{t\dagger}(g')) = \mathrm{Tr}(D^t(\theta, m) D^{t\dagger}(\theta', m')) = 1 \tag{116}$$

Sign representation:

$$\mathrm{Tr}(D^s(\theta, m) D^{s\dagger}(\theta', m')) = \mathrm{Tr}((-1)^m (-1)^{m'}) = (-1)^{m+m'} \tag{117}$$

k-th representation:

$$\begin{aligned}\mathrm{Tr}(D^k(\theta,m)D^{k\dagger}(\theta',m')) &= \mathrm{Tr}(e^{ik\sigma_z\theta}\sigma_x^m(e^{ik\sigma_z\theta'}\sigma_x^{m'})^\dagger)\\ &= \mathrm{Tr}(e^{ik\sigma_z\theta}\sigma_x^{m+m'}e^{-ik\sigma_z\theta'})\\ &= \delta_{mm'}\mathrm{Tr}(e^{ik\sigma_z(\theta-\theta')})\\ &= \delta_{mm'}(e^{ik(\theta-\theta')}+e^{-ik(\theta-\theta')})\end{aligned} \tag{118}$$

Inserting this into (eq. 115) we obtain:

$$h_E(\mathbf{x},k) = \frac{1}{4\pi}\iint \mathrm{d}\theta\mathrm{d}\theta' \sum_{m,m'} |\theta,m\rangle\langle\theta',m'| \left( f_t + f_s(-1)^{m+m'} + 2\sum_{k>0} f_k\delta_{mm'}(e^{ik(\theta-\theta')}+e^{-ik(\theta-\theta')})\right) \tag{119}$$

The expression simplifies if we go from the basis characterized by the angles $\theta$ to the angular momentum basis characterized by the eigenvalues $l$ of the angular momentum operator $L$. The new basis $|l,m\rangle$ is completely defined by the relation

$$\langle l,m|\phi,n\rangle = \frac{1}{\sqrt{2\pi}}\delta_{mn}e^{-il\phi}. \tag{120}$$

$L$ can then be defined as

$$L = \sum_{l,m} l\,|l,m\rangle\langle l,m| \tag{121}$$

where $l = -\infty,..,-1,0,1,..\infty$. We can see that $L$ really generates rotations:

$$e^{-iL\theta}|\phi,n\rangle = e^{-iL\theta}\sum_{l=-\infty}^{\infty}|l,n\rangle\frac{1}{\sqrt{2\pi}}e^{-il\phi} = \sum_{l=-\infty}^{\infty}|l,n\rangle\frac{1}{\sqrt{2\pi}}e^{-il(\phi+\theta)} = |\theta+\phi,n\rangle \tag{122}$$

Transforming to the angular momentum basis, eq. (119) takes the form

$$
\begin{aligned}
h_E(\mathbf{x},k) &= \frac{1}{4\pi}\iint \mathrm{d}\theta\mathrm{d}\theta' \sum_{m,m'}\sum_{l,l'} |l,m\rangle \langle l,m|\theta,m\rangle \left( f_t + f_s(-1)^{m+m'} + 2\sum_{k>0} f_k \delta_{mm'}(e^{ik(\theta-\theta')} + e^{-ik(\theta-\theta')}) \right) \\
&\quad \langle\theta',m'|l',m'\rangle \langle l',m'| \\
&= \frac{1}{8\pi^2}\iint \mathrm{d}\theta\mathrm{d}\theta' \sum_{m,m'}\sum_{l,l'} |l,m\rangle \Big( f_t e^{-il\theta}e^{il'\theta'} + f_s e^{-il\theta}e^{il'\theta'}(-1)^{m+m'} \\
&\quad +2\sum_{k>0} f_k \delta_{mm'}(e^{i(k-l)\theta}e^{i(l'-k)\theta'} + e^{-i(k+l)\theta}e^{i(k+l')\theta'}) \Big) \langle l',m'| \\
&= \frac{1}{2}\sum_{m,m'}\sum_{l,l'} |l,m\rangle \left( f_t \delta_{l,0}\delta_{l',0} + f_s \delta_{l,0}\delta_{l',0}(-1)^{m+m'} + 2\sum_{k>0} f_k \delta_{mm'}(\delta_{k,l}\delta k, l' + \delta_{k,-l}\delta k, -l') \right) \langle l',m'| \\
&= \frac{1}{2}\sum_{m,m'} \left( f_t |0,m\rangle \langle 0,m'| + f_s(-1)^{m+m'} |0,m\rangle \langle 0,m'| + 2\sum_{l\neq 0} f_l |l,m\rangle \langle l,m| \right)
\end{aligned}
\tag{123}
$$

where the coefficients $f_l$ have to satisfy the constraint $f_l = f_{-l}\,\forall l$. If we define redefine the coefficient for the trivial and sign representation as $f_{t'} := f_t - f_s$ and $f_0 := f_s$ we can simplify the expression further:

$$
\begin{aligned}
h_E(\mathbf{x},k) &= \frac{1}{2}\sum_{m,m'} \left( f_{t'} |0,m\rangle \langle 0,m'| + f_0 \left(1 + (-1)^{m+m'}\right) |0,m\rangle \langle 0,m'| + 2\sum_{l\neq 0} f_l |l,m\rangle \langle l,m| \right) \\
&= \frac{1}{2}\sum_{m,m'} \left( f_{t'} |0,m\rangle \langle 0,m'| + f_0 2\delta_{mm'} |0,m\rangle \langle 0,m'| + 2\sum_{l\neq 0} f_l |l,m\rangle \langle l,m| \right) \\
&= \frac{1}{2}\sum_{m,m'} f_{t'} |0,m\rangle \langle 0,m'| + \sum_{l=-\infty}^{\infty}\sum_{m} f_l |l,m\rangle \langle l,m|
\end{aligned}
\tag{124}
$$

We see that the second term only depends on $l$, i.e. only the part corresponding to rotations makes a non-trivial contribution. For this reason, we can identify it with the electric energy for $U(1)$ if we consider $O(2)$, or $\mathbb{Z}_N$ for the dihedral groups $D_{2N}$. The first term, however, takes into account reflections but only for the $l = 0$ eigenstate of the angular momentum operator.

### 3.3.5 Dihedral group $D_{2N}$

The dihedral group can be viewed as a truncation for $O(2)$ where the angle $\theta$ characterizing the rotations only takes discrete values. The set describing the group can be defined as

$$D_{2N} = \{g = (p, m) \equiv R\,(2\pi/N)^p\, S^m | p \in [0, N-1) \,\text{and}\, m \in \{0, 1\}\} \tag{125}$$

However, not all dihedral groups inherit their properties from $O(2)$. The structure of the irreducible representations is only the same for $N$ being odd and $N \geq 3$. Dihedral groups with even $N$ have two additional sign representations. Therefore, we will focus in the following on the former. Since the irreducible representations are the same, the $U$ operator will have the same form as in the case of $O(2)$ with the substitution $\theta = \frac{2\pi}{N}p$. The same calculations from above for the electric energy hold true for the dihedral group (under the restriction that $N$ has to be odd and $N \geq 3$). The only difference is that the rotations are finite which implies a finite maximal value for the angular momentum operator. Thus, for $D_{2N}$ - which consists of N rotations - the sum over $l$ in the final expression only contains $N$ terms. Thus, the electric Hamiltonian for $D_{2N}$ can be written as:

$$h_E(\mathbf{x}, k) = \frac{1}{2}\sum_{m,m'} f_{t'}\,|0, m\rangle\,\langle 0, m'| + \sum_{l=-(N-1)/2}^{(N-1)/2}\sum_{m} f_l\,|l, m\rangle\,\langle l, m| \tag{126}$$

In particular, the relevant group for implementation later on, $D_6$, has the electric link Hamiltonian:

$$h_E(\mathbf{x}, k) = \frac{1}{2}\sum_{m,m'} f_{t'}\,|0, m\rangle\,\langle 0, m'| + \sum_{l=-1}^{1}\sum_{m} f_l\,|l, m\rangle\,\langle l, m| \tag{127}$$

The other Hamiltonians have exactly the same form as for $O(2)$ with the substitution $\theta = \frac{2\pi}{N}p$

$$\begin{aligned}
H_M &= M\sum_{\mathbf{x}}(-1)^{\mathbf{x}}\psi^\dagger(\mathbf{x})\psi(\mathbf{x}) = M\sum_{\mathbf{x}}(-1)^{\mathbf{x}}\left(\psi_1^\dagger(\mathbf{x})\psi_1(\mathbf{x}) + \psi_2^\dagger(\mathbf{x})\psi_2(\mathbf{x})\right)\\
H_{GM} &= \lambda_{GM}\sum_{\mathbf{x},k}\left(\psi_1^\dagger(\mathbf{x}),\quad \psi_2^\dagger(\mathbf{x})\right) e^{i\frac{2\pi}{N}\hat{p}\sigma_z}\sigma_x^{\hat{m}}(\mathbf{x}, k)\begin{pmatrix}\psi_1(\mathbf{x})\\ \psi_2(\mathbf{x})\end{pmatrix} + H.c.\\
H_B &= \lambda_B\sum_{\text{plaquettes } p}\mathrm{Tr}\left(U_1(\mathbf{p})U_2(\mathbf{p})U_3^\dagger(\mathbf{p})U_4^\dagger(\mathbf{p})\right) + H.c.
\end{aligned} \tag{128}$$

The dihedral group $D_6$ will be of particular interest later on as it is the smallest non-abelian group. It is symmetry group of the triangle and isomorphic to the symmetric group $S_3$. It can be viewed as a subgroup of $SO(3)$ and its double cover $SU(2)$ in the following way: Every rotation $R \in SO(3)$ can be written in terms of the Euler angles $\alpha, \beta, \gamma$

$$R(\alpha, \beta, \gamma) = e^{i\alpha J_z} e^{i\beta J_x} e^{i\gamma J_z} \tag{129}$$

where $J_z$ is the generator for rotations in z-direction and $J_x$ the one for rotations in x-direction. The group $D_6$ can then be obtained by restricting the parameter space to $\alpha = \{0, \frac{2\pi}{3}, \frac{4\pi}{3}\}$ (corresponding to $\frac{2\pi}{3}$-rotations around the z-axis), $\beta = \{0, \pi\}$ (reflections along the x-axis) and $\gamma = 0$.

# 4 Digital quantum simulation of lattice gauge theories

In this chapter, we will first review basic ingredients required for a simulation of lattice gauge theories with ultracold atoms, in particular the concept of a stator, used for mediating three- and four-body interactions, will be explained. Afterwards, an algorithm for the simulation of lattice gauge theories in three dimensions will be proposed. To back the validity of this simulation scheme, bounds on the trotterization error will be provided.

## 4.1 Stators

A natural method to realize interactions in systems of ultracold atoms is given by atomic collisions. Under typical conditions in ultracold atom experiments, i.e. low densities and low energies, these are dominated by elastic two-body scattering. Its theory is well understood and the Hamiltonian can be calculated exactly (see section 2). Three-and four body processes, however, are suppressed and at the same time only allow for an approximate mathematical description, which makes it much harder to map the Hamiltonian from ultracold atoms to the system one would like to simulate. For the purpose of quantum simulation it makes therefore sense to design a scheme in which interactions involving three or more atoms can be rewritten as a sequence of only two-body collisions. This is particularly relevant for lattice gauge theories since gauge-matter interactions and plaquette interactions are three, respectively four body terms (see section 3).

One approach to this problem is the concept of a *Stator* which will be presented briefly in this section (a detailed discussion can be found in [60]. It is based on the idea of using an auxiliary degree of freedom to mediate interactions via entanglement. Putting it in more mathematical terms, we consider a Hilbert spaces $H_A$ representing the physical d.o.f., where the interaction is supposed to be implemented, and a Hilbert space $H_B$ for the auxiliary d.o.f. (sometimes called control in the following). We denote the operators acting on the Hilbert space $H$ by $\mathcal{O}(H)$. A stator S can then be defined as an element which acts on a state in $H_A$ but is itself a state in $H_B$, i.e. $S \in \mathcal{O}(H_A) \times H_B$. Thus the name "Stator", a mixture of a state and an operator. It can be prepared by acting on some initial state $|in_B\rangle \in H_B$ with a unitary $\mathcal{U}_{AB} \in \mathcal{O}(H_A \times H_B)$:

$$S = \mathcal{U}_{AB} |in_B\rangle \in \mathcal{O}(H_A) \times H_B \tag{130}$$

Mathematically speaking, a stator is an isometry that maps a state $|\psi_A\rangle \in H_A$ to the tensor product $U_{AB}(|\psi_A\rangle \otimes |in_B\rangle) \in H_A \times H_B$. This can be viewed as an entangling operation between the physical state $|\psi_A\rangle$ and the auxiliary state $|in_B\rangle$.
If this entangling procedure is chosen in a certain way operations acting on the physical Hilbert space can implemented by acting only on the auxiliary state. Assume we want to realize a Hamiltonian $H \in \mathcal{O}(H_A)$ in the physical Hilbert space. For that, we need to design a stator S and a hermitian operator $H' \in H_B$ in the auxiliary Hilbert space in such a way that the following eigenoperator relation [60] holds:

$$H'S = SH \tag{131}$$

An analogue relation for the time evolution follows directly, since $H$ and $H'$ are hermitian operators:

$$e^{-iH't}S = Se^{-iHt} \tag{132}$$

Therefore, by creating such a stator of the physical and auxiliary Hilbert spaces, we can obtain time evolution of the physical state:

$$e^{-iH't}\mathcal{U}_{AB}\,|\psi_A\rangle\,|in_B\rangle = e^{-iH't}S\,|\psi_A\rangle = Se^{-iHt}\,|\psi_A\rangle \tag{133}$$

i.e. we end up with the desired time evolution of the physical state $|\psi_A\rangle$. However, it is still entangled with the auxiliary state which means that one can either perform another operation using the stator $S$ or disentangle both states. This would lead to a product state with the auxiliary state going back to its initial state:

$$\mathcal{U}_{AB}^{\dagger}e^{-iH't}\mathcal{U}_{AB}\,(|\psi_A\rangle \otimes |in_B\rangle) = |in_B\rangle \otimes e^{-iHt}\,|\psi_A\rangle \tag{134}$$

In the upcoming sections, for the purpose of quantum simulation of lattice gauge theories, the physical and auxiliary Hilbert spaces will be represented by ultracold atoms. A sequence of two body collisions between the auxiliary atoms and the physical atoms will create the stator that allows realizing the full time evolution by acting locally on the auxiliary Hilbert space.

## 4.2 Quantum simulation of lattice gauge theory in three dimensions

Next, we shall focus on the quantum simulation of lattice gauge theories in three dimensions. So far, there have been digital proposals in one or two dimensions [42, 43, 50, 57], one building upon the concept of a stator [42]. The motivation for increasing the dimension is obvious since we ultimately want to simulate phenomena in nature which still lack a complete understanding. Although investigations in lower dimensions have revealed lots of interesting physical effects, the behavior of a system can crucially depend on the dimension. That makes quantum simulations in three dimensions a reasonable next step.

First of all, we will briefly present the Hamiltonian of lattice gauge theory in three dimensions (following chapter 3) and split it into the individual parts which will be implemented independently. Notation will be used according to figure 3. A fermion residing at lattice site $\mathbf{x}$ will be denoted by $\psi^{\dagger j}_m(\mathbf{x})$ where $j$ indicates the representation under gauge transformations and $m$ the specific component of the representation. Since the representation $j$ remains fixed it will be neglected later on for convenience. A gauge field residing on the link pointing from site $\mathbf{x}$ in direction $k$ will be denoted by $U^j_{mn}(\mathbf{x}, k)$ . $j$ again characterizes the representation and its components under left and right transformations are denoted $m$, respectively $n$. In this notation the locally gauge invariant Hamiltonian in three dimensions involves four different terms:

1. The plaquette interactions, the magnetic part, diagonal in the group representation basis:

$$
\begin{aligned}
H_B = \sum_{\text{plaquette } \mathbf{p}} H_B(\mathbf{p}) &= \lambda_B \sum_{\mathbf{x}} \mathrm{Tr}(U(\mathbf{x},1)U(\mathbf{x}+\hat{1},2)U^\dagger(\mathbf{x}+\hat{2},1)U^\dagger(\mathbf{x},2)) + h.c. \\
&+ \mathrm{Tr}(U(\mathbf{x},3)U(\mathbf{x}+\hat{3},1)U^\dagger(\mathbf{x}+\hat{1},3)U^\dagger(\mathbf{x},1)) + h.c. \\
&+ \mathrm{Tr}(U(\mathbf{x},2)U(\mathbf{x}+\hat{2},3)U^\dagger(\mathbf{x}+\hat{3},2)U^\dagger(\mathbf{x},3)) + h.c. \\
&=: \sum_{\mathbf{x}} H_{B,1}(\mathbf{x}) + H_{B,2}(\mathbf{x}) + H_{B,3}(\mathbf{x}) \\
&= \sum_{\mathbf{x}\,\text{even}} H_{B,1}(\mathbf{x}) + H_{B,2}(\mathbf{x}) + H_{B,3}(\mathbf{x}) + \sum_{\mathbf{x}\,\text{odd}} H_{B,1}(\mathbf{x}) + H_{B,2}(\mathbf{x}) + H_{B,3}(\mathbf{x}) \\
&=: H_{B,1e} + H_{B,2e} + H_{B,3e} + H_{B,1o} + H_{B,2o} + H_{B,3o}
\end{aligned}
\tag{135}
$$

   It is important to mention that all the different magnetic terms commute. Thus, even a trotterized time evolution will lead to an exact time evolution for the magnetic Hamilto-

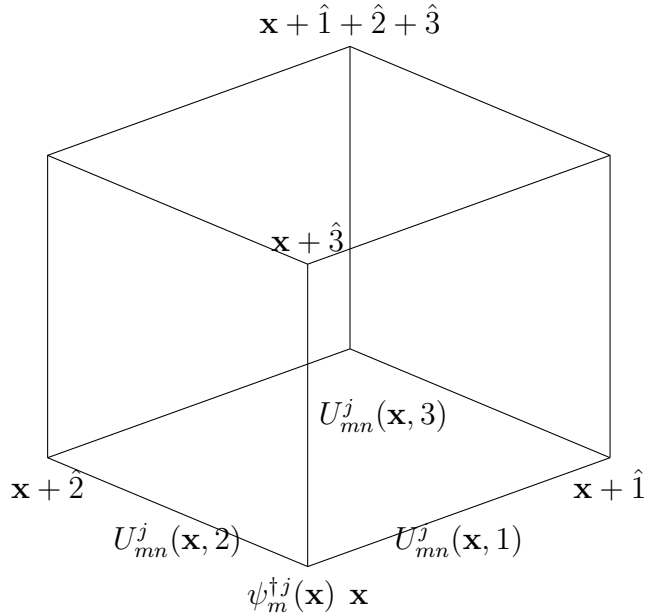


Figure 3: Notation of matter d.o.f. at lattice sites and gauge d.o.f. on the links in a unit cube

nian.

2. The electric part, diagonal in the representation basis:

$$H_E = \lambda_E \sum_{\mathbf{x},k} h_E(\mathbf{x},k) \tag{136}$$

with

$$h_E(\mathbf{x},k) = \sum_{j,m,n} f(j)\,|jmn\rangle\,\langle jmn| \tag{137}$$

The first two interactions are pure gauge interactions and constitute the Kogut-Susskind Hamiltonian.

3. The fermionic mass term:

$$H_M = M \sum_{\mathbf{x}} (-1)^{x_1+x_2+x_3}\ \psi^\dagger(\mathbf{x})\psi(\mathbf{x}) \tag{138}$$

The alternating minus sign comes from the staggering of the fermions.

4. The gauge-matter interactions:

$$\begin{aligned} H_{GM} &= \sum_{\mathbf{x}} \sum_{k=1}^{3} H_{GM}(\mathbf{x}, k) \\ &= \lambda_{GM} \sum_{\mathbf{x}} \sum_{k=1}^{3} \psi_m^\dagger(\mathbf{x}) U_{mn}(\mathbf{x}, k) \psi_n(\mathbf{x}, \hat{k}) + h.c. \\ &= \sum_{\mathbf{x}\,\text{even}} H_{GM}(\mathbf{x}, 1) + H_{GM}(\mathbf{x}, 2) + H_{GM}(\mathbf{x}, 3) + \sum_{\mathbf{x}\,\text{odd}} H_{GM}(\mathbf{x}, 1) + H_{GM}(\mathbf{x}, 2) + H_{GM}(\mathbf{x}, 3) \\ &=: H_{GM,1e} + H_{GM,2e} + H_{GM,3e} + H_{GM,1o} + H_{GM,2o} + H_{GM,3o} \end{aligned} \tag{139}$$

Compared to the magnetic Hamiltonian, the different terms of the gauge-matter Hamiltonian do not commute if they share the same fermion.
Summing up, we obtain the Hamiltonian of lattice gauge theory in three dimensions in full generality, split into the parts which are implemented independently:

$$\begin{aligned} H &= H_B + H_E + H_M + H_{GM} \\ &= H_{B,1e} + H_{B,2e} + H_{B,3e} + H_{B,1o} + H_{B,2o} + H_{B,3o} + H_E + H_M \\ &+ H_{GM,1e} + H_{GM,2e} + H_{GM,3e} + H_{GM,1o} + H_{GM,2o} + H_{GM,3o} \end{aligned} \tag{140}$$

## 4.3 The implementation

In this section we want to discuss the implementation of the individual parts of the Hamiltonian. To create plaquette and gauge-matter interactions by means of a stator - as described in section 4.1 - we introduce an auxiliary degree of freedom in the middle of every second cube (either all even or odd ones) and assign to it a Hilbert space $\tilde{H}$ similar to the Hilbert spaces on the links (see Fig 4). The reason for not placing them in every cube is that the interactions can not be implemented in neighboring cubes at the same time. This is a consequence of the fact that stators can not share a degree of freedom. The plaquette between two neighboring cubes, for example, can only be entangled with one of the ancillas to generate the magnetic interactions. Thus, the Hamiltonian needs to be realized for even and odd cubes separately.

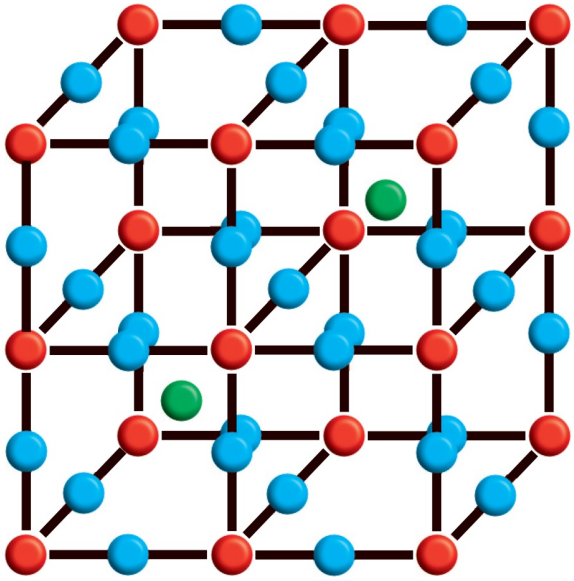

Figure 4: The physical system consists of the gauge fields residing on the links (blue) and the matter fields on the vertices (red). The auxiliary degrees of freedom (green) are located in the center of every second cube (either even or odd) and can be rigidly moved to the center of the neighboring cube without affecting any other degree of freedom.

### 4.3.1 Plaquette interactions

For the plaquette interactions, the basic stator we will use is the so called group element stator,

$$S_i = \int |g_i\rangle \langle g_i| \otimes |\tilde{g}\rangle \, \mathrm{d}g \tag{141}$$

where the first Hilbert space belongs to the gauge field residing on link $i$ and the second one to the aforementioned auxiliary d.o.f. in the center of the cube. The resulting entangled state can be created by the unitary

$$\mathcal{U}_i = \int |g_i\rangle \langle g_i| \otimes \tilde{\Theta}_g^\dagger \, \mathrm{d}g \tag{142}$$

acting on the initial state $|\tilde{in}\rangle = |\tilde{e}\rangle$. We repeat a similar entangling operation $\mathcal{U}_i$ for the three other links of the plaquette (e.g. the links 1,2,3,4 of cube $\mathbf{x}$) and obtain a plaquette stator of the form

$$S_\square^{1234}(\mathbf{x}) = \mathcal{U}_\square^{1234}(\mathbf{x}) \, |\tilde{in}\rangle = \mathcal{U}_1(\mathbf{x})\mathcal{U}_2(\mathbf{x})\mathcal{U}_3^\dagger(\mathbf{x})\mathcal{U}_4^\dagger(\mathbf{x}) \, |\tilde{in}\rangle \tag{143}$$

The crucial part is that it fulfills the relation

$$\mathrm{Tr}(\tilde{U}+\tilde{U}^\dagger)S_\square = S_\square \mathrm{Tr}(U_1 U_2 U_3^\dagger U_4^\dagger + h.c.) \tag{144}$$

i.e. acting locally with $\tilde{H}_B(\mathbf{x}) = \lambda_B \mathrm{Tr}(\tilde{U}(\mathbf{x}) + h.c.)$ on the control of the cube enables us to realize the magnetic time evolution for this plaquette. The required sequence for that is

$$\mathcal{U}_{B,1}(\mathbf{x}) = \mathcal{U}_\square^{1234\,\dagger}(\mathbf{x})\, e^{-i\tilde{H}_B(\mathbf{x})\tau}\, \mathcal{U}_\square^{1234}(\mathbf{x}) \tag{145}$$

whose action on the plaquette state $|\psi_{1234}\rangle$, the tensor product of the four link states, and the auxiliary state $|\tilde{in}\rangle$ is a pure time evolution of the physical state:

$$\mathcal{U}_{B,1}(\mathbf{x})\, |\psi_{1234}\rangle\, |\tilde{in}\rangle = |\tilde{in}\rangle\, e^{-iH_B(\mathbf{x})\tau}\, |\psi_{1234}\rangle \tag{146}$$

We can create the other two plaquette terms by choosing the appropriate stators and applying the above sequence. To describe them conveniently, we first define some abbreviations for the gauge field operators in a unit cube according to Fig. 5.

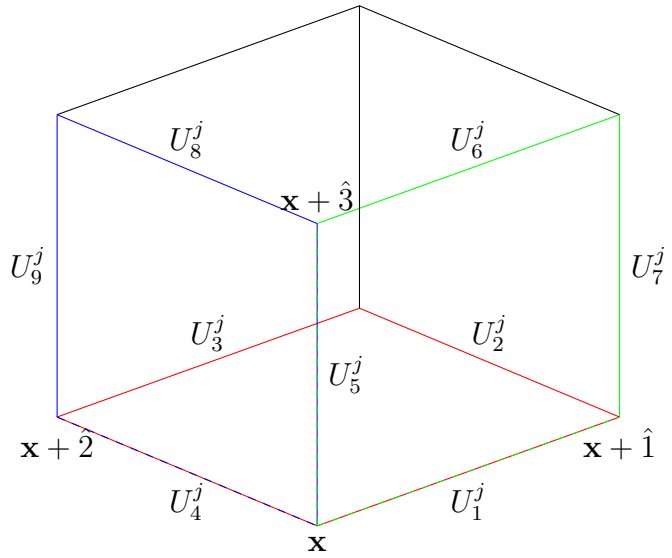


$$\begin{aligned}
U_1^j &= U^j(\mathbf{x},1)\\
U_2^j &= U^j(\mathbf{x}+\hat{1},2)\\
U_3^j &= U^j(\mathbf{x}+\hat{2},1)\\
U_4^j &= U^j(\mathbf{x},2)\\
U_5^j &= U^j(\mathbf{x},3)\\
U_6^j &= U^j(\mathbf{x}+\hat{3},1)\\
U_7^j &= U^j(\mathbf{x}+\hat{1},3)\\
U_8^j &= U^j(\mathbf{x}+\hat{3},2)\\
U_9^j &= U^j(\mathbf{x}+\hat{2},3)
\end{aligned}$$

Figure 5: The different plaquettes of a unit cube and their corresponding gauge field operators

Using this notation, we create the stator used already in the example above

$$S_\square^{1234}(\mathbf{x}) = \mathcal{U}_\square^{1234}(\mathbf{x})\, |\tilde{in}\rangle \tag{147}$$

corresponding to the red plaquette in the figure below. The sequence $\mathcal{U}_{B,1}(\mathbf{x})$ gives us the time evolution under the Hamiltonian $H_{B,1}(\mathbf{x})$. If we do it for all even cubes we obtain $H_{B,1e}$, respectively $H_{B,1o}$ for the odd cubes. In the same fashion we can use the stator

$$S_{\square}^{5671}(\mathbf{x}) = \mathcal{U}_{\square}^{5671}(\mathbf{x}) \, |\tilde{in}\rangle \tag{148}$$

corresponding to the green plaquette, to perform the sequence $\mathcal{U}_{B,2}(\mathbf{x})$. This would result in an effective implementation of $H_{B,2e}$ and $H_{B,2o}$ if applied to all even or odd cubes. Finally, the stator

$$S_{\square}^{5894}(\mathbf{x}) = \mathcal{U}_{\square}^{5894}(\mathbf{x}) \, |\tilde{in}\rangle \tag{149}$$

corresponding to the blue plaquette, allows the implementation of $H_{B,3e}$ and $H_{B,3o}$ by the sequence $\mathcal{U}_{B,3}(\mathbf{x})$ for all cubes.
Summarizing, we can formulate an algorithm to implement the plaquette interactions. We start with one control atom placed in the center of every even cube and do the following three steps:

1. Create the stator: Move all controls to the gauge fields on link 4 and create the unitary

$$\mathcal{U}_{4e}^{\dagger} = \prod_{\mathbf{x}\, even} \mathcal{U}_{4}^{\dagger}(\mathbf{x}) \tag{150}$$

Bring the controls back to the center of every cube. We repeat the same process with link 3 to obtain the unitary

$$\mathcal{U}_{3e}^{\dagger} = \prod_{\mathbf{x}\, even} \mathcal{U}_{3}^{\dagger}(\mathbf{x}) \tag{151}$$

Finally, for the links 2 and 1:

$$\mathcal{U}_{2e} = \prod_{\mathbf{x}\, even} \mathcal{U}_{2}(\mathbf{x}) \tag{152}$$

$$\mathcal{U}_{1e} = \prod_{\mathbf{x}\, even} \mathcal{U}_{1}(\mathbf{x}) \tag{153}$$

So in total we get:

$$\mathcal{U}_{B,1e} = \mathcal{U}_{1e}\mathcal{U}_{2e}\mathcal{U}_{3e}^{\dagger}\mathcal{U}_{4e}^{\dagger} = \prod_{\mathbf{x}\ even} \mathcal{U}_{B,1}(\mathbf{x}) \tag{154}$$

2. For the controls we turn on the Hamiltonian $\tilde{H}_{B,e} = \sum_{\mathbf{x}\ even} \tilde{H}_B(\mathbf{x})$ for a period $\tau$ resulting in the time evolution

$$\tilde{V}_{Be} = e^{-i\tilde{H}_{B,e}\tau} \tag{155}$$

3. In the last step we have to undo the stator by creating the inverse of the first step, i.e. $\mathcal{U}_{B,1e}^{\dagger}$.

The above procedure is applied to a state $|\psi(t)\rangle\,|\tilde{in}\rangle$ at time t. Thanks to relation (144) we get:

$$|\psi(t+\tau)\rangle\,|\tilde{in}\rangle = \mathcal{U}_{B,1e}^{\dagger}\tilde{V}_{Be}\mathcal{U}_{B,1e}\,|\psi(t)\rangle\,|\tilde{in}\rangle = W_{B,1e}\,|\psi(t)\rangle\,|\tilde{in}\rangle \tag{156}$$

with

$$W_{B,1e} = e^{-i\sum_{\mathbf{x}\ even} H_{B,1}\tau} = e^{-iH_{B,1e}\tau} \tag{157}$$

Since our magnetic Hamiltonian consists of three parts we have to repeat the procedure with the two stators from eq.(148) and (149). We can thus create $W_{B,2e} = e^{-iH_{B,2e}\tau}$ and $W_{B,3e} = e^{-iH_{B,3e}\tau}$.

Now we move the control atoms to the odd cubes. Here we repeat the steps for the even cubes so that we can implement $W_{B,1o}, W_{B,2o}, W_{B,3o}$. This gives us then the whole magnetic time evolution.

It is important to note here that the different parts of the magnetic Hamiltonian commute with each other so that we can really implement them independently.

### 4.3.2 Gauge-Matter interactions

After expressing the four-body plaquette interaction as a sequence of two-body interactions, we want to obtain the three-body interactions of the matter with the gauge field in a similar way. Its Hamiltonian for a link emanating from the vertex $\mathbf{x}$ in direction $k$ has the form

$$H_{GM}(\mathbf{x},k) = \lambda_{GM}\psi^{\dagger}_m(\mathbf{x})U_{mn}(\mathbf{x},k)\psi_n(\mathbf{x}+\hat{k}) + h.c. \tag{158}$$

An important ingredient to split this interaction in two-body terms is the following unitary operator between the fermion at vertex $\mathbf{x}$ and the gauge field on link $(\mathbf{x},k)$:

$$U_W(\mathbf{x},k) = e^{iZ_{mn}(\mathbf{x},k)\psi^{\dagger}_m(\mathbf{x})\psi_n(\mathbf{x})} \tag{159}$$

with $Z_{mn}$ defined by eq.$(84)$. Its meaning gets more apparent if we assume the gauge group $G$ is compact; then, we obtain

$$U_W(\mathbf{x},k) = e^{i\hat{\phi}^a(\mathbf{x},k)\psi^{\dagger}_m(\mathbf{x})T^a_{mn}\psi_n(\mathbf{x})} = e^{i\hat{\phi}^a Q^a} \tag{160}$$

an interaction of the "vector potential $\hat{\phi}^a$ with the fermionic charge $Q^a$. It can therefore be interpreted as a fermionic transformation whose parameter is an operator. The idea is now to use this transformation to map a pure fermionic tunneling term into the desired gauge-matter interactions. This can be done by means of the Baker-Campbell Hausdorff formula which underlies the following relation:

$$U_W(\mathbf{x},k)\psi^{\dagger}_n U_W(\mathbf{x},k)^{\dagger} = \psi^{\dagger}_m U_{mn}(\mathbf{x},k) \tag{161}$$

Thus, defining the fermionic tunneling Hamiltonian as

$$H_t(\mathbf{x},k) = \lambda_{GM}(\psi^{\dagger}_m(\mathbf{x})\psi_m(\mathbf{x}+\hat{\mathbf{k}}) + h.c.) \tag{162}$$

allows writing the Hamiltonian $H_{GM}$ as a sequence of two-body interactions:

$$H_{GM}(\mathbf{x},k) = U_W(\mathbf{x},k)H_t(\mathbf{x},k)U^{\dagger}_W(\mathbf{x},k) \tag{163}$$

Similarly to the plaquette interactions, we have to be careful with the implementation of $H_{GM}$ since every fermion must not interact with more than one link. As every fermion is connected to six links in three dimensions we have to split up the process in six steps. We start by realizing $H_{GM,1}$ but only for even links (see Figure 6). We apply the sequence:

1. Move gauge degrees of freedom to the beginning of the link and let them interact with the fermion to obtain the unitary

$$\mathcal{U}^{\dagger}_{W,1e} = \prod_{\mathbf{x}\, even} \mathcal{U}^{\dagger}_{W}(\mathbf{x}, 1) \tag{164}$$

Then we bring the link degrees of freedom back to their original position.

2. Allow tunneling on these links for time $\tau$:

$$\mathcal{U}_{t,1e} = \prod_{\mathbf{x}\, even} \mathcal{U}_{t}(\mathbf{x}, 1) \tag{165}$$

with

$$\mathcal{U}_{t}(\mathbf{x}, k) = e^{-iH_t(\mathbf{x},k)\tau} \tag{166}$$

3. According to eq.$(163)$ we move the link degrees again to the fermion and let them interact to generate

$$\mathcal{U}_{W,1e} = \prod_{\mathbf{x}\, even} \mathcal{U}_{W}(\mathbf{x}, 1) \tag{167}$$

This gives us in total

$$\mathcal{U}_{W,1e}\mathcal{U}_{t,1e}\mathcal{U}^{\dagger}_{W,1e} = e^{-i\sum_{\mathbf{x}\, even} H_{GM}(\mathbf{x},1)\tau} = W_{GM,1e} \tag{168}$$

In the same way we can create $W_{GM,2e}, W_{GM,3e}, W_{GM,1o}, W_{GM,2o}, W_{GM,3o}$.

Using stators, there is an alternative way of realizing the gauge-matter interaction. It requires more steps but on the other hand doesn't require moving the physical degrees of freedom as in the procedure above. This might be beneficial since we have to move the controls anyway to create the plaquette interactions. The sequence goes as follows:

1. We start by letting the controls - initially placed in all even cubes in the state $|\tilde{in}\rangle = |\tilde{e}\rangle$ - interact with the the gauge links $U_1 = U(\mathbf{x}, 1)$ according to $(141)$

$$\mathcal{U}_{1e} = \prod_{\mathbf{x}\, even} \mathcal{U}_{1}(\mathbf{x}) \tag{169}$$

to create the group element stator $S_1$.

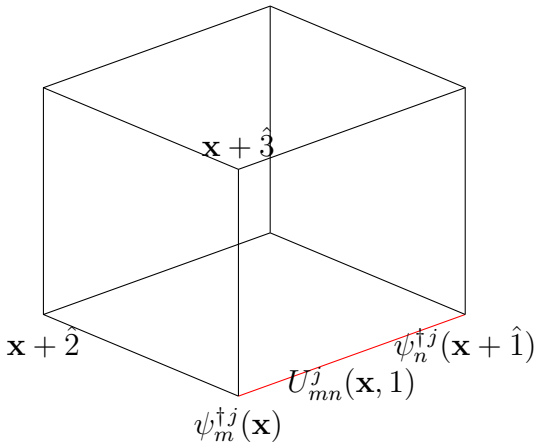


Figure 6: Link belonging to $H_{GM,1}$ for which the implementation sequence is exemplarily shown

2. Then we move the control from the link to the fermion at vertex $\mathbf{x}$ and realize the interaction

$$\tilde{\mathcal{U}}^{\dagger}_{W,1e} = \prod_{\mathbf{x}\ even} \tilde{\mathcal{U}}^{\dagger}_{W}(\mathbf{x},1) \tag{170}$$

which is the same interaction as $\mathcal{U}_W(\mathbf{x},1)$ but between the control and the fermion $\psi(\mathbf{x})$ and not between fermion and gauge link. Due to the property of the group element stator $S_1$ the interaction from the control with the fermion will be translated in an interaction between the fermion and the link.

3. Afterwards we can allow for pure tunneling between the fermions which gives rise to

$$\mathcal{U}_{t,1e} = \prod_{\mathbf{x}\ even} \mathcal{U}_{t}(\mathbf{x},1) \tag{171}$$

with

$$\mathcal{U}_t(\mathbf{x},1) = e^{-i\lambda_{GM}(\psi^{\dagger}_m(\mathbf{x})\psi_m(\mathbf{x}+\hat{1})+h.c.)\tau} \tag{172}$$

4. Following eq.(163) we have to apply $\tilde{\mathcal{U}}^{\dagger}_{W}(\mathbf{x},1)$ for all even cubes which is again realized by an interaction between the control and the fermion $\psi(\mathbf{x})$.

$$\tilde{\mathcal{U}}_{W,1e} = \prod_{\mathbf{x}\, even} \tilde{\mathcal{U}}_W(\mathbf{x}, 1) \tag{173}$$

5. Finally, we have to undo the group element stator between the auxiliary state and the gauge field on the link:

$$\mathcal{U}_{1e}^{\dagger} = \prod_{\mathbf{x}\, even} \mathcal{U}_1^{\dagger}(\mathbf{x}) \tag{174}$$

The resulting sequence is:

$$\begin{aligned}
&\mathcal{U}_{1e}^{\dagger}\tilde{\mathcal{U}}_{W,1e}\mathcal{U}_{t,1e}\tilde{\mathcal{U}}_{W,1e}^{\dagger}\mathcal{U}_{1e}\,|\psi\rangle\,|\tilde{in}\rangle \\
&= \mathcal{U}_{1e}^{\dagger}\tilde{\mathcal{U}}_{W,1e}\mathcal{U}_{t,1e}\tilde{\mathcal{U}}_{W,1e}^{\dagger}S_{1e}\,|\psi\rangle \\
&= \mathcal{U}_{1e}^{\dagger}S_{1e}\mathcal{U}_{W,1e}\mathcal{U}_{t,1e}\mathcal{U}_{W,1e}^{\dagger}\,|\psi\rangle \\
&= |\tilde{in}\rangle\, e^{-iH_{GM,1e}}\,|\psi\rangle \\
&= |\tilde{in}\rangle\, W_{GM,1e}\,|\psi\rangle
\end{aligned} \tag{175}$$

We repeat this procedure for the link $U_2$ and $U_3$ which gives us $W_{GM,2e}$ and $W_{GM,3e}$. After that we move the controls to the odd cubes and repeat the whole procedure which gives us the full gauge matter interaction.
The electric part $W_E = e^{-iH_E\tau}$ and the matter part $W_M = e^{-iH_M\tau}$ are local terms of our Hamiltonian which is why we can implement them just by acting locally on the physical degrees of freedom.
We can now write down the whole sequence for a time step $\tau$ combining commuting terms:

$$W(\tau) = W_M W_E W_{GM,3o} W_{GM,2o} W_{GM,1o} W_{GM,3e} W_{GM,2e} W_{GM,1e} W_B \tag{176}$$

## 4.4 Shaping of the lattice

Although we managed to formulate the complete Hamiltonian in terms of two-body interactions, some care has to be taken when realizing the sequence with ultracold atoms in optical lattices. The gauge-matter interactions require a pure tunneling term between neighbouring fermions, i.e. the link atoms - which are normally located between the two - are not allowed

to interact. Therefore, we do not have to construct the lattice in the usual naive way but rather to shift the link atoms away from the tunneling path between the fermions. It is important to emphasize here that in the digitization framework the fermions will only be allowed to tunnel in one direction at a time. This means that in the direction of tunneling the Wannier functions will overlap between neighbouring sites. In the other directions, however, they can be localized by increasing the lattice depth. This has to be done to an extent that it will no longer overlap with the wave function of the link atoms. Thus, we can optimize the shift of the link atoms and the intensity of the laser trapping the matter fermions.

One way to construct such a lattice would be to pick the atomic species representing our matter, gauge and auxiliary degrees of freedom and the trapping frequencies in such a way that each optical potential is visible for only one them. The lattice for the atomic species corresponding to matter is a standard cubic lattice which can be designed by three pairs of counterpropagating lasers leading to a potential of the form (choosing orthogonal polarizations):

$$V_{mat}(x,y,z) = V_{mat,x}\cos\left(\frac{2\pi}{\lambda_{mat}}x+\frac{\pi}{2}\right)^2 + V_{mat,y}\cos\left(\frac{2\pi}{\lambda_{mat}}y+\frac{\pi}{2}\right)^2 + V_{mat,z}\cos\left(\frac{2\pi}{\lambda_{mat}}z+\frac{\pi}{2}\right)^2 \tag{177}$$

The lattice spacing s is therefore $s := \frac{\lambda_{mat}}{2}$. Since we have full control over the amplitudes $V_{mat}$ by varying the laser intensity we can easily prevent any tunneling or allow tunneling in only one direction which is necessary for the simulation scheme.

But to implement tunneling for even vortices only (resp. odd) and the staggering of the fermions we need an additional potential which can unbalance even and odd lattice sites. One possibility for that is:

$$V_{stag}(x,y,z) = V_{stag}\cos\left(\frac{\pi}{2s}(x+y+z)+\phi(t)\right)^2 \tag{178}$$

This can be realized with a pair of counterpropagating lasers pointing in direction $\frac{1}{\sqrt{3}}(1,1,1)$ with a wavelength $\lambda_{stag} = \frac{4s}{\sqrt{3}} = \frac{2\lambda_{mat}}{\sqrt{3}} \approx 1.15\lambda_{mat}$. The standard configuration, where no Hamiltonian term is realized, is reached if we set $V_{stag} = 0$ and increase the intensity of the other lasers to a point where no tunneling occurs. Starting from this configuration, the individual Hamiltonians are implemented as follows:

For realizing the staggering of the fermions, we need to smoothly increase the intensity $V_{stag}$ of the staggering potential as this will create an energy difference between even and odd

minima. We then let the system evolve for some time and finally reduce $V_{stag}$ until we reach again the standard configuration.

For tunneling along x-direction at even sites we smoothly lower $V_{mat,x}$ while keeping $V_{mat,y}$ and $V_{mat,z}$ high to allow for tunneling in x-direction only and tune $\phi(t)$ to the value $\pi/4$ such that tunneling will only occur at even sites. For tunneling along y- and z-directions we apply similar procedures with $V_{mat,x}$ replaced by $V_{mat,y}$ and $V_{mat,z}$ respectively. The difference in implementing tunneling at odd instead of even lattice sites is to tune the phase $\phi(t)$ not to $\pi/4$ but $-\pi/4$. The smoothness of all this operations is required to ensure that the atoms remain in the lowest Bloch band at all times.

Constructing the lattice for the link atoms is a bit more difficult compared with two dimensions where it is just a rotated square lattice. In 3D, the spacing in all three directions is not the same anymore. Therefore, the lattice is not just a cubic one but has a more complex elementary cell. Thus, the setup becomes a bit more complicated. One solution to the problem is to use 4 pairs of counterpropagating lasers of wavelength $2s/\sqrt{3}$ along the directions $k_1 := \frac{1}{\sqrt{3}}(1,1,1)$, $k_2 := \frac{1}{\sqrt{3}}(1,-1,1)$, $k_3 := \frac{1}{\sqrt{3}}(1,1,-1)$ and $k_4 := \frac{1}{\sqrt{3}}(1,-1,-1)$. Choosing the same polarization for all of them, we can ensure constructive interference between all of them which will lead to a deepening of the optical potential. The interference terms are very beneficial because it allows for a stricter separation between the link lattice and the other lattices and therefore reduces disturbances during e.g. the tunneling of the matter fermions. The resulting potential is of the following form:

$$\begin{aligned} V_{link}(x,y,z) = V_{link,0}(&\cos(\pi(x+y+z))^2 + \cos(\pi(x-y+z))^2 \\ &+ \cos(\pi(x+y-z))^2 + \cos(\pi(x-y-z))^2 \\ &+ 2\cos(\pi(x+y+z))\cos(\pi(x-y+z)) + 2\cos(\pi(x+y+z))\cos(\pi(x+y-z)) \\ &+ 2\cos(\pi(x+y+z))\cos(\pi(x-y-z)) + 2\cos(\pi(x-y+z))\cos(\pi(x+y-z)) \\ &+ 2\cos(\pi(x-y+z))\cos(\pi(x-y-z)) + 2\cos(\pi(x+y-z))\cos(\pi(x-y-z))) \end{aligned} \tag{179}$$

As mentioned earlier, it is necessary to move the link atoms out of the tunneling path between the fermions. Thus, we move the whole link lattice along the $(1,1,1)$-direction to ensure pure tunneling along all three directions. The desired shift we want to realize is:

$$
\begin{aligned}
x &\to x + \alpha\frac{s}{\pi} \\
y &\to y + \alpha\frac{s}{\pi} \\
z &\to z + \alpha\frac{s}{\pi}
\end{aligned}
\tag{180}
$$

for some phase $\alpha$ with $-\frac{\pi}{4} \leq \alpha < \frac{\pi}{4}$. The minimum distance for the link atoms from the lattice is then $|\alpha|\frac{\sqrt{2}s}{\pi}$. The optimum value for $\alpha$ in that regard is $-\pi/4$ with a minimum distance of $s/\sqrt{2}$. Any of these shifts can be achieved by introducing phases to the pairs of lasers. They have to be $-3\alpha$ for the $k_1$-direction, $-\alpha$ for $k_2$, $-\alpha$ for $k_3$ and $\alpha$ for $k_4$. The resulting amplitudes of their standing waves are proportional to:

$$
\begin{aligned}
k_1 &: \cos(\pi(x+y+z) - 3\alpha) \\
k_2 &: \cos(\pi(x-y+z) - \alpha) \\
k_3 &: \cos(\pi(x+y-z) - \alpha) \\
k_4 &: \cos(\pi(x-y-z) + \alpha)
\end{aligned}
\tag{181}
$$

resulting in an optical potential of the form:

$$
\begin{aligned}
V_{link}(x,y,z) = V_{link,0}(&\cos(\pi(x+y+z) - 3\alpha)^2 + \cos(\pi(x-y+z) - \alpha)^2 \\
&+ \cos(\pi(x+y-z) - \alpha)^2 + \cos(\pi(x-y-z) + \alpha)^2 \\
&+ 2\cos(\pi(x+y+z) - 3\alpha)\cos(\pi(x-y+z) - \alpha) \\
&+ 2\cos(\pi(x+y+z) - 3\alpha)\cos(\pi(x+y-z) - \alpha) \\
&+ 2\cos(\pi(x+y+z) - 3\alpha)\cos(\pi(x-y-z) + \alpha) \\
&+ 2\cos(\pi(x-y+z) - \alpha)\cos(\pi(x+y-z) - \alpha) \\
&+ 2\cos(\pi(x-y+z) - \alpha)\cos(\pi(x-y-z) + \alpha) \\
&+ 2\cos(\pi(x+y-z) - \alpha)\cos(\pi(x-y-z) + \alpha))
\end{aligned}
\tag{182}
$$

The lattice for the auxiliary atoms is again a cubic lattice of spacing 2s. It can be set up in the standard way by three counterpropagating lasers of wavelength $\lambda_{aux} = 4s = 2\lambda_{mat}$. The challenge here is to do it in a way that it is moveable in all three dimensions as the auxiliary atoms mediate the interactions by atomic collisions. This can be done, for example, by tuning the phase shift of the lasers.

## 4.5 Error bounds for trotterized time evolutions

Apart from experimental errors, the previously described simulation scheme will also involve errors coming from its digital nature. In this section, we shall analyze these errors in detail. We will first derive bounds for a general Hamiltonian consisting of several terms which are implemented independently. In the second part these bounds will be applied for the case of lattice gauge theories in arbitrary dimension and with an arbitrary gauge group. Finally, we will adapt these results to some cases of relevance.

### 4.5.1 Error bounds for general trotterized time evolutions

In the following, a bound for the error between the time evolution of a quantum mechanical system with Hamiltonian $H = \sum_j H_j$ and its trotterized, approximate time evolution (in M steps) is derived, where all Hamiltonians $H_j$ are implemented independently. To approximate the real time evolution one can arrange the time evolutions of the different $H_j$ in various sequences. The focus will be on the standard trotter formula (the first order formula) and the second order formula which is still feasible for implementation. Higher order formulas, however, would require more experimental effort in the sense that the tunability of the experimental parameters would have to be more precise, and the number of operations required for a single time step would increase exponentially with the order of approximation. Therefore these higher-order formulas are neglected in the following discussion.

**First order formula** The standard approach to a trotterized time evolution $\mathcal{U}_M(t)$ is a product of all the individual time evolutions [12], i.e.

$$\mathcal{U}_M(t) = (\prod_j e^{-iH_j \frac{t}{M}})^M \tag{183}$$

The difference to the physical time evolution $\mathcal{U}(t)$ expressed in the operator norm has the form:

$$\begin{aligned} \|\mathcal{U}(t) - \mathcal{U}_M(t)\| &= \left\| e^{-itH} - (\prod_j e^{-iH_j \frac{t}{M}})^M \right\| \\ &= \left\| (e^{-i\frac{t}{M}\sum_j H_j})^M - (\prod_j e^{-iH_j \frac{t}{M}})^M \right\| \end{aligned} \tag{184}$$

Setting $g := e^{-i\frac{t}{M}\sum_j H_j}$, $h := \prod_j e^{-iH_j\frac{t}{M}}$ and using the finite geometric series one obtains:

$$\begin{aligned} \left\|g^M - h^M\right\| &= \left\|(g-h)\sum_{m=0}^{M-1} h^m g^{M-1-m}\right\| \\ &= \|g-h\|\,\left\|g^{M-1} + g^{M-2}h + ... + h^{N-1}\right\| \\ &\leq \|g-h\|\,M \end{aligned} \tag{185}$$

To find the upper bound for $\|g-h\|$ we follow [77] and use in addition the unitarity of $g$ and $h$. Defining $\lambda := -it/M$, we get:

$$\begin{aligned} \|g-h\| &= \left\|e^{-i\frac{t}{M}\sum_{j=1}^p H_j} - \prod_j e^{-iH_j\frac{t}{M}}\right\| \\ &= \left\|\int_0^\lambda dt \int_0^t ds \sum_{k=1}^{p-1} e^{\lambda H_1} e^{\lambda H_2} ... e^{\lambda H_{k-1}} e^{tH_k} e^{(t-s)\sum_{j=k+1}^p H_j} \left[\sum_{k+1}^p H_j, H_k\right] e^{s\sum_{j=k+1}^p H_j} e^{(\lambda-t)\sum_{j=k}^p H_j}\right\| \\ &\leq \frac{|\lambda|^2}{2}\sum_{k=1}^{p-1}\left\|\left[\sum_{k+1}^p H_j, H_k\right]\right\| \end{aligned} \tag{186}$$

Combining the two estimates gives us the upper bound on the trotterization error:

$$\begin{aligned} \|\mathcal{U}(t) - \mathcal{U}_M(t)\| &= \left\|e^{-itH} - (\prod_j e^{-iH_j\frac{t}{M}})^M\right\| \\ &\leq \frac{t^2}{2M}\sum_{k=1}^{p-1}\left\|\left[\sum_{j=k+1}^p H_j, H_k\right]\right\| \\ &\leq \frac{t^2}{2M}\sum_{j<k}\|[H_j, H_k]\| \end{aligned} \tag{187}$$

**Second order formula** To get a better scaling with the number of time steps we can apply trotterization sequence in reverse order after the usual trotterized time evolution [78], i.e.

$$\mathcal{U}_{2,M} = \left(e^{-iH_1\frac{t}{2M}} ... e^{-iH_{p-1}\frac{t}{2M}} e^{-iH_p\frac{t}{M}} e^{-iH_{p-1}\frac{t}{2M}} ... e^{-iH_1\frac{t}{2M}}\right)^M \tag{188}$$

From an implementation point of view this decomposition can be realized straightforwardly once we know how to obtain the sequence for the first order. Following again the proof in [77] adjusted to unitary operators, an upper bound for the trotterization error of a Hamiltonian

consisting of two terms is derived first to obtain the bound for the whole sequence recursively ($\lambda = -it/M$):

$$
\begin{aligned}
&\left\| e^{\lambda(H_1+H_2)} - e^{(\lambda/2)H_1} e^{\lambda H_2} e^{(\lambda/2)H_1} \right\| \\
=&\left\| \frac{1}{2} \int_0^\lambda dt \int_0^t ds \int_0^s du\, e^{(t/2)H_1} e^{tH_2} \right. \\
&\left. \left( \frac{1}{2} e^{(u/2)H_1} [H_1,[H_1,H_2]] e^{-(u/2)H_1} + e^{-uH_2} [H_2,[H_1,H_2]] e^{uH_2} \right) e^{(t/2)H_1} e^{(\lambda-t)(H_1+H_2)} \right\| \\
=&\frac{1}{12} \left( \|[[H_1,H_2],H_2]\| + \frac{1}{2} \|[[H_1,H_2],H_1]\| \right) =: \Delta_2(H_1,H_2)
\end{aligned}
\tag{189}
$$

By applying this estimate now recursively, we obtain an error bound for an arbitrary number p of Hamiltonians:

$$
\begin{aligned}
&\left\| e^{\lambda \sum_{j=1}^p H_j} - e^{(\lambda/2)H_1} \ldots e^{(\lambda/2)H_{p-1}} e^{\lambda H_p} e^{(\lambda/2)H_{p-1}} \ldots e^{(\lambda/2)H_1} \right\| \\
=&\left\| e^{\lambda \sum_{j=1}^p H_j} - e^{(\lambda/2)H_1} e^{\lambda \sum_{j=2}^p H_j} e^{(\lambda/2)H_1} \right. \\
&\left. + e^{(\lambda/2)H_1} e^{\lambda \sum_{j=2}^p H_j} e^{(\lambda/2)H_1} - e^{(\lambda/2)H_1} \ldots e^{(\lambda/2)H_{p-1}} e^{\lambda H_p} e^{(\lambda/2)H_{p-1}} \ldots e^{(\lambda/2)H_1} \right\| \\
\leq&\left\| e^{\lambda \sum_{j=1}^p H_j} - e^{(\lambda/2)H_1} e^{\lambda \sum_{j=2}^p H_j} e^{(\lambda/2)H_1} \right\| \\
&+ \left\| e^{(\lambda/2)H_1} \left( e^{\lambda \sum_{j=2}^p H_j} - e^{(\lambda/2)H_2} \ldots e^{(\lambda/2)H_{p-1}} e^{\lambda H_p} e^{(\lambda/2)H_{p-1}} \ldots e^{(\lambda/2)H_2} \right) e^{(\lambda/2)H_1} \right\| \\
\leq&\Delta_2 \left( \lambda H_1, \lambda \sum_{j=2}^p H_j \right) + \left\| e^{\lambda \sum_{j=2}^p H_j} - e^{(\lambda/2)H_2} \ldots e^{(\lambda/2)H_{p-1}} e^{\lambda H_p} e^{(\lambda/2)H_{p-1}} \ldots e^{(\lambda/2)H_2} \right\|
\end{aligned}
\tag{190}
$$

Thus, after recursion we arrive at the following inequality:

$$\begin{aligned}
&\left\| e^{\lambda \sum_{j=1}^{p} H_j} - e^{(\lambda/2)H_1} ... e^{(\lambda/2)H_{p-1}} e^{\lambda H_p} e^{(\lambda/2)H_{p-1}} ... e^{(\lambda/2)H_1} \right\| \\
\leq & \sum_{k=1}^{p-1} \Delta_2(\lambda H_k, \lambda(H_{k+1} + .. + H_p)) \\
= & \frac{|\lambda|^3}{12} \sum_{k=1}^{p-1} \|[[H_k, H_{k+1} + .. + H_p], H_{k+1} + .. + H_p]\| + \frac{1}{2}\|[[H_k, H_{k+1} + .. + H_p], H_k]\| \\
= & \frac{t^3}{12M^3} \sum_{k=1}^{p-1} \|[[H_k, H_{k+1} + .. + H_p], H_{k+1} + .. + H_p]\| + \frac{1}{2}\|[[H_k, H_{k+1} + .. + H_p], H_k]\|
\end{aligned} \tag{191}$$

With this inequality we can estimate the error for the full time evolution after M steps using the bound from the first order formula (see eq. (185)):

$$\begin{aligned}
\|\mathcal{U}(t) - \mathcal{U}_{2,M}(t)\| &= \left\| e^{-itH} - (e^{-iH_1 \frac{t}{2M}} ... e^{-iH_{p-1} \frac{t}{2M}} e^{-iH_p \frac{t}{M}} e^{-iH_{p-1} \frac{t}{2M}} ... e^{-iH_1 \frac{t}{2M}})^M \right\| \\
&= \left\| (e^{-i \frac{t}{M} \sum_j H_j})^M - (e^{-iH_1 \frac{t}{2M}} ... e^{-iH_{p-1} \frac{t}{2M}} e^{-iH_p \frac{t}{M}} e^{-iH_{p-1} \frac{t}{2M}} ... e^{-iH_1 \frac{t}{2M}})^M \right\| \\
&\leq M \left\| e^{-i \frac{t}{M} \sum_j H_j} - e^{-iH_1 \frac{t}{2M}} ... e^{-iH_{p-1} \frac{t}{2M}} e^{-iH_p \frac{t}{M}} e^{-iH_{p-1} \frac{t}{2M}} ... e^{-iH_1 \frac{t}{2M}} \right\| \\
&= \frac{t^3}{12M^2} \sum_{k=1}^{p-1} \|[[H_k, H_{k+1} + .. + H_p], H_{k+1} + .. + H_p]\| + \frac{1}{2} \|[[H_k, H_{k+1} + .. + H_p], H_k]\|
\end{aligned} \tag{192}$$

### 4.5.2 Error bounds for trotterized time evolutions in lattice gauge theory

Having estimated the trotterization error in general, we can now specify this bound for lattice gauge theories. This is an important task since we have to balance experimental errors and errors caused by the digitization. The experimental errors increase with the number of trotterization steps whereas the digitization errors decreases. Therefore, the more precisely we bound the trotterization errors, the less steps are required for the implementation. This would significantly reduce the experimental errors.

The Hamiltonian for a lattice gauge theory in $d$ dimensions with an arbitrary gauge group can be written in the form (see chapter 3 for details):

$$H_{LGT} = H_B + H_E + H_M + H_{GM} \tag{193}$$

with the plaquette Hamiltonian

$$H_B = \lambda_B \sum_{\text{plaquettes } p} \text{Tr}\left(U_1(\mathbf{p})U_2(\mathbf{p})U_3^\dagger(\mathbf{p})U_4^\dagger(\mathbf{p})\right) + H.c. \tag{194}$$

the electric Hamiltonian

$$H_E = \sum_{\mathbf{x},k} \sum_j f(j) \left|jmn\right\rangle \left\langle jmn\right| \tag{195}$$

the matter Hamiltonian

$$H_M = M \sum_{\mathbf{x}} (-1)^{\mathbf{x}} \psi^\dagger(\mathbf{x})\psi(\mathbf{x}) \tag{196}$$

and the gauge-matter Hamiltonian

$$H_{GM} = \lambda_{GM} \sum_{\mathbf{x},k} \psi_m^\dagger(\mathbf{x}) U_{mn}(\mathbf{x},k)\psi_n(\mathbf{x}+\hat{k}) + H.c. \tag{197}$$

Since the different parts of the Hamiltonian can not be implemented simultaneously, they are split up in the digitized simulation scheme. The parts which can be implemented in one step are the matter Hamiltonian and the electric Hamiltonian. The magnetic part has to be realized in several steps but since these parts commute with one another, we can consider the magnetic Hamiltonian as a whole. The gauge-matter interactions are implemented for each type of link independently, i.e. 2d steps in total. They, however, have a non-zero commutator which is why they need to be analyzed individually. Hence, for the computation of the trotterization error we divide the Hamiltonian into the following pieces:

$$H_{LGT} = H_B + H_E + H_M + \sum_{i=1}^{2d} H_{GM,i} \tag{198}$$

**First order formula** By inspection of eq. (187) we see that for an upper bound on the digitization error of the standard trotter formula, the commutator among all different parts of the Hamiltonian in eq. (198) has to be computed and its operator norm has to be estimated. Since the derivations are very lengthy we will refer the interested reader to the Appendix. With the commutators from there we can obtain the trotterization error for the first order formula:

$$
\begin{aligned}
&\|\mathcal{U}(t) - \mathcal{U}_M(t)\| \\
=&\left\| e^{-itH} - (\prod_j e^{-iH_j \frac{t}{M}})^M \right\| \\
\leq&\frac{t^2}{2M}\left( \| \left[H_E, H_B\right] \| + \|[H_{GM}, H_E]\| + \|H_{GM}, H_M\| + \sum_{k=1}^{2d-1}\sum_{j=k+1}^{2d} \| \left[H_{GM,j}, H_{GM,k}\right] \| \right) \\
=&\frac{t^2 d_U \mathcal{N}_{links}}{M}\left( \lambda_B\lambda_E 4(d-1)\max_j |f(j)| + \lambda_{GM}\lambda_E \max_j |f(j)| + M\lambda_{GM} + \lambda_{GM}^2 \frac{2d-1}{4} \right)
\end{aligned}
\tag{199}
$$

**Second order formula** To bound the error of the second order formula we need to calculate nested commutators according to eq.(192). The calculations of them can be found in the Appendix. With all nested commutators at hand we can estimate the total trotterization error with the second order formula:

$$
\begin{aligned}
&\|\mathcal{U}(t) - \mathcal{U}_{2,M}(t)\| \\
\leq&\frac{t^3 \mathcal{N}_{links} d_U}{6M^2}\left[ 16\lambda_E\lambda_B \max_j |f(j)|(d-1)\left( 2\lambda_E \max_j |f(j)| + \lambda_B d_U (d-1) \right) \right. \\
&+\lambda_{GM}\lambda_E \max_j |f(j)| \left( 2\lambda_{GM} d_U (2(2d-1)+1) + \lambda_E \max_j |f(j)| \right) \\
&\left. +\lambda_{GM} M\left(4d\lambda_{GM} + M\right) + \lambda_{GM}^3 (2d-1)\left( \frac{1}{3}(4d-1) + \frac{1}{2} \right) \right]
\end{aligned}
\tag{200}
$$

If we assume a cubic lattice with L lattice sites per side we can express the number of links in terms of this quantity L depending on the dimension d:

$$
\mathcal{N}_{links} = d(L-1)L^{d-1} \tag{201}
$$

Thus, the total trotterization error in terms of L is:

$$
\begin{aligned}
&\|\mathcal{U}(t) - \mathcal{U}_{2,M}(t)\| \\
\leq &\frac{t^3 d(L-1)L^{d-1}d_U}{6M^2}\left[16\lambda_E\lambda_B \max_j |f(j)|(d-1)\left(2\lambda_E \max_j |f(j)| + \lambda_B d_U(d-1)\right)\right. \\
&+\lambda_{GM}\lambda_E \max_j |f(j)|\left(2\lambda_{GM}d_U(2(2d-1)+1) + \lambda_E \max_j |f(j)|\right) \\
&\left.+\lambda_{GM}M\left(4d\lambda_{GM} + M\right) + \lambda_{GM}^3(2d-1)\left(\frac{1}{3}(4d-1) + \frac{1}{2}\right)\right]
\end{aligned} \tag{202}
$$

It is noteworthy that the errors scale with system size and not with higher powers of the system size which might be the case in a more general setting. The reason for that is that the interactions are local. This is an indicator that the bounds are reasonable.

### 4.5.3 Special cases

In the last section, we want to apply the derived bounds from above to some special cases. The first case is dimension two where the formula reduces to:

$$
\begin{aligned}
\|\mathcal{U}(t) - \mathcal{U}_{2,M}(t)\| \leq \frac{t^3(L-1)Ld_U}{3M^2}&\left(16\lambda_E\lambda_B \max_j |f(j)|\{2\lambda_E \max_j |f(j)| + \lambda_B d_U\}\right. \\
&+\lambda_{GM}\lambda_E \max_j |f(j)|\{14\lambda_{GM}d_U + \lambda_E \max_j |f(j)|\} \\
&\left.+\lambda_{GM}M\{8\lambda_{GM} + M\} + \frac{17}{2}\lambda_{GM}^3\right)
\end{aligned} \tag{203}
$$

If we also specify the gauge group the error bound will only depend on the coupling constant and the volume of our lattice. One important gauge group for quantum simulations of lattice gauge theories is $\mathbb{Z}_N$ as a truncation of $U(1)$. For finite N the electric Hamiltonian of $\mathbb{Z}_N$ lattice gauge theory has the form

$$
H_E = \lambda_E \sum_{x,k} 1 - P(x,k) - P^\dagger(x,k) \tag{204}
$$

where the P operator is unitary. Therefore, we can set $\max_j |f(j)| = 2$ (neglecting the constant term). Since the gauge group is abelian the dimension of the representation is $d_U = 1$. The error bound then reduces to:

$$\begin{aligned}\|\mathcal{U}(t)-\mathcal{U}_{2,M}(t)\| \leq \frac{t^3(L-1)L}{3M^2}\,(&32\lambda_E\lambda_B\{4\lambda_E+\lambda_B\}\\ &+\lambda_{GM}\lambda_E 4\{7\lambda_{GM}+\lambda_E\}\\ &+\lambda_{GM}M\{8\lambda_{GM}+M\}+\frac{17}{2}\lambda_{GM}^3\Big)\end{aligned} \tag{205}$$

The same can be done for the dihedral groups $D_N$. Their significance comes from the approximation of the orthogonal group O(2) in the limit $N \to \infty$. In chapter 3 it was shown that the electric part of the Hamiltonian of $D_N$ has a similar form as the one corresponding to $\mathbb{Z}_N$ and we can set $\max_j |f(j)| = 2$. The difference for the estimate is that the typical representation for the $U$-operators under the gauge group $D_N$ is two dimensional ($d_U = 2$). The resulting error bound is then:

$$\begin{aligned}|\mathcal{U}(t)-\mathcal{U}_{2,M}(t)\| \leq \frac{2t^3(L-1)L}{3M^2}\,(&64\lambda_E\lambda_B\{2\lambda_E+\lambda_B\}\\ &+\lambda_{GM}\lambda_E 4\{14\lambda_{GM}+\lambda_E\}\\ &+\lambda_{GM}M\{8\lambda_{GM}+M\}+\frac{17}{2}\lambda_{GM}^3\Big)\end{aligned} \tag{206}$$

The same error bounds can be derived in three dimensions. For $\mathbb{Z}_N$ one obtains:

$$\begin{aligned}\|\mathcal{U}(t)-\mathcal{U}_{2,M}(t)\| \leq \frac{t^3(L-1)L^2}{M^2}\,(&64\lambda_E\lambda_B\{2\lambda_E+\lambda_B\}\\ &+2\lambda_{GM}\lambda_E\{11\lambda_{GM}+\lambda_E\}\\ &+\lambda_{GM}M\{6\lambda_{GM}+\frac{1}{2}M\}+\frac{125}{12}\lambda_{GM}^3\Big)\end{aligned} \tag{207}$$

For the dihedral group $D_N$ one obtains:

$$\begin{aligned}\|\mathcal{U}(t)-\mathcal{U}_{2,M}(t)\| \leq \frac{2t^3(L-1)L^2}{M^2}\,(&128\lambda_E\lambda_B\{\lambda_E+\lambda_B\}\\ &+2\lambda_{GM}\lambda_E\{22\lambda_{GM}+\lambda_E\}\\ &+\lambda_{GM}M\{6\lambda_{GM}+\frac{1}{2}M\}+\frac{125}{12}\lambda_{GM}^3\Big)\end{aligned} \tag{208}$$

# 5 Implementation of lattice gauge theories with a dihedral gauge group

Quantum simulations of lattice gauge theories with dynamical fermions and gauge fields in more than 1+1 dimensions is a difficult task. One of the reasons being that the plaquette interactions only come into play in dimension 2 and higher. Thus, we propose a way to implement one of the simpler non-abelian gauge groups, the dihedral group $D_N$ which converges in the large-N limit to O(2), with ultracold atoms. Our scheme is in principle applicable to all dihedral groups but the focus is put on the simplest non-abelian one which is $D_6$. It is isomorphic to the group of permutations $S_3$. The underlying idea is to use a product Hilbert space to represent the gauge fields residing on the links. The same applies for the auxiliary Hilbert space. In practice this can be done by using two atoms, e.g. two different hyperfine levels of the same atomic species. This drastically reduces the number of levels in every system. If $m$ levels in the first and $n$ levels in the second system are required to represent a certain state, a single system would need $m \times n$ levels.

## 5.1 Simulating system

Focusing again on the lattice gauge theory of $D_6$, as explained in section 3, we first want to discuss the system we will use as a platform to perform the quantum simulation. The proposed implementation can be carried out in either two or three dimensions. In both cases the lattice is constructed by lasers generating optical potentials and trapping different atomic species. For the exact construction in two dimensions we refer to [42], for the construction in three dimensions we refer to the general algorithm presented in chapter 4. In the following we will concentrate on the latter and built the implementation upon this scheme. The two dimensional version can also easily be derived from that. The most important ingredients, the atomic species, represent the dynamical fields of our theory. For the matter fields it is crucial to use fermionic atoms to obtain the correct commutation relations. Since the dimension of the only faithful representation of the dihedral groups is two, and we thus have two fermionic d.o.f. $\psi_1$ and $\psi_2$, it is very natural to choose an $F = 1/2$ hyperfine level to describe the matter fields. This is an advantage compared to the abelian case where only one fermionic d.o.f. exists and one has to make sure that other $m_F$ states in the same hyperfine level do not disturb the simulation. The fermionic operators $\psi_1$ and $\psi_2$ are associated with the $F = 1/2$ multiplet in the following way:

$$\begin{aligned}\psi_1 &\to |F = 1/2; m_F = 1/2\rangle \\ \psi_2 &\to |F = 1/2; m_F = -1/2\rangle\end{aligned} \tag{209}$$

To simulate the gauge field and auxiliary degrees of freedom we will use, as mentioned above, the tensor product of two systems. The reason for that becomes clear when looking at the structure of their Hilbert space. We denote the dihedral group $D_6$ as

$$D_6 = \{(p, m)|p \in \{0, 1, 2\}, m \in \{0, 1\}\} \tag{210}$$

where $p$ corresponds to rotations and $m$ to reflections (for a detailed discussion of the group properties see section 3). Using the group element representation basis, the Hilbert space of the gauge fields then exhibits the product structure:

$$\mathcal{H}_{control} = \mathcal{H}_{link} = \bigoplus_{p,m} span\{|p, m\rangle\} \cong \bigoplus_{p=0}^{2} span\{|p\rangle\} \otimes \bigoplus_{m=0}^{1} span\{|m\rangle\} =: \mathcal{H}_3 \otimes \mathcal{H}_2 \tag{211}$$

This group structure already suggests to use a tensor product of a three-level and a two-level system to represent the gauge field d.o.f. and the auxiliary d.o.f.. One possible choice is atoms in the $F_3 = 1$ hyperfine multiplet (the index 3 will label the three-level system) and on the other hand atoms in the $F_2 = 1/2$ multiplet (the index 2 will label the three-level system), but in principle any three-level resp. two-level system can be chosen. We identify:

$$\begin{aligned}|p = 0\rangle &\equiv |F_3 = 1, m_F = 0\rangle \\ |p = 1\rangle &\equiv |F_3 = 1, m_F = 1\rangle \\ |p = 2\rangle &\equiv |F_3 = 1, m_F = -1\rangle \\ |m = 0\rangle &\equiv |F_2 = \frac{1}{2}, m_F = \frac{1}{2}\rangle \\ |m = 1\rangle &\equiv |F_2 = \frac{1}{2}, m_F = -\frac{1}{2}\rangle\end{aligned} \tag{212}$$

Every state of the Hilbert space on the link can be obtained as a tensor product of the two multiplets, e.g. $|p = 1, m = 1\rangle = |F_3 = 1, m_F = 1\rangle \otimes |F_2 = \frac{1}{2}, m_F = -\frac{1}{2}\rangle$. The corresponding creation operators on some link $(\mathbf{x}, k)$ are described by $a^\dagger_{m_F}(\mathbf{x}, k)$ with $m_F = -1, 0, 1$ for the three-level system and $c^\dagger_{m_F}(\mathbf{x}, k)$ with $m_F = -1/2, 1/2$ for the two-level system.
Since the Hilbert space structure for the link and auxiliary d.o.f. is the same, we can use another

atomic species in the same hyperfine multiplets to simulate the controls. To distinguish the two species we will denote all the auxiliary states with a tilde, i.e. the three level states by $|\tilde{p}\rangle$ and the two-level states by $|\tilde{m}\rangle$. Their creation operators are called $b^\dagger_{m_F}(\mathbf{x}, k)$ with $m_F = -1, 0, 1$ for the three-level system and $d^\dagger_{m_F}(\mathbf{x}, k)$ with $m_F = -1/2, 1/2$ for the two-level system. The resulting setup - for convenience in two dimensions - is depicted in Fig. 7.

It will turn out useful to define unitary operators $P_3, Q_3$ and $P_2, Q_2$ acting on the three-level respectively two-level system of the link Hilbert space. The same operators acting on the auxiliary Hilbert space will be denoted with an additional tilde, i.e. $\tilde{P}_3, \tilde{Q}_3$ and $\tilde{P}_2, \tilde{Q}_2$. They are defined as:

$$\begin{aligned} P_3 |p\rangle &= e^{i\frac{2\pi}{3}p} |p\rangle \\ Q_3 |p\rangle &= |p+1\rangle \, (cyclically) \\ P_2 |m\rangle &= e^{i\pi m} |m\rangle = (-1)^m |m\rangle \\ Q_2 |m\rangle &= |m+1\rangle \, (cyclically) \end{aligned} \tag{213}$$

We see that the operators acting on the three-level system fulfill the $\mathbb{Z}_3$ algebra whereas the operators acting on the two-level system fulfill the $\mathbb{Z}_2$ algebra. All interactions between the constituents of the simulating system from above are mediated by two-body scattering (for a detailed discussion see chapter 2). The only additional ingredient we have to add to the experimental setup is a magnetic field. The necessity for that will become clear during the implementation with the scattering term as we will need to preserve $m_F$ for both atoms. This can be achieved by lifting the degeneracy for the hyperfine multiplets in different ways such that a transition changing $m_F$ will cost energy. A natural way to do that is by introducing a uniform magnetic field corresponding to the magnetic Hamiltonian (Zeeman shift):

$$H_Z = \mu_B g_F m_F B \tag{214}$$

where $\mu_B$ is the Bohr magneton and $g_F$ the hyperfine Lande factor. Since the energy splitting is supposed to be different for the two atoms we need to choose species with different Lande factor. Another possible approach to realize the energy splitting is to address single species which however requires alternative methods (e.g. use of AC Stark effect).

At some points of the implementation we also need to spatially separate the different $m_F$ levels which can be achieved by applying a magnetic field gradient, for example in z-direction: $\mathbf{B}(z) = bz\hat{e}_z$. Since the magnetic potential is not uniform anymore the different $m_F$ levels will

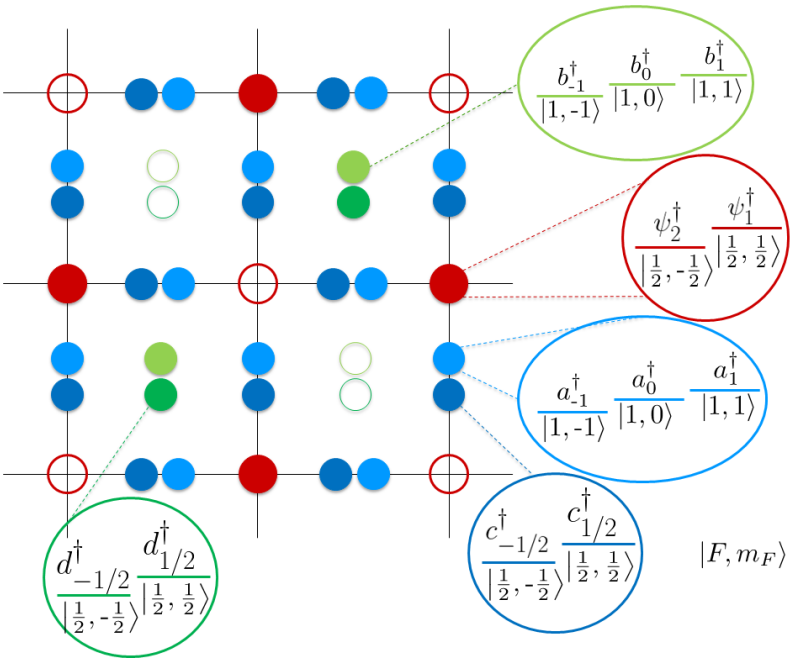


Figure 7: The $D_6$ simulating system consists of one atomic species on the vertices representing the matter (red circles) and two for each the gauge field on the links and the controls located at the centers of every second plaquette (resp. cube in three dimensions).

experience forces, pointing in different directions for $m_F$ levels with opposite sign. The overall harmonic trapping potential on the other hand will lead to an equilibrium position within the harmonic well. By choosing the Lande factors of the atomic species and tuning the magnetic field gradient one can then tailor the scattering interactions in an $m_F$-dependent way due to fully controlling the overlap between the atomic wave functions. In the case of two atoms in the $F = 1$ multiplet ($F_1 = F_2 = 1$) and a sufficient spatial separation, one could create terms only containing the $m_{F,1} = 0$ and $m_{F,2}$ states. One could also choose an $F = 1/2$ multiplet with a very small Lande factor and an $F = 1$ multiplet with a large Lande factor so that only the $m_F = 0$ component would interact with the two-level system.

Similar manipulations using a magnetic field gradient have already been employed. A selective trapping of the $m_F = 0$ component has already been accomplished in experiment while the other components were pushed out of the trap [79]. Weaker gradients should therefore enable a spatial $m_F$-splitting inside the trap.

## 5.2 Implementation of the digital simulation

With the presented simulating system and the necessary background from the previous chapters we can finally implement the digital simulation scheme for the lattice gauge theory of $D_6$.

### 5.2.1 Standard configuration of the lattice

Before starting the simulation we should define the starting configuration of our simulation system. As already explained in chapter 3, the standard configuration for the lattice is reached if the staggering potential $V_{stag}(x, y, z)$ for the matter fields is switched off and the optical potential $V_{mat}(x, y, z)$ is sufficiently deep such that no tunneling occurs. Furthermore, the potentials $V_{link}(x, y, z)$ and $V_{aux}(x, y, z)$ need to have deep minima as well preventing any tunneling. For the latter the potential barriers between the different minima will be kept high throughout the whole implementation since we only need to allow for tunneling of the matter fermions at some point.

The loading of the atoms proceeds as follows: The auxiliary and link lattice are loaded with one atom per minimum. The initial states of the auxiliary atoms in the group representation basis are the ones corresponding to the neutral element, i.e $|\tilde{in}\rangle = |\tilde{e}\rangle$. This means we have to prepare the state $|\tilde{F}_3 = 1; \tilde{m}_F = 0\rangle$ for the three-level system and $|\tilde{F}_2 = 1/2; \tilde{m}_F = 1/2\rangle$ for the two level system. The link atoms are prepared in the singlet state $|000\rangle$ (see eq.(82)) corresponding to the trivial representation. Thus, in terms of the hyperfine states representing the group element basis, this translates as an equal superposition of all possible states. All the atoms are cooled to a degree that they will certainly occupy the motional ground state with energies $E_{0,aux}$ and $E_{0,link}$.

For the matter fermions we need to achieve half-filling with empty even minima and fully occupied odd minima (energy $E_{0,mat}$) for the reasons described below. As we are dealing with the non-abelian gauge $D_6$, the non-trivial representation of the matter fields under the gauge group is two-dimensional. This means that we have to prepare the fermionic species in the $|F = 1/2; m_F = 1/2\rangle$ state for the first component and in the $|F = 1/2; m_F = -1/2\rangle$ state for the second component and put one of each in an odd minima. This will give us the gauge-invariant Dirac sea state $|D\rangle$ (see section 3.3.1). Together with the $|0\rangle$ state of the gauge fields we obtain the global singlet state from eq. (88).

As mentioned in the previous section, we also need to introduce a uniform magnetic field (or an AC Stark effect) to lift the degeneracy of the ground state. and induce energy splittings

($\Delta E_{aux}$,$\Delta E_{link}$ and $\Delta E_{mat}$ respectively) between the different $m_F$ components.
We can finally define the non-interacting Hamiltonian $H_0$ which will be present throughout the whole implementation:

$$\begin{aligned} H_0 &= \sum_{\mathbf{x}} (E_{0,mat} + \Delta E_{mat})\, \psi_1^\dagger(\mathbf{x})\psi_1(\mathbf{x}) + (E_{0,mat} - \Delta E_{mat})\, \psi_2^\dagger(\mathbf{x})\psi_2(\mathbf{x}) \\ &= \sum_{\mathbf{x},k} \sum_{m_F} (E_{0,link,a} + \Delta E_{link,a}\, m_F)\, a_{m_F}^\dagger(\mathbf{x},k) a_{m_F}(\mathbf{x},k) \\ &= \sum_{\mathbf{x},k} \sum_{m_F} (E_{0,link,c} + \Delta E_{link,c}\, m_F)\, c_{m_F}^\dagger(\mathbf{x},k) c_{m_F}(\mathbf{x},k) \\ &= \sum_{\mathbf{x}} \sum_{m_F} (E_{0,aux,b} + \Delta E_{aux,b}\, m_F)\, b_{m_F}^\dagger(\mathbf{x}) b_{m_F}(\mathbf{x}) \\ &= \sum_{\mathbf{x}} \sum_{m_F} (E_{0,aux,d} + \Delta E_{aux,d}\, m_F)\, d_{m_F}^\dagger(\mathbf{x}) d_{m_F}(\mathbf{x}) \end{aligned} \tag{215}$$

All parts of the digital simulations are added on top of $H_0$. To recover the desired Hamiltonian H we move to an interaction picture , i.e. we will work in a rotating frame with respect to $H_0$ and make use of the rotating wave approximation.

### 5.2.2 The mass Hamiltonian

The mass Hamiltonian in three dimensions takes the form

$$H_M = M \sum_{\mathbf{x}} (-1)^{x_1+x_2+x_3} \psi^\dagger(\mathbf{x})\psi(\mathbf{x}) \tag{216}$$

with $\psi^\dagger(\mathbf{x})\psi(\mathbf{x}) = \psi_1^\dagger(\mathbf{x})\psi_1(\mathbf{x}) + \psi_2^\dagger(\mathbf{x})\psi_2(\mathbf{x})$. Thus, the corresponding time evolution for a time step $\tau$ is:

$$W_M = e^{-iH_M\tau} \tag{217}$$

The implementation of this term can be achieved by smoothly increasing the staggering potential $V_{stag}(x,y,z)$, as described in section 5.4. This allows to raise the energy of the even minima by an amount $M_{even}$ resulting in the Hamiltonian

$$H'_M = M_{even} \sum_{\mathbf{x}} (1 + (-1)^{x_1+x_2+x_3}) \psi^\dagger(\mathbf{x})\psi(\mathbf{x}) \tag{218}$$

If we realize this Hamiltonian for a time $\frac{M_{even}}{M}\tau$ we obtain the desired unitary evolution $W_M$, up to an irrelevant global phase.

### 5.2.3 The stator

For the creation of the plaquette interactions and the gauge-matter interactions it is required to construct the group element stator (see chapter 4 for a detailed discussion):

$$S = \int dg \, |g\rangle \langle g| \otimes |\tilde{g}\rangle \tag{219}$$

where $\sim$ denotes the auxiliary system and the part without the $\sim$ the physical system. If we want to create this stator for a certain link $i$ from the state corresponding to the neutral element $|\tilde{in}\rangle = |\tilde{e}\rangle$ we have to apply

$$\mathcal{U}_i = \int dg \, |g\rangle_i \langle g|_i \otimes \tilde{\Theta}^\dagger_g \tag{220}$$

Specifying this equation to the gauge group $D_6$ we obtain the following interaction between the d.o.f. on each link and the ones of the control:

$$\begin{aligned}
\mathcal{U}_i \, |\tilde{in}\rangle &= \sum_p \sum_m |p,m\rangle_i \langle p,m|_i \otimes \tilde{\Theta}^\dagger_{p,m} \, |\tilde{0},\tilde{0}\rangle \\
&= \sum_p \sum_m |p,m\rangle_i \langle p,m|_i \otimes |\tilde{p} + (-1)^{\tilde{m}} 0, \tilde{m}\rangle \\
&= \sum_p \sum_m |p,m\rangle_i \langle p,m|_i \otimes |\tilde{p},\tilde{m}\rangle \\
&= \sum_p \sum_m |p,m\rangle_i \langle p,m|_i \otimes \tilde{Q}_3^p \tilde{Q}_2^m \, |\tilde{0},\tilde{0}\rangle \\
&= \tilde{Q}_3^{\hat{p}} \tilde{Q}_2^{\hat{m}} \, |\tilde{0},\tilde{0}\rangle
\end{aligned} \tag{221}$$

By choosing $|\tilde{0},\tilde{0}\rangle$ as our initial state the creation of the stator reduces to an interaction between the three-level systems and an interaction between the two-level systems which can be implemented in parallel. They can be written as

$$\mathcal{U}_3 := \tilde{Q}_3^{\hat{p}} = e^{-i\frac{3}{2\pi}\log \tilde{Q}_3 \log P_3} = \tilde{V}_3^\dagger \mathcal{U}_3' \tilde{V}_3 \tag{222}$$

with $\tilde{V}_3$ mapping from the Q-basis into the P-basis and

$$\mathcal{U}_3' = e^{-i\frac{3}{2\pi}\log\tilde{P}_3\log P_3} \tag{223}$$

The mapping to the P-basis is required since this will allow to express the interaction in terms of the angular momentum operator.
Respectively for the two-level systems:

$$\mathcal{U}_2 := \tilde{Q}_2^{\hat{m}} = e^{-i\frac{1}{\pi}\log\tilde{Q}_2\log P_2} = \tilde{V}_2^{\dagger}\mathcal{U}_2'\tilde{V}_2 \tag{224}$$

with

$$\mathcal{U}_2' = e^{-i\frac{1}{\pi}\log\tilde{P}_2\log P_2} \tag{225}$$

The basis transformations $\tilde{V}_3$ and $\tilde{V}_2$ are local interactions on the auxiliary atoms that can be implemented by adressing them with optical/RF fields. Thus, we express this unitary transformation for all auxiliary atoms, $\tilde{V}_{3,all}$, as a time evolution under a Hamiltonian, denoted $\tilde{H}_{3,all}$:

$$\begin{aligned}\tilde{H}_{3,all} = \sum_{\mathbf{x}} \Big[ &(\sqrt{3}-1)b_0^{\dagger}(\mathbf{x})b_0(\mathbf{x}) + \frac{1}{2}(1+2\sqrt{3})b_{\pm1}^{\dagger}(\mathbf{x})b_{\pm1}(\mathbf{x}) \\ &+ \frac{1}{2}b_1^{\dagger}(\mathbf{x})b_{-1}(\mathbf{x}) - b_1^{\dagger}(\mathbf{x})b_0(\mathbf{x}) - b_{-1}^{\dagger}(\mathbf{x})b_0(\mathbf{x}) + H.c.\Big]\end{aligned} \tag{226}$$

The basis transformation from the Q-basis to the P-basis is then generated by $V_{3,all} = e^{-i\tilde{H}_{3,all}\frac{\pi}{2\sqrt{3}}}$.
The similar transformation for the two-level system is much simpler, as it is just a Hadamard transform. Applied to all atoms it takes the form:

$$\tilde{V}_{2,all} = \frac{1}{\sqrt{2}}(\tilde{\sigma}_{x,all} + \tilde{\sigma}_{z,all}) = e^{i\frac{\pi}{2\sqrt{2}}\sum_{\mathbf{x}}(\tilde{\sigma}_x+\tilde{\sigma}_z)} \tag{227}$$

The more difficult part is the implementation of $\mathcal{U}_3'$ and $\mathcal{U}_2'$. Starting with $\mathcal{U}_3'$, we first express the $P_3$-operators in terms of the z-component of the hyperfine angular momentum operator $F_{z,3}$. The action of $log(P_3)$ on the $F = 1$ hyperfine angular momentum states $|F_3 = 1; m_F = 1\rangle$, $|F_3 = 1; m_F = 0\rangle$, $|F_3 = 1; m_F = -1\rangle$ - which represent our three-level system - can be expressed in their basis:

$$\log P_3 = \log \begin{pmatrix} e^{i\frac{2\pi}{3}} & 0 & 0 \\ 0 & 1 & 0 \\ 0 & 0 & e^{-i\frac{2\pi}{3}} \end{pmatrix} = i\frac{2\pi}{3} \begin{pmatrix} 1 & 0 & 0 \\ 0 & 0 & 0 \\ 0 & 0 & -1 \end{pmatrix} = i\frac{2\pi}{3} F_{z,3} \tag{228}$$

We can therefore write the $\mathcal{U}_3'$ - interaction in terms of the z-components of the hyperfine angular momentum:

$$\mathcal{U}_3' = e^{i\frac{2\pi}{3}\tilde{F}_{z,3}F_{z,3}} \tag{229}$$

We want to use two-body scattering processes to implement this interaction. For the two $F = 1$ multiplets of the auxiliary and the link atom, the unitary describing the scattering process takes the form (for details see chapter 2):

$$\mathcal{U}_{scat} = e^{-i\alpha\sum_{j=0}^{2} g_j(\tilde{F}_3 \cdot F_3)^j} \tag{230}$$

where $\alpha = \frac{2\pi}{\mu}\int_0^{T_0} \mathcal{O}(t)dt$ is the Wannier functions' overlap integrated over the whole interaction duration $T_0$. To make this equal to eq. (229) we need to make use of the magnetic field we introduced in the last section. This comes from the appearance of $\tilde{F}_{3,x}F_{3,x}$ and $\tilde{F}_{3,y}F_{3,y}$ terms that involve transitions between different $m_F$ and $\tilde{m}_F$ values. To suppress this processes, we can give them an energy penalty by introducing a magnetic field, lifting the degeneracy of the hyperfine states (Zeeman splitting). This adds an energy term $E(m_F) = \mathcal{E}m_F$ to the Hamiltonian of the link atoms and to the Hamiltonian of the auxiliary atoms, $\tilde{E}(\tilde{m}_F) = \tilde{\mathcal{E}}\tilde{m}_F$. Since the atomic collision conserves the sum of the z-components of the angular momentum, $m_F + \tilde{m}_F$, the transition $m_F \to m_F'$ is characterized by an energy cost $(m_F' - m_F)(\mathcal{E} - \tilde{\mathcal{E}})$. If we require $\mathcal{E} \neq \tilde{\mathcal{E}}$, the scattering process will conserve both $m_F$ and $\tilde{m}_F$. Enforcing this constraint on eq.(230), gives us

$$\mathcal{U}_{scat} = e^{-i\alpha(\eta_0 N_{tot}\tilde{N}_{tot} + \eta_1 F_{z,3}\tilde{F}_{z,3} + \eta_2 \tilde{N}_0 N_0)} \tag{231}$$

where $\eta_0 = g_0 + \frac{3}{2}g_2, \eta_1 = g_1 - \frac{1}{2}g_2, \eta_2 = 3g_2, N_{tot} = \sum_{m_F} a_{m_F}^\dagger a_{m_F}, \tilde{N}_{tot} = \sum_{m_F} b_{m_F}^\dagger b_{m_F}, N_0 = a_0^\dagger a_0$ and $\tilde{N}_0 = b_0^\dagger b_0$. For the exact values of the $g$'s in terms of the scattering lengths see section 2.5.

The shaping of the lattice is done in a way that no tunneling in the link and the auxiliary lattice is possible. As every well is loaded with one atom we can set $N_{tot} = \tilde{N}_{tot} = 1$. Hence, the first term in the exponential gives only rise to a global phase. When tuning the parameter $\alpha$

we have to be a bit careful since the overlap integral has to be positive. On the other hand, without further specification (e.g. the atomic species) we can not tell whether the parameters $\eta$ are positive or negative. We therefore set $\alpha = -\frac{2\pi}{3\eta_1}$ under the assumption that $\eta_1$ is negative. If it is positive we set $\alpha = \frac{2\pi}{3\eta_1}$ which would give us the conjugate $\mathcal{U}_3'^{\dagger}$ by following the same procedure. Its conjugate $\mathcal{U}_3'$ could then be obtained by doing a flipping operation in the exact same way as explained later on for the case of taking the conjugate of $\mathcal{U}_3'$. Focusing now on the case $\eta_1 < 0$ we get

$$\mathcal{U}_{scat} = e^{i\frac{2\pi}{3}(F_{z,3}\tilde{F}_{z,3} + \frac{\eta_2}{\eta_1}\tilde{N}_0 N_0)} \tag{232}$$

up to a global phase. To eliminate the undesired second term in the exponential we apply a magnetic field gradient as explained in section 5.1 so that a spatial separation between the different $m_F$ -respectively $\tilde{m}_F$ - components occurs. This allows to shape the atomic wave function in a way that only the $m_F = 0$ and $\tilde{m}_F = 0$ components will overlap. However, we have to take into account that the different levels of the hyperfine multiplet will acquire relative phases during the time evolution under a magnetic field gradient. This can be remedied by switching the sign of the magnetic field and repeating the process (this technique will be applied for all future scattering events of this kind). All relative phases then cancel each other and we end up with a scattering term of the form:

$$\mathcal{V}_{scat} = e^{-i\beta N_0 \tilde{N}_0} \tag{233}$$

We tune overlap and interacting time such that $\beta = 2\pi(\kappa + \frac{\eta_2}{3\eta_1}) > 0 (\kappa \in \mathbb{Z}$ can be chosen as the smallest allowed integer). Combining it with $\mathcal{U}_{scat}$ we get

$$\mathcal{V}_{scat}\mathcal{U}_{scat} = e^{i\frac{2\pi}{3}F_{z,3}\tilde{F}_{z,3}}\, e^{-i2\pi\kappa\tilde{N}_0 N_0} = e^{i\frac{2\pi}{3}F_{z,3}\tilde{F}_{z,3}} = \mathcal{U}_3' \tag{234}$$

where in the last step we used the fact that since $\kappa \in \mathbb{Z}$ the second unitary has no effect whatsoever. We finally found a way to create the stator but we also need to explain how to undo the stator, i.e. create $\mathcal{U}_3'^{\dagger}$. One way of implementing it is by flipping locally the $\tilde{m}_F = 1$ and $\tilde{m}_F = -1$ levels of the auxiliary atoms, which is equivalent to mapping $\tilde{F}_{z,3}$ into $-\tilde{F}_{z,3}$. It can be achieved by addressing the control atoms with lasers or RF light. Denoting the spin flipping by $\tilde{V}_{F,3}$ we can obtain $\mathcal{U}_3'^{\dagger}$ by the sequence (again ignoring global phases):

$$\mathcal{V}_{scat}\tilde{V}_{F,3}\mathcal{U}_{scat}\tilde{V}_{F,3}^{\dagger} = e^{-i\beta N_0\tilde{N}_0}e^{i\frac{2\pi}{3}(-\tilde{F}_{z,3}F_{z,3}+\frac{\eta_2}{\eta_1}\tilde{N}_0N_0)} = e^{-i\frac{2\pi}{3}F_{z,3}\tilde{F}_{z,3}} = \mathcal{U}_3'^{\dagger} \tag{235}$$

In a similar fashion we want to create now the unitary operator $\mathcal{U}_2'$ from two-body scattering. We first write $\mathcal{U}_2'$ in terms of the z-component of the angular momentum operator $F_{z,2}$. The action of $\log P_2$ on the two level system - consisting of $|F_2 = 1/2; m_F = 1/2\rangle$ and $|F_2 = 1/2; m_F = -1/2\rangle$ - is given by:

$$\log P_2 = \log \sigma_z = \log\left(e^{i\frac{\pi}{2}(1-\sigma_z)}\right) = i\frac{\pi}{2}(1-\sigma_z) = i\frac{\pi}{2}(1-2F_{z,2}) \tag{236}$$

Hence, $\mathcal{U}_2'$ can be written in the form:

$$\mathcal{U}_2' = e^{-i\frac{1}{\pi}(i\frac{\pi}{2})^2(1-\sigma_z)(1-\tilde{\sigma}_z)} = e^{i\frac{\pi}{4}}e^{-i\frac{\pi}{4}\sigma_z}e^{-i\frac{\pi}{4}\tilde{\sigma}_z}e^{i\pi F_{z,2}\tilde{F}_{z,2}} \tag{237}$$

The first term is a global phase and can be ignored. The second and third term are local operations which can be implemented by adressing the respective atoms by external fields. The more difficult part is the two-body-interaction between the auxiliary and the link atom. It will be realized by an atomic collision between the two. Since both are in the $F = 1/2$ multiplet the total angular momentum can only take two values ($F_{tot} = 0$ or $F_{tot} = 1$) which simplifies the expression. The corresponding scattering term $\mathcal{U}_{scat,2}$ is

$$\mathcal{U}_{scat,2} = e^{-i\gamma(g_0N_{tot}\tilde{N}_{tot}+g_1F_2\cdot\tilde{F}_2)} \tag{238}$$

where $\gamma$ is again the Wannier functions' overlap integrated over the time of interaction. As for the three-level system, the different energy splittings due to the magnetic field will conserve the $m_F$ and $\tilde{m}_F$ values. Moreover, tunneling is forbidden for both lattices so that $N_{tot} = \tilde{N}_{tot} = 1$ and we can ignore the resulting global phase. We end up with the constrained scattering term:

$$\mathcal{U}_{scat,2} = e^{-i\gamma g_1F_{z,2}\cdot\tilde{F}_{z,2}} \tag{239}$$

If we tune the overlap and interaction time such that $\gamma = -\frac{\pi}{g_1}$, we obtain the desired two-body interaction of $\mathcal{U}_2'$. We assumed again that the parameter $g_1$ is negative. If it is positive, we can choose $\gamma = \frac{\pi}{g_1}$ and finally get $\mathcal{U}_2'^{\dagger}$ (if we take the conjugate of the local terms as well). Either way, we would then need to implement the conjugate which is done again by a spin flip of the $\tilde{m}_F = 1/2$ and $\tilde{m}_F = -1/2$ state, denoted as $V_{F,2}$. For the $g_1 < 0$ case the conjugate $\mathcal{U}_2'^{\dagger}$ is obtained by the sequence

$$e^{i\frac{\pi}{4}\tilde{\sigma}_z}e^{i\frac{\pi}{4}\sigma_z}\tilde{V}_{F,2}\mathcal{U}_{scat,2}\tilde{V}_{F,2}^{\dagger} = e^{i\frac{\pi}{4}\tilde{\sigma}_z}e^{i\frac{\pi}{4}\sigma_z}e^{-i\pi F_{z,2}\tilde{F}_{z,2}} = \mathcal{U}_2'^{\dagger} \tag{240}$$

### 5.2.4 Plaquette interaction

Knowing how to construct the stator, the implementation of the plaquette interaction is straightforward. Since we have to split them in different parts (see chapter 4), we start with $H_{B,1e}$, the type 1 plaquettes of the even cubes, where the auxiliary atoms are placed in the standard configuration. We follow the three steps of the algorithm given in section 4.3.1:

1. We create the stator for the plaquettes. It can be constructed out of the unitaries $\mathcal{U}_2 = \tilde{V}_2^{\dagger}\mathcal{U}_2'\tilde{V}_2$ and $\mathcal{U}_3 = \tilde{V}_3^{\dagger}\mathcal{U}_3'\tilde{V}_3$ responsible for creating the group element stator as discussed in the last section. Thus, if we move the lattice of the auxiliary atoms to a link $i$ and tailor the interactions accordingly, we can build the stator for all links i in even cubes:

$$\mathcal{U}_{ie} = \tilde{V}_{3,all}^{\dagger}\tilde{V}_{2,all}^{\dagger}\prod_{\mathbf{x}\,even}\mathcal{U}_{3,i}'(\mathbf{x})\,\mathcal{U}_{2,i}'(\mathbf{x})\,\tilde{V}_{2,all}\tilde{V}_{3,all} \tag{241}$$

   The desired plaquette stator can therefore be obtained by repeating this procedure with all four links. The basis transformations $\tilde{V}_3$ and $\tilde{V}_2$ have to be done only in the beginning and at the end which reduces the sequence to:

$$\mathcal{U}_{B,1e} = \tilde{V}_{3,all}^{\dagger}\tilde{V}_{2,all}^{\dagger}\mathcal{U}_{1e}'\mathcal{U}_{2e}'\mathcal{U}_{3e}'^{\dagger}\mathcal{U}_{4e}'^{\dagger}\tilde{V}_{2,all}\tilde{V}_{3,all} \tag{242}$$

   where $\mathcal{U}_{ie}'$ is defined as $\mathcal{U}_{ie}' = \prod_{\mathbf{x}\,even}\mathcal{U}_{3,i}'(\mathbf{x})\,\mathcal{U}_{2,i}'(\mathbf{x})$. This gives us the entangled state between the four links and the auxiliary degree of freedom which allows mediating the plaquette interactions.

2. The next step is a local operation on the auxiliary Hilbert space which generates the time evolution in the physical Hilbert space (for details see section 4.3.1). We need to realize the interaction $\tilde{V}_B = e^{-i\tilde{H}_B\tau}$ of the control with $\tilde{H}_B$ being the control Hamiltonian:

$$\tilde{H}_B = \lambda_B \mathrm{Tr}\,(\tilde{U} + \tilde{U}^{\dagger}) \tag{243}$$

   In our case this is a local interaction since we represent our control system by two atoms.

The Hamiltonian $\tilde{H}_B$ takes the form (see chapter 3 for details on the magnetic Hamiltonian) :

$$\begin{aligned}\tilde{H}_B &= \lambda_B \,\mathrm{Tr}(\tilde{U} + \tilde{U}^\dagger) \\ &= \lambda_B \,\mathrm{Tr}\left(\sum_p \sum_m |\tilde{p}, \tilde{m}\rangle \langle \tilde{p}, \tilde{m}| \; e^{i\frac{2\pi}{3}\sigma_z p}\sigma_x^m + H.c.\right) \\ &= \lambda_B \,\mathrm{Tr}\begin{pmatrix} e^{i\frac{2\pi}{3}\hat{p}}\,(1-\hat{m}) & e^{i\frac{2\pi}{3}\hat{p}}\hat{m} \\ e^{-i\frac{2\pi}{3}\hat{p}}\,\hat{m} & e^{-i\frac{2\pi}{3}\hat{p}}\,(1-\hat{m}) \end{pmatrix} + H.c. \\ &= \lambda_B\,(\tilde{P}_3 + \tilde{P}_3^\dagger)(1-\hat{m}) + H.c \\ &= 2\lambda_B\,(\tilde{P}_3 + \tilde{P}_3^\dagger)(1-\hat{m})\end{aligned} \tag{244}$$

The hat over $m$ and $p$ indicates that they are operators acting on the auxiliary Hilbert space with eigenvalues $m$ and $p$ for the state $|\tilde{p}, \tilde{m}\rangle$. We can already see that $\tilde{P}_3 + \tilde{P}_3^\dagger$ is acting on the three-level system whereas $(1-\hat{m})$ is acting on the two-level system. We therefore have to implement the time-evolution of a two-body interaction:

$$\tilde{V}_B = e^{-i\tilde{H}_B\tau} = e^{-i2\lambda_B\,(\tilde{P}_3+\tilde{P}_3^\dagger)(1-\hat{m})\tau} \tag{245}$$

We first compute $\tilde{P}_3+\tilde{P}_3^\dagger$ acting on the three level system of the hyperfine states $|\tilde{F}_3 = 1; m_F = 1\rangle$, $|\tilde{F}_3 = 1; m_F = 0\rangle$ and $|\tilde{F}_3 = 1; m_F = -1\rangle$:

$$\tilde{P}_3 + \tilde{P}_3^\dagger = \begin{pmatrix} 2\cos\frac{2\pi}{3} & 0 & 0 \\ 0 & 2 & 0 \\ 0 & 0 & 2\cos\frac{2\pi}{3} \end{pmatrix} = \begin{pmatrix} -1 & 0 & 0 \\ 0 & 2 & 0 \\ 0 & 0 & -1 \end{pmatrix} = -\mathbb{I} + 3\tilde{N}_0 \tag{246}$$

Thus, we get for the interaction $\tilde{V}_B$:

$$\begin{aligned}\tilde{V}_B = e^{-i\tilde{H}_B\tau} = e^{-i2\lambda_B\,(\tilde{P}_3+\tilde{P}_3^\dagger)(1-\hat{m})\tau} &= e^{-i2\lambda_B\,(-\mathbb{I}+3\tilde{N}_0)\tilde{N}_{1/2}\tau} \\ &= e^{i2\lambda_B\tilde{N}_{1/2}\tau}\,e^{-i6\lambda_B\tilde{N}_0\tilde{N}_{1/2}\tau}\end{aligned} \tag{247}$$

The first exponential is a local term of the two-level system which can be implemented by means of optical/RF fields. The second term requires scattering between the two auxiliary atoms. The relevant scattering term for angular momentum $F = 1$ and $F = 1/2$ is:

$$\mathcal{U}_{scat,3} = e^{-i\delta\left(g_{1/2}\sum_m d_m^\dagger d_m \sum_n b_n^\dagger b_n + g_{3/2}\tilde{F}_2\cdot\tilde{F}_3\right)} \tag{248}$$

where $\delta$ denotes again the integrated overlap of the Wannier functions. As in the previous cases - since the different energy splittings due to the magnetic field conserve $\tilde{m}_F$ - we can remove terms which change $\tilde{m}_F$. The unitary for the scattering process reduces to:

$$\mathcal{U}_{scat,3} = e^{-i\delta\left(g_{1/2}\sum_m d_m^\dagger d_m \sum_n b_n^\dagger b_n + g_{3/2}\tilde{F}_{z,2}\tilde{F}_{z,3}\right)} \tag{249}$$

To achieve $\tilde{m}_F$-dependent overlaps, we again apply a magnetic field gradient which spatially separates the $\tilde{m}_F$-components. If we choose the Lande-factors of the atomic species and design the magnetic field gradient in the right way, we can tune the overlap such that only the $\tilde{m}_F = 0$-component and the $\tilde{m}_F = 1/2$-component experience scattering with each other. With additional tuning of the interaction time we can set $\delta = \frac{6\lambda_B\tau}{g_{1/2}}$ and finally obtain:

$$\mathcal{U}_{scat,3} = e^{-i6\lambda_B\tilde{N}_0\tilde{N}_{1/2}\tau} \tag{250}$$

which is up to local operations the desired unitary $V_B$. This interaction will be implemented in parallel for all cubes where auxiliary atoms are placed, i.e. in this case for the even cubes. Hence, the overall interaction of this step is

$$\tilde{V}_{Be} = e^{-i\tilde{H}_{B,e}\tau} \tag{251}$$

with $\tilde{H}_{B,e} = \sum_{\mathbf{x}\,even}\tilde{H}_B(\mathbf{x})$.

3. In the third and last step we have to undo the stator. This can be done by just doing the hermitian conjugate of the first step, i.e. the sequence:

$$\mathcal{U}_{B,1e}^\dagger = \tilde{V}_{3,all}^\dagger\tilde{V}_{2,all}^\dagger\mathcal{U}_{4e}'\mathcal{U}_{3e}'\mathcal{U}_{2e}'^\dagger\mathcal{U}_{1e}'^\dagger\tilde{V}_{2,all}\tilde{V}_{3,all} \tag{252}$$

According to eq.(156) these three steps give us $W_{B,1e}$, the time evolution for a time step $\tau$ of the first part of the plaquette interaction at even cubes:

$$\mathcal{U}_{B,1e}^\dagger\tilde{V}_{Be}\mathcal{U}_{B,1e} = W_{B,1e} \tag{253}$$

If we repeat now the same procedure but with the links corresponding to the second and third plaquette term, we obtain $W_{B,2e}$ and $W_{B,3e}$. To realize the odd cubes evolution, we move the auxiliary atoms to the centers of the odd cubes and repeat all of the above. This results in the time evolutions $W_{B,1o}$,$W_{B,2o}$ and $W_{B,3o}$. Then we bring the auxiliary atoms back to the centers of the even cubes.

### 5.2.5 Gauge-matter interactions

For the Gauge-matter interactions on a link $(\mathbf{x}, k)$ we have to implement the Hamiltonian

$$\begin{aligned} H_{GM}(\mathbf{x},k) &= \lambda_{GM}\,\psi_a^\dagger(\mathbf{x})U_{ab}(\mathbf{x},k)\psi_b(\mathbf{x}+\hat{k}) + H.c. \\ &= \lambda_{GM}\,\psi_a^\dagger(\mathbf{x})\,(e^{i\frac{2\pi}{3}\sigma_z\hat{p}}\sigma_x^{\hat{m}})_{ab}\,\psi_b(\mathbf{x}+\hat{k}) + H.c. \\ &= \lambda_{GM}\,\psi_a^\dagger(\mathbf{x})\,(e^{i\frac{2\pi}{3}\sigma_z\hat{p}})_{ab}(\sigma_x^{\hat{m}})_{bc}\,\psi_c(\mathbf{x}+\hat{k}) + H.c. \\ &= \lambda_{GM}\,\psi_a^\dagger(\mathbf{x})\,(U_p)_{ab}(\mathbf{x},k)\,(U_m)_{bc}(\mathbf{x},k)\,\psi_c(\mathbf{x}+\hat{k}) + H.c. \end{aligned} \tag{254}$$

with $U_p \equiv e^{i\frac{2\pi}{3}\sigma_z\hat{p}}$ and $U_m \equiv \sigma_x^{\hat{m}}$. We can use the product structure of U to implement the gauge-matter part via two-body interactions. The key ingredient for that is the Baker-Campbell-Hausdorff formula. We first need to define two unitaries, one that corresponds to $U_p$:

$$\mathcal{U}_{W,p}(\mathbf{x},k) = e^{\log(U_p)_{ab}(\mathbf{x},k)\,\psi_a^\dagger(\mathbf{x})\psi_b(\mathbf{x})} = e^{i\frac{2\pi}{3}\hat{p}\,(\psi_1^\dagger(\mathbf{x})\psi_1(\mathbf{x})-\psi_2^\dagger(\mathbf{x})\psi_2(\mathbf{x}))} \tag{255}$$

and another one corresponding to $U_m$:

$$\mathcal{U}_{W,m}(\mathbf{x},k) = e^{\log(U_m)_{ab}(\mathbf{x},k)\,\psi_a^\dagger(\mathbf{x})\psi_b(\mathbf{x})} = e^{i\frac{\pi}{2}\hat{m}\,(\psi_1^\dagger(\mathbf{x})\psi_1(\mathbf{x})+\psi_2^\dagger(\mathbf{x})\psi_2(\mathbf{x})-\psi_1^\dagger(\mathbf{x})\psi_2(\mathbf{x})-\psi_2^\dagger(\mathbf{x})\psi_1(\mathbf{x}))} \tag{256}$$

With these definitions at hand we can get the following relation by applying twice the Baker-Campbell-Hausdorff formula:

$$\mathcal{U}_{W,p}(\mathbf{x},k)\mathcal{U}_{W,m}(\mathbf{x},k)\psi_n^\dagger(\mathbf{x})\mathcal{U}_{W,m}^\dagger(\mathbf{x},k)\mathcal{U}_{W,p}^\dagger(\mathbf{x},k) = \psi_a^\dagger(\mathbf{x})(U_p)_{ab}(\mathbf{x},k)(U_m)_{bn}(\mathbf{x},k) \tag{257}$$

The gauge-matter Hamiltonian can then be written as

$$H_{GM}(\mathbf{x},k) = \mathcal{U}_{W,p}(\mathbf{x},k)\mathcal{U}_{W,m}(\mathbf{x},k)H_t(\mathbf{x},k)\mathcal{U}_{W,m}^\dagger(\mathbf{x},k)\mathcal{U}_{W,p}^\dagger(\mathbf{x},k) \tag{258}$$

with the tunneling Hamiltonian

$$H_t(\mathbf{x}, k) = \lambda_{GM}\, \psi_a^\dagger(\mathbf{x})\psi_a(\mathbf{x} + \hat{k}) + H.c. \tag{259}$$

Defining its time evolution as

$$\mathcal{U}_t(\mathbf{x}, k) = e^{-iH_t(\mathbf{x},k)\tau} \tag{260}$$

we can write the sequence to realize the time evolution of the Gauge-Matter interaction on the link $(\mathbf{x}, k)$:

$$W_{GM}(\mathbf{x}, k) = \mathcal{U}_{W,p}(\mathbf{x}, k)\mathcal{U}_{W,m}(\mathbf{x}, k)\mathcal{U}_t(\mathbf{x}, k)\mathcal{U}_{W,m}^\dagger(\mathbf{x}, k)\mathcal{U}_{W,p}^\dagger(\mathbf{x}, k) \tag{261}$$

The crucial thing to note here is that all the terms involve only two-body interactions which allows an implementation with ultracold atoms as we will see in the following. We can not implement all gauge-matter interactions at once as the fermions on the vertices are only allowed to interact with one link at a time. Focusing on the links in the $\hat{1}$-direction for the even cubes, we aim to realize the time evolution

$$W_{GM,1e} = e^{-iH_{GM,1e}\tau} \tag{262}$$

with $H_{GM,1e} = \sum_{\mathbf{x}even} H_{GM}(\mathbf{x}, 1)$. Since we want to keep the lattice of the matter and link degrees of freedom fixed, these interactions will be mediated by the control atoms. Thus, following the algorithm presented in section 4.3.2, we first need to create the group element stator between the auxiliary atoms and the link atoms. This can be done by moving the auxiliary atoms to the $\hat{1}$-links and generate the sequence (as discussed in section. 5.2.3):

$$\mathcal{U}_{1e} = \tilde{V}_{3,all}^\dagger \tilde{V}_{2,all}^\dagger \prod_{\mathbf{x}\, even} \mathcal{U}'_{3,\mathrm{link1}}(\mathbf{x})\, \mathcal{U}'_{2,\mathrm{link1}}(\mathbf{x})\, \tilde{V}_{2,all}\tilde{V}_{3,all} \tag{263}$$

Afterwards, the two terms $\mathcal{U}_{W,p}^\dagger$ and $\mathcal{U}_{W,m}^\dagger$ have to be implemented by two-body scattering processes but between the fermions and the auxiliary atoms due to the stator construction, therefore denoted as $\tilde{\mathcal{U}}_{W,p}$ and $\tilde{\mathcal{U}}_{W,m}$. Starting with $\tilde{\mathcal{U}}_{W,p}^\dagger$, we first write it in terms of the angular momentum operator respectively the second quantized operators $\psi_1$ and $\psi_2$ for the fermions:

$$\tilde{\mathcal{U}}_{W,p}^\dagger(\mathbf{x}, k) = e^{-i\frac{2\pi}{3}\hat{p}\,(\psi_1^\dagger(\mathbf{x})\psi_1(\mathbf{x}) - \psi_2^\dagger(\mathbf{x})\psi_2(\mathbf{x}))} = e^{-i\frac{2\pi}{3}\tilde{F}_{z,3}\,(\psi_1^\dagger(\mathbf{x})\psi_1(\mathbf{x}) - \psi_2^\dagger(\mathbf{x})\psi_2(\mathbf{x}))} \tag{264}$$

Now we have to tailor the atomic collision between the $\tilde{F}_3 = 1$ and the $F = 1/2$ multiplet accordingly. The magnetic field again lifts the degeneracy of the hyperfine levels and thereby preventing any transitions changing the $m_F$-values. An important difference to previous scattering processes is that the fermion number is not locally conserved but only globally, the total number of auxiliary atoms, however, still is ($\tilde{N}_{3,tot} = \sum_m b_m^\dagger b_m = 1$). Taking all that into account, the unitary for the scattering is given by:

$$\mathcal{U}_{scat,4} = e^{-i\alpha(g_{1/2}(\psi_1^\dagger\psi_1+\psi_2^\dagger\psi_2)+g_{3/2}\tilde{F}_{z,3}(\psi_1^\dagger\psi_1-\psi_2^\dagger\psi_2))} \tag{265}$$

If we tune the overlap such that $\alpha = \frac{2\pi}{3g_{3/2}}$ we obtain

$$\mathcal{U}_{scat,4} = e^{-i\frac{2\pi g_{1/2}}{3g_{3/2}}(\psi_1^\dagger\psi_1+\psi_2^\dagger\psi_2)} e^{-i\frac{2\pi}{3}\tilde{F}_{z,3}(\psi_1^\dagger\psi_1-\psi_2^\dagger\psi_2)} \tag{266}$$

The second exponential gives rise to the desired interaction $\tilde{\mathcal{U}}_{W,p}^\dagger$ whereas the first term is a fermion-dependent phase, denoted from now on as

$$V_{W'}(\theta) = e^{-i\theta\psi^\dagger\psi} \tag{267}$$

where $\theta = \frac{2\pi g_{1/2}}{3g_{3/2}}$ and $\psi^\dagger\psi = \psi_1^\dagger\psi_1 + \psi_2^\dagger\psi_2$. A discussion of these phases will be done later on. Before, the implementation of $\tilde{\mathcal{U}}_{W,m}^\dagger$ as scattering between the fermions and the two-level system is explained. It has the form:

$$\begin{aligned}
\tilde{\mathcal{U}}_{W,m}^\dagger &= e^{-i\frac{\pi}{2}\hat{m}\,(\psi_1^\dagger\psi_1+\psi_2^\dagger\psi_2-\psi_1^\dagger\psi_2-\psi_2^\dagger\psi_1)} \\
&= e^{-i\frac{\pi}{2}\tilde{N}_{-1/2}\,(\psi_1^\dagger\psi_1+\psi_2^\dagger\psi_2-\psi_1^\dagger\psi_2-\psi_2^\dagger\psi_1)} \\
&= V_{H,fer} e^{-i\frac{\pi}{2}\tilde{N}_{-1/2}\,(\psi_1^\dagger\psi_1+\psi_2^\dagger\psi_2-\psi_1^\dagger\psi_1+\psi_2^\dagger\psi_2)} V_{H,fer} \\
&= V_{H,fer} e^{-i\pi\tilde{N}_{-1/2}\psi_2^\dagger\psi_2} V_{H,fer}
\end{aligned} \tag{268}$$

where $\tilde{N}_{-1/2} = d_{-1/2}^\dagger d_{-1/2}$ and $V_{H,fer} = \frac{1}{\sqrt{2}}(\sigma_{x,fer} + \sigma_{z,fer})$ a Hadamard transform on the fermions which can be implemented by means of optical/RF fields. The remaining two-body interaction is realized as the scattering between the $F = 1/2$ states of the control atoms and the fermions. It can be described by the following unitary:

$$\mathcal{U}_{scat,5} = e^{-i\eta\left(g_0\sum_m d_m^\dagger d_m(\psi_1^\dagger\psi_1+\psi_2^\dagger\psi_2)+g_1\tilde{F}_{z,2}(\psi_1^\dagger\psi_1-\psi_2^\dagger\psi_2)\right)} \tag{269}$$

We switch on a magnetic field gradient designed in a way that only the $m_F = -1/2$-components of the auxiliary atom and the fermion overlap. Moreover,The interaction time should be tuned such that $\eta = \frac{\pi}{g_0+g_1}$ which finally gives rise to:

$$\mathcal{U}_{scat,5} = e^{-i\eta\left(g_0 d^\dagger_{-1/2} d_{-1/2}\psi_2^\dagger\psi_2 + g_1 d^\dagger_{-1/2} d_{-1/2}\psi_2^\dagger\psi_2\right)} = e^{-i\pi d^\dagger_{-1/2} d_{-1/2}\,\psi_2^\dagger\psi_2} \tag{270}$$

Since the implementation of $\tilde{\mathcal{U}}^\dagger_{W,p}$ and $\tilde{\mathcal{U}}^\dagger_{W,m}$ is done in parallel for all even cubes we get the sequence

$$\prod_{\mathbf{x}\,even} \tilde{\mathcal{U}}^\dagger_{W,m}(\mathbf{x},1)\tilde{\mathcal{U}}^\dagger_{W,p}(\mathbf{x},1)V_{W'}(\theta) \tag{271}$$

In the next step we implement the tunneling $\mathcal{U}_{t,1e}$ in the 1-direction for even cubes. This can be achieved by decreasing the potential barrier between neighboring lattice sites as explained in detail in section 4.4 for the general algorithm. We get

$$\mathcal{U}_{t,1e} = \prod_{\mathbf{x}even} \mathcal{U}_t(\mathbf{x},1) \tag{272}$$

After the tunneling we need to realize the conjugate of $\tilde{\mathcal{U}}^\dagger_{W,p}$ and $\tilde{\mathcal{U}}^\dagger_{W,m}$, i.e. $\tilde{\mathcal{U}}_{W,p}$ and $\tilde{\mathcal{U}}_{W,m}$. One way of creating $\tilde{\mathcal{U}}_{W,p}$ is by doing a spin flipping operation $\tilde{V}_{F,3}$ for the three-level system of the control which results in:

$$\begin{aligned} \tilde{V}_{F,3}\tilde{\mathcal{U}}^\dagger_{W,p}\tilde{V}^\dagger_{F,3} &= \tilde{\mathcal{U}}_{W,m} \\ \tilde{V}_{F,3}V_{W'}(\theta)\tilde{V}^\dagger_{F,3} &= V_{W'}(\theta) \end{aligned} \tag{273}$$

For the creation of $\tilde{\mathcal{U}}_{W,m}$ we observe that $\tilde{\mathcal{U}}^\dagger_{W,m}$ is a $\pi$-gate and the operator $d^\dagger_{-1/2}d_{-1/2}\psi_2^\dagger\psi_2$ only takes integer values. Therefore the unitary $\tilde{\mathcal{U}}^\dagger_{W,m}$ is real and therefore - since it is diagonal- conjugate to itself. Hence, we just repeat the steps from above for the creation of $\tilde{\mathcal{U}}^\dagger_{W,m}$. The sequence we finally obtain is

$$\prod_{\mathbf{x}\,even} V_{W'}(\theta)\tilde{\mathcal{U}}_{W,p}(\mathbf{x},1)\tilde{\mathcal{U}}_{W,m}(\mathbf{x},1) \tag{274}$$

In the last step we need to undo the stator, which is done by the conjugate of the first step, $\mathcal{U}^\dagger_{1e}$ (explained in detail in the previous section on the stator). We can then summarize by writing

down the whole sequence acting on the stator $S_1 = \mathcal{U}_{1e} |\tilde{in}\rangle$ created in the beginning :

$$\begin{aligned}
&\mathcal{U}_{1e}^{\dagger} \prod_{\mathbf{x}\, even} V_{W'}(\theta)\tilde{\mathcal{U}}_{W,p}(\mathbf{x},1)\tilde{\mathcal{U}}_{W,m}(\mathbf{x},1)\mathcal{U}_t(\mathbf{x},1)\tilde{\mathcal{U}}_{W,m}^{\dagger}(\mathbf{x},1)\tilde{\mathcal{U}}_{W,p}^{\dagger}(\mathbf{x},1)V_{W'}(\theta)S_1 \\
=&\mathcal{U}_{1e}^{\dagger}S_1 \prod_{\mathbf{x}\, even} V_{W'}(\theta)\mathcal{U}_{W,p}(\mathbf{x},1)\mathcal{U}_{W,m}(\mathbf{x},1)\mathcal{U}_t(\mathbf{x},1)\mathcal{U}_{W,m}^{\dagger}(\mathbf{x},1)\mathcal{U}_{W,p}^{\dagger}(\mathbf{x},1)V_{W'}(\theta) \\
=&|\tilde{in}\rangle\, V_{W'}(\theta) \prod_{\mathbf{x}\, even} W_{GM}(\mathbf{x},1)V_{W'}(\theta) \\
=&|\tilde{in}\rangle\, V_{W'}(\theta)W_{GM,1e}V_{W'}(\theta)
\end{aligned} \tag{275}$$

We finally get the desired gauge-matter interactions up to the fermionic phases $V_{W'}(\theta)$. However, if we consider the whole lattice it can be shown that the phases correspond to a static vector potential of zero magnetic field and are therefore unphysical [42]. If we repeat the whole procedure from above for the other links we obtain the gauge-matter interactions $W_{GM,2e}$,$W_{GM,3e}$,$W_{GM,1o}$,$W_{GM,2o}$ and $W_{GM,3o}$.

### 5.2.6 Electric Hamiltonian

The electric Hamiltonian for the gauge group $D_6$ acts on the gauge fields residing on the links. If we choose its second part - which corresponds pure rotations only - in accordance with the electric energy of $\mathbb{Z}_3$ (see chapter 3 for details) we obtain, using the notation of previous sections:

$$H_E = \lambda_E \sum_{\mathbf{x},k} h_E(\mathbf{x},k) \tag{276}$$

with

$$h_E(\mathbf{x},k) = \frac{1}{2} f_{t'} \sum_{m,m'} |0,m\rangle \langle 0,m'| + f_r(1 - P_3 - P_3^{\dagger}) \otimes \mathbb{I}_2 \tag{277}$$

If we also express the interactions of the first part in terms of operators acting on the link atoms, we end up with:

$$\begin{aligned}
h_E(\mathbf{x},k) = &\frac{1}{2} f_{t'} a_0^{\dagger} a_0 \otimes (1 + \sigma_x) + f_r(1 - P_3 - P_3^{\dagger}) \otimes \mathbb{I}_2 \\
&\frac{1}{2} f_{t'} a_0^{\dagger} a_0 \otimes (1 + \sigma_x) + f_r \sum_{m_F=-1}^{1} (1 + |m_F|) a_{m_F}^{\dagger} a_{m_F} \otimes \mathbb{I}_2
\end{aligned} \tag{278}$$

The first Hilbert space represents the three-level system, the second one the two-level system. The coefficient $f_r$ is the overall coefficient for the electric part corresponding to pure rotations, equivalently to $\mathbb{Z}_3$. We have to implement the time evolution:

$$W_E = e^{-iH_E\tau} = \prod_{\mathbf{x},k} e^{-ih_E(\mathbf{x},k)\tau} \tag{279}$$

with

$$e^{-ih_E\tau} = e^{-i\frac{\lambda_E f_{t'}}{2}a_0^\dagger a_0\tau} e^{-i\frac{\lambda_E f_{t'}}{2}a_0^\dagger a_0\sigma_x\tau} e^{-i\lambda_E f_r \sum_{m_F}(1+|m_F|)a_{m_F}^\dagger a_{m_F}\tau} \tag{280}$$

The first and the third exponential are local terms of the atoms and can be addressed by external fields. The second term is implemented by two-body scattering similar to the one for the plaquette interaction. Following the steps there, we obtain the unitary:

$$\mathcal{U}_{scat,3} = e^{-i\gamma g_{1/2}N_0N_{1/2}} \tag{281}$$

Tuning overlap and interaction time such that $\gamma = \frac{\lambda_E f_{t'}\tau}{g_{1/2}}$ and combining it with the local interaction $\mathcal{V}_{E,2} = e^{i\frac{\lambda_E f_{t'}\tau}{2}N_{1/2}}$, gives us:

$$\mathcal{V}_{E,2}\mathcal{U}_{scat,3} = e^{i\frac{\lambda_E f_{t'}\tau}{2}N_{1/2}} e^{-i\lambda_E f_{t'}N_0N_{1/2}\tau} = e^{-i\frac{\lambda_E f_{t'}}{2}N_0\sigma_z\tau} \tag{282}$$

If we then perform a Hadamard transform on the two-level system we get the desired interaction:

$$V_{H,2}\mathcal{V}_{E,2}\mathcal{U}_{scat,3}V_{H,2} = e^{-i\frac{\lambda_E f_{t'}}{2}N_0\sigma_x} = e^{-i\frac{\lambda_E f_{t'}}{2}a_0^\dagger a_0\sigma_x\tau} \tag{283}$$

which gives us the electric Hamiltonian up to local interactions. We have finally implemented all interactions by using local interactions on the atoms and tailoring the appropriate two-body scattering terms.

## 5.3 Experimental errors

The errors affecting the precision of the simulation are twofold. On the one hand, we have trotterization errors coming from the digitization. They are intrinsic and discussed in detail in section 4.5. On the other hand, there will be experimental errors in the implementation. Unlike trotterization errors, they may break the gauge symmetry and increase with a larger number of time steps M. This concerns in particular gates that do not depend on the length $\tau$ of the time

step but require a fixed amount of time. Thus, the number M must be chosen in way to balance digitization and implementation errors.

Some of the sources of errors are shared with many other cold atom experiments. The first one is decoherence, e.g. caused by spontaneous scattering of lattice photons with the atoms. This has been relatively well under control nowadays, reducing the corresponding timescales to several minutes [3, 80, 81]. Other factors contributing to decoherence are fluctuations of the magnetic field which are also present in many cold atom experiments. Secondly, one needs to ensure that the atoms remain in the lowest Bloch band throughout the whole implementation. Hence, it is of crucial importance to shape the lattice and move the atoms in an adiabatic way. This has to be taken into account in our simulation scheme when the auxiliary atoms are moved or when the matter lattice is deformed to allow for tunneling. However, such techniques have become well-controlled [3, 82].

Errors more specific to this proposal are connected with the two-body scattering. It requires a high degree of control over the overlap of the atomic wavefunctions and the time of interaction during these collisions. One of the ingredients to achieve that is the ability to design and manipulate the magnetic field gradient in a precise manner. Moreover, for the implementation of local terms the turning on/off and the duration of laser pulses need to be under high control.

# 6 Summary and Conclusions

In this thesis on quantum simulation of lattice gauge theories with ultracold atoms, two main results were achieved: On the one hand a digital simulation scheme was proposed to realize lattice gauge theories in 3+1 dimensions including dynamical fermions using only two-body interactions. On the other hand, following the aforementioned simulation scheme, an implementation of a lattice gauge theory with a non-abelian gauge group - the dihedral group $D_6$ - was proposed, mapping the Hamiltonian of lattice gauge theory exactly to the Hamiltonian of ultracold atoms. However, since the time evolution is performed in a trotterized manner, intrinsic errors occur. These were studied in detail as a good bound on the trotterization error gives more leeway to experimental errors.

The key ingredient of the three-dimensional simulation scheme is an auxiliary system which can be entangled with the physical system. This allows to create an object called stator which mediates the complicated three and four-body interactions of lattice gauge theory only by two-body interactions as desired for implementations with ultracold atoms. Moreover, it should be emphasized that all time evolutions in this algorithm are individually gauge invariant. The corresponding gauge group has to be either a compact Lie group or a finite group which is not a restriction for all relevant theories. In the case of compact Lie groups, the local Hilbert spaces of the gauge fields have an infinite dimension and therefore need to be truncated for a feasible implementation. However, as the construction of the stator is done in group space, the truncation has to be done there as well and can not be in the typically used representation space. Examples for such truncations are $\mathbb{Z}_N$ for $U(1)$ or - as proposed in this thesis - $D_N$ for $O(2)$ (or $SO(3)$).

For the implementation of the lattice gauge theory with dihedral group $D_6$ - isomorphic to the symmetric group $S_3$ - we exploited the group structure of $D_6$ as a semidirect product. This allowed us to represent the gauge fields by a tensor product of a three-level and a two-level system and thus simplified the implementation. The potential gain from this procedure would be even higher for more complicated gauge groups exhibiting a semidirect product structure. This idea might pave the way for other realizations of lattice gauge theories with non-abelian gauge groups in more than 1+1 dimensions including dynamical fermionic matter. This is a non-trivial step since in two and more spatial dimensions plaquette interactions, which are not present in one dimension, occur. An advantage of implementing these plaquette interaction by the construction of stators is that the interactions are strong since no perturbation theory is required

as compared to quantum simulations without an auxiliary system. Moreover, no sophisticated experimental techniques such as Feshbach resonances are required. However, precise control over atomic collisions is needed in order to obtain the desired time evolution. In particular since gates entangling the auxiliary system with the physical system do not depend on the simulated time and are thus more prone to experimental errors.

Future efforts on experimental techniques can therefore be targeted at the controllability of the relevant parameters, i.e. in particular fine tuning of the overlap integrals and the interaction time during scattering processes. The generation and experimental control of superlattices is important as well in order to create a staggering potential for the dynamical fermions. Also conducting experiments on simpler models - as currently set up for the Schwinger model - is a very promising direction as it can serve as a proof of principle for the validity of quantum simulations of lattice gauge theories. The Schwinger model is particularly well suited for this task since it has accurate analytical and numerical results to compare experimental results with. Successful experiments might encourage more work in this direction.

From the theoretical point of view, a logical next step is to think of possibilities to realize more complex gauge groups. One step towards that goal is to find suitable ways to truncate compact gauge groups like for example $SU(2)$ in a meaningful manner.

# Appendix

For the bounds on the trotterization error of the digital quantum simulation (presented in chapter 4) a computation of commutators and nested commutators of the different parts of the Hamiltonian is required. Since the calculation of these commutators for a general lattice gauge theory are very lengthy, they are shifted to the Appendix.

## First order

For the first order formula the ordinary commutators need to be computed. Starting with the commutator between gauge-matter interactions on different links $i$ and $j$, we obtain:

$$
\begin{aligned}
&[H_{GM,i}, H_{GM,j}] \\
=&\left[\sum_{x,k_i} \lambda_{GM}\, \psi_m^\dagger(x) U_{mn}(x,k_i)\psi_n(x+k_i) + h.c, \sum_{y,k_j} \lambda_{GM}\, \psi_m^\dagger(y) U_{mn}(y,k_j)\psi_n(y+k_j) + h.c\right] \\
=&\lambda_{GM}^2 \sum_{x/\{boundary\}} \Big[\psi_m^\dagger(x) U_{mn}(x,k_i)\psi_n(x+k_i) + h.c, \psi_{m'}^\dagger(x) U_{m'n'}(x,k_j)\psi_{n'}(x+k_j) + h.c\Big] \\
+&\Big[\psi_m^\dagger(x) U_{mn}(x,k_i)\psi_n(x+k_i) + h.c, \psi_{m'}^\dagger(x+k_i-k_j) U_{m'n'}(x+k_i-k_j,k_j)\psi_{n'}(x+k_i) + h.c\Big] \\
=&\lambda_{GM}^2 \sum_{x/\{boundary\}} \Big[\psi_n^\dagger(x+k_i) U_{nm}^\dagger(x,k_i)\psi_m(x), \psi_{m'}^\dagger(x) U_{m'n'}(x,k_j)\psi_{n'}(x+k_j)\Big] - h.c. \\
+&\Big[\psi_m^\dagger(x) U_{mn}(x,k_i)\psi_n(x+k_i), \psi_{n'}^\dagger(x+k_i) U_{n'm'}^\dagger(x+k_i-k_j,k_j)\psi_{m'}(x+k_i-k_j)\Big] - h.c \\
=&\lambda_{GM}^2 \sum_{x/\{boundary\}} \psi_n^\dagger(x+k_i) U_{nm}^\dagger(x,k_i) U_{mn'}(x,k_j)\psi_{n'}(x+k_j) - h.c. \\
+&\psi_m^\dagger(x) U_{mn}(x,k_i) U_{nm'}^\dagger(x+k_i-k_j,k_j)\psi_{m'}(x+k_i-k_j) - h.c.
\end{aligned}
\tag{284}
$$

To estimate the norm of this term the $\psi$- and $U$-operators need to be expressed in terms of tunneling terms and unitary operators as already discussed in section 4.3.2:

$$
\begin{aligned}
&[H_{GM,i}, H_{GM,j}] \\
=&\lambda_{GM}^2 \sum_{x/\{boundary\}} \psi_n^\dagger(x+k_i) U_{nm}^\dagger(x,k_i) U_{mn'}(x,k_j) \psi_{n'}(x+k_j) - h.c. \\
+&\psi_m^\dagger(x) U_{mn}(x,k_i) U_{nm'}^\dagger(x+k_i-k_j,k_j) \psi_{m'}(x+k_i-k_j) - h.c. \\
=&\lambda_{GM}^2 \sum_{x/\{boundary\}} e^{\log U^\dagger(x,k_i)_{ab} \psi_a^\dagger(x+k_i)\psi_b(x+k_i)} e^{\log U(x,k_j)_{ab}\psi_a^\dagger(x+k_i)\psi_b(x+k_i)} \\
&(\psi_n^\dagger(x+k_i)\psi_n(x+k_j) - h.c.) e^{-\log U(x,k_j)_{ab}\psi_a^\dagger(x+k_i)\psi_b(x+k_i)} e^{-\log U^\dagger(x,k_i)_{ab}\psi_a^\dagger(x+k_i)\psi_b(x+k_i)} \\
+&e^{\log U(x,k_i)_{ab}\psi_a^\dagger(x)\psi_b(x)} e^{\log U^\dagger(x+k_i-k_j,k_j)_{ab}\psi_a^\dagger(x)\psi_b(x)} \\
&(\psi_n^\dagger(x)\psi_n(x+k_i-k_j) - h.c.) e^{-\log U^\dagger(x+k_i-k_j,k_j)_{ab}\psi_a^\dagger(x)\psi_b(x)} e^{\log U(x,k_i)_{ab}\psi_a^\dagger(x)\psi_b(x)} \\
=&\lambda_{GM}^2 \sum_{x/\{boundary\}} \mathcal{U}_{W1}^\dagger \mathcal{U}_{W2} (\psi_n^\dagger(x+k_i)\psi_n(x+k_j) - h.c.) \mathcal{U}_{W2}^\dagger \mathcal{U}_{W1} \\
+&\mathcal{U}_{W3}\mathcal{U}_{W4}^\dagger (\psi_n^\dagger(x)\psi_n(x+k_i-k_j) - h.c.) \mathcal{U}_{W4}\mathcal{U}_{W3}^\dagger
\end{aligned}
\tag{285}
$$

Since the $\mathcal{U}$'s are unitary, the operator norm of this commutator can be estimated as:

$$
\begin{aligned}
\| [H_{GM,i}, H_{GM,j}] \| &\leq \lambda_{GM}^2 \sum_{x/\{boundary\}} \|\psi_n^\dagger(x)\psi_n(x+k_i-k_j) - h.c.\| + \|\psi_n^\dagger(x)\psi_n(x+k_i-k_j) - h.c.\| \\
&\leq \lambda_{GM}^2 \frac{\mathcal{N}_{links}}{2d} 2 d_U = \lambda_{GM}^2 \frac{\mathcal{N}_{links}}{d} d_U
\end{aligned}
\tag{286}
$$

where $d_U$ is the dimension of the representation of $U$ under the gauge group and therefore the operator norm of the tunneling term. In the next step the commutator between the matter- and gauge-matter interactions is calculated:

$$
\begin{aligned}
&[H_M, H_{GM,i}] \\
=&\left[\sum_x M(-1)^x \psi^\dagger_{n'}(x)\psi_{n'}(x), \sum_{y,k_i} \lambda_{GM}\psi^\dagger_m(y)U_{mn}(y,k_i)\psi_n(y+k_i) + h.c\right] \\
=&\sum_x M\lambda_{GM}\Big[(-1)^x\psi^\dagger_{n'}(x)\psi_{n'}(x) + (-1)^{x+k_i}\psi^\dagger_{n'}(x+k_i)\psi_{n'}(x+k_i), \\
&\psi^\dagger_m(x)U_{mn}(x,k_i)\psi_n(x+k_i) + h.c.\Big] \\
=&\sum_x M\lambda_{GM}\left[(-1)^x\psi^\dagger_{n'}(x)\psi_{n'}(x), \psi^\dagger_m(x)U_{mn}(x,k_i)\psi_n(x+k_i)\right] - h.c. \\
+&\left[(-1)^{x+k_i}\psi^\dagger_{n'}(x+k_i)\psi_{n'}(x+k_i), \psi^\dagger_m(x)U_{mn}(x,k_i)\psi_n(x+k_i)\right] - h.c. \\
=&\sum_x M\lambda_{GM}(-1)^x\psi^\dagger_m(x)U_{mn}(x,k_i)\psi_n(x+k_i) - h.c. \\
-&(-1)^{x+k_i}\psi^\dagger_m(x)U_{mn}(x,k_i)\psi_n(x+k_i) - h.c. \\
=&2\sum_x M\lambda_{GM}(-1)^x\psi^\dagger_m(x)U_{mn}(x,k_i)\psi_n(x+k_i) - h.c.
\end{aligned}
\tag{287}
$$

We rewrite this expression again in terms of the unitary operators $\mathcal{U}_W$ which allows us to bound the commutator in the following way:

$$
\begin{aligned}
\| [H_M, H_{GM,i}] \| &= \left\| 2\sum_x M\lambda_{GM}(-1)^x\psi^\dagger_m(x)U_{mn}(x,k_i)\psi_n(x+k_i) - h.c. \right\| \\
&= \left\| 2\sum_x M\lambda_{GM}(-1)^x\mathcal{U}_W(\psi^\dagger_n(x)\psi_n(x+k_i) - h.c.)\mathcal{U}^\dagger_W \right\| \\
&\leq 2M\lambda_{GM}\mathcal{N}_{links}d_U
\end{aligned}
\tag{288}
$$

For the commutator with the electric part the whole gauge-matter interaction is considered as every part of the gauge-matter Hamiltonian does not commute with $H_E$. We obtain:

$$
\begin{aligned}
&[H_{GM}, H_E] \\
=&\left[\sum_{x,k} \lambda_{GM}\, \psi_m^\dagger(x) U_{mn}(x,k) \psi_n(x+k) + h.c., \sum_{y,k'} \lambda_E \sum_j f(j)\, |jmn\rangle \langle jmn| \right] \\
=&\sum_{x,k} \lambda_{GM} \lambda_E \max_j |f(j)| \left[\psi_m^\dagger(x) U_{mn}(x,k) \psi_n(x+k) + h.c., \sum_j \frac{f(j)}{\max_j |f(j)|}\, |jmn\rangle \langle jmn| \right]
\end{aligned}
\tag{289}
$$

To bound this expression from above we write the gauge-matter interaction again in terms of the unitary operators $\mathcal{U}_W$:

$$
\begin{aligned}
&\| [H_{GM}, H_E] \| \\
\leq&\sum_{x,k} \lambda_{GM} \lambda_E \max_j |f(j)| \left\| \left[\mathcal{U}_W(\psi_n^\dagger(x)\psi_n(x+k) + h.c.)\mathcal{U}_W^\dagger, \sum_j \frac{f(j)}{\max_j |f(j)|}\, |jmn\rangle \langle jmn| \right] \right\| \\
\leq&\sum_{x,k} \lambda_{GM} \lambda_E \max_j |f(j)| 2 \left\|\psi_n^\dagger(x)\psi_n(x+k) + h.c.\right\| \left\| \sum_j \frac{f(j)}{\max_j |f(j)|}\, |jmn\rangle \langle jmn| \right\| \\
=&\mathcal{N}_{links} \lambda_{GM} \lambda_E \max_j |f(j)| 2 d_U
\end{aligned}
\tag{290}
$$

The last commutator is the one between the magnetic and electric Hamiltonian:

$$
\begin{aligned}
&[H_B, H_E] \\
=&\left[\sum_{plaquettes} \lambda_B Tr(U_1 U_2 U_3^\dagger U_4^\dagger) + h.c., \sum_{x,k} \lambda_E \sum_j f(j)\, |jmn\rangle \langle jmn| \right] \\
=&\lambda_B \lambda_E \sum_{x,k} \sum_{l=1}^{2(d-1)} \max_j |f(j)| \left[Tr(U_{l1} U_{l2} U_{l3}^\dagger U_{l4}^\dagger) + h.c., \sum_j \frac{f(j)}{\max_j |f(j)|}\, |jmn\rangle \langle jmn| \right]
\end{aligned}
\tag{291}
$$

where in the last step we used the fact that every link is contained in 2(d-1) plaquettes labeled by l. Taking the operator norm results in the bound:

$$
\begin{aligned}
&\| [H_B, H_E] \| \\
\leq &\lambda_B \lambda_E \mathcal{N}_{links} 2(d-1) \max_j |f(j)| \left\| \left[ Tr(U_1 U_2 U_3^\dagger U_4^\dagger) + h.c., \sum_j \frac{f(j)}{\max_j |f(j)|} |jmn\rangle \langle jmn| \right] \right\| \\
\leq &\lambda_B \lambda_E \mathcal{N}_{links} 4(d-1) \max_j |f(j)| \left\| Tr(U_1 U_2 U_3^\dagger U_4^\dagger) + h.c. \right\| \left\| \sum_j \frac{f(j)}{\max_j |f(j)|} |jmn\rangle \langle jmn| \right\| \\
= &\lambda_B \lambda_E \mathcal{N}_{links} 4(d-1) \max_j |f(j)| \left\| \int dg_1 dg_2 dg_3 dg_4 \, |g_1 g_2 g_3 g_4\rangle \langle g_1 g_2 g_3 g_4| \, Tr(D^j(g_1 g_2 g_3^{-1} g_4^{-1})) + h.c. \right\| \\
= &\lambda_B \lambda_E \mathcal{N}_{links} 4(d-1) \max_j |f(j)| \\
&\left\| \int dg_1 dg_2 dg_3 dg_4 \, |g_1 g_2 g_3 g_4\rangle \langle g_1 g_2 g_3 g_4| \, 2Re\{Tr(D^j(g_1 g_2 g_3^{-1} g_4^{-1}))\} \right\| \\
= &\lambda_B \lambda_E \mathcal{N}_{links} 4(d-1) \max_j |f(j)| 2max_{g \in G} |Re\{Tr(D^j(g)\}| \\
\leq &\lambda_B \lambda_E \mathcal{N}_{links} 8(d-1) \max_j |f(j)| d_U
\end{aligned}
\tag{292}
$$

We can be sure that the estimate in the last step is the best one can do since it is realized for the neutral element.

## Second order

For a bound on the second-order formula we need to calculate all nested commutators. We start with the magnetic Hamiltonian since it commutes with everything apart from the electric Hamiltonian.

$$
\begin{aligned}
&\| \, [[H_B, H_E], H_E] \, \| \\
=&\left\| \left[ \lambda_B \lambda_E \sum_{links} \sum_{l=1}^{2(d-1)} \max_j |f(j)| \left[ Tr(U_{l1} U_{l2} U_{l3}^\dagger U_{l4}^\dagger) + h.c., \sum_j \frac{f(j)}{\max_j |f(j)|} |jmn\rangle \langle jmn| \right], \right. \right. \\
&\left. \left. \sum_{links} \lambda_E \sum_j f(j) |jmn\rangle \langle jmn| \right] \right\| \\
\leq& \lambda_E^2 \lambda_B \max_j |f(j)|^2 \sum_{links} \sum_{l=1}^{2(d-1)} 4 \\
&\left\| \left[ \left[ Tr(U_{l1} U_{l2} U_{l3}^\dagger U_{l4}^\dagger) + h.c., \sum_j \frac{f(j)}{\max_j |f(j)|} |jmn\rangle \langle jmn| \right], \sum_{j'} \frac{f(j')}{\max_{j'} |f(j')|} |j'mn\rangle \langle j'mn| \right] \right\| \\
\leq& \lambda_E^2 \lambda_B \max_j |f(j)|^2 \sum_{links} \sum_{l=1}^{2(d-1)} 4 \times 8 d_U \\
=& \lambda_E^2 \lambda_B \max_j |f(j)|^2 \mathcal{N}_{links} 64 (d-1) d_U
\end{aligned}
\tag{293}
$$

In a similar way we can compute:

$$
\begin{aligned}
&\| \left[ [H_B, H_E], H_B \right] \| \\
=&\left\| \left[ \lambda_B \lambda_E \sum_{links} \sum_{l=1}^{2(d-1)} \max_j |f(j)| \left[ Tr(U_{l1} U_{l2} U_{l3}^\dagger U_{l4}^\dagger) + h.c., \sum_j \frac{f(j)}{\max_j |f(j)|} |jmn\rangle \langle jmn| \right], \right. \right. \\
&\left. \left. \sum_{plaquettes} \lambda_B Tr(U_1 U_2 U_3^\dagger U_4^\dagger) + h.c. \right] \right\| \\
\leq&\lambda_E \lambda_B^2 \max_j |f(j)| \sum_{links} \sum_{l=1}^{2(d-1)} 2(d-1) \\
&\left\| \left[ \left[ Tr(U_{l1} U_{l2} U_{l3}^\dagger U_{l4}^\dagger) + h.c., \sum_j \frac{f(j)}{\max_j |f(j)|} |jmn\rangle \langle jmn| \right], Tr(U_1 U_2 U_3^\dagger U_4^\dagger) + h.c. \right] \right\| \\
\leq&\lambda_E \lambda_B^2 \max_j |f(j)| \sum_{links} \sum_{l=1}^{2(d-1)} 2(d-1) \times 16 d_U^2 \\
=&\lambda_E \lambda_B^2 \max_j |f(j)| \mathcal{N}_{links} 64 (d-1)^2 d_U^2
\end{aligned}
\tag{294}
$$

The next commutator is the one for the electric Hamiltonian. Since we already calculated the commutator for the magnetic part $H_B$ the only non-commuting Hamiltonian remains the gauge-matter interaction.

$$
\begin{aligned}
&\| \left[ \left[ H_E, H_{GM} \right], H_{GM} \right] \| \\
=&\left\| \left[ \sum_{x,k} \lambda_{GM} \lambda_E \max_j |f(j)| \left[ \sum_j \frac{f(j)}{\max_j |f(j)|} \left| jmn \right\rangle \left\langle jmn \right|, \psi_m^\dagger(x) U_{mn}(x,k) \psi_n(x+k) + h.c. \right], \right. \right. \\
&\left. \left. \sum_{y,k'} \lambda_{GM} \psi_m^\dagger(y) U_{mn}(y,k') \psi_n(y+k') + h.c. \right] \right\| \\
\leq& \lambda_{GM}^2 \lambda_E \max_j |f(j)| \sum_{x,k} \sum_{l=1}^{2(2d-1)+1} \\
&\left\| \left[ \left[ \sum_j \frac{f(j)}{\max_j |f(j)|} \left| jmn \right\rangle \left\langle jmn \right|, \psi_m^\dagger(x) U_{mn}(x,k) \psi_n(x+k) + h.c. \right], \right. \right. \\
&\left. \left. \psi_m^\dagger(x_l) U_{mn}(x_l,k_l) \psi_n(x_l+k_l) + h.c. \right] \right\| \\
\leq& \lambda_{GM}^2 \lambda_E \max_j |f(j)| \sum_{x,k} \sum_{l=1}^{2(2d-1)+1} 4 \times \| \sum_j \frac{f(j)}{\max_j |f(j)|} \left| jmn \right\rangle \left\langle jmn \right| \| \| U_W (\psi_m^\dagger(x) \psi_n(x+k) + h.c.) U_W^\dagger \|^2 \\
=& \lambda_{GM}^2 \lambda_E \max_j |f(j)| \mathcal{N}_{links} (2(2d-1)+1) 4 d_U^2
\end{aligned}
\tag{295}
$$

In a similar fashion we calculate the other nested commutator for $H_E$:

$$
\begin{aligned}
&\| \left[ \left[ H_E, H_{GM} \right], H_E \right] \| \\
=&\left\| \left[ \sum_{x,k} \lambda_{GM} \lambda_E \max_j |f(j)| \left[ \sum_j \frac{f(j)}{\max_j |f(j)|} |jmn\rangle \langle jmn| , \psi_m^\dagger(x) U_{mn}(x,k) \psi_n(x+k) + h.c. \right], \right.\right. \\
&\left.\left. \sum_{links} \sum_{j'} \frac{f(j')}{\max_{j'} |f(j')|} |j'mn\rangle \langle j'mn| \right] \right\| \\
\leq& \lambda_{GM} \lambda_E^2 \max_j |f(j)|^2 \sum_{x,k} \\
&\left\| \left[ \left[ \sum_j \frac{f(j)}{\max_j |f(j)|} |jmn\rangle \langle jmn| , \psi_m^\dagger(x) U_{mn}(x,k) \psi_n(x+k) + h.c. \right], \sum_{j'} \frac{f(j')}{\max_{j'} |f(j')|} |j'mn\rangle \langle j'mn| \right] \right\| \\
\leq& \lambda_{GM} \lambda_E^2 \max_j |f(j)|^2 \sum_{x,k} 4 \times \left\| \sum_j \frac{f(j)}{\max_j |f(j)|} |jmn\rangle \langle jmn| \right\|^2 \left\| U_W (\psi_m^\dagger(x) \psi_n(x+k) + h.c.) U_W^\dagger \right\| \\
&= \lambda_{GM} \lambda_E^2 \max_j |f(j)|^2 \mathcal{N}_{links} 4 d_U
\end{aligned}
\tag{296}
$$

The next term are the nested commutators for the matter Hamiltonian. The only part of the Hamiltonian that does not commute with it are the gauge-matter interactions:

$$
\begin{aligned}
&\| \left[ \left[ H_M, H_{GM} \right], H_{GM} \right] \| \\
=&\left\| \left[ 2\lambda_{GM} M \sum_{x,k} (-1)^x \psi_m^\dagger(x) U_{mn}(x,k) \psi_n(x+k) - h.c., \sum_{y,k'} \lambda_{GM} \, \psi_m^\dagger(y) U_{mn}(y,k') \psi_n(y+k') + h.c. \right] \right\| \\
\leq& 2\lambda_{GM}^2 M \sum_{x,k} \sum_{l=1}^{2(2d-1)} \left\| \left[ \psi_m^\dagger(x) U_{mn}(x,k) \psi_n(x+k) - h.c., \psi_{m'}^\dagger(x_l) U_{m'n'}(x_l,k_l) \psi_{n'}(x_l+k_l) + h.c. \right] \right\| \\
&+ \left\| \left[ \psi_m^\dagger(x) U_{mn}(x,k) \psi_n(x+k) - h.c., \psi_m^\dagger(x) U_{mn}(x,k) \psi_n(x+k) + h.c. \right] \right\| \\
=& 2\lambda_{GM}^2 M \sum_{x,k} \left( \sum_{l=1}^{2(2d-1)} \| U_{W,l} U_W H_t(x_l,k_l) U_W^\dagger U_{W,l}^\dagger \| \right) + 2 \| \psi_n^\dagger(x) \psi_n(x) - \psi_n^\dagger(x+k) \psi_n(x+k) \| \\
=& 2\lambda_{GM}^2 M \sum_{x,k} 2(2d-1) d_U + 2 d_U \\
=& \lambda_{GM}^2 M \mathcal{N}_{links} 8 d d_U
\end{aligned}
\tag{297}
$$

The other commutator for $H_M$ takes the much simpler form:

$$
\begin{aligned}
&\| \left[ \left[ H_M, H_{GM} \right], H_M \right] \| \\
=&2\lambda_{GM} M^2 \left\| \left[ \sum_{x,k} (-1)^x \psi_m^\dagger(x) U_{mn}(x,k) \psi_n(x+k) - h.c., \sum_y (-1)^y \psi_{m'}^\dagger(y) \psi_{m'}(y) \right] \right\| \\
=&2\lambda_{GM} M^2 \Bigg\| \sum_{x,k} \left[ \psi_m^\dagger(x) U_{mn}(x,k) \psi_n(x+k), \psi_{m'}^\dagger(x) \psi_{m'}(x) \right] + h.c. \\
&- \left[ \psi_m^\dagger(x) U_{mn}(x,k) \psi_n(x+k), \psi_{m'}^\dagger(x+k) \psi_{m'}(x+k) \right] + h.c. \Bigg\| \\
=&2\lambda_{GM} M^2 \left\| \sum_{x,k} -\psi_m^\dagger(x) U_{mn}(x,k) \psi_n(x+k) + h.c - \psi_m^\dagger(x) U_{mn}(x,k) \psi_n(x+k) + h.c \right\| \\
\leq&4\lambda_{GM} M^2 \mathcal{N}_{links} \| U_W H_t U_W^\dagger \| \\
=&4\lambda_{GM} M^2 \mathcal{N}_{links} d_U
\end{aligned}
\tag{298}
$$

In the last step the nested commutator among the different gauge-matter hamiltonians needs to be computed:

$$
\begin{aligned}
&\| \left[ \left[ H_{GM,i}, H_{GM,j} \right], H_{GM,l} \right] \| \\
=&\Bigg\| \Bigg[ \lambda_{GM}^2 \sum_{x/\{boundary\}} \psi_n^\dagger(x+k_i) U_{nm}^\dagger(x,k_i) U_{mn'}(x,k_j) \psi_{n'}(x+k_j) - h.c. \\
&+\psi_m^\dagger(x) U_{mn}(x,k_i) U_{nm'}^\dagger(x+k_i-k_j,k_j) \psi_{m'}(x+k_i-k_j) - h.c., \\
&\sum_{y,k_l} \lambda_{GM}\, \psi_m^\dagger(y) U_{mn}(y,k_l) \psi_n(y+k_l) + h.c \Bigg] \Bigg\| \\
\leq&\lambda_{GM}^3 \sum_{x/\{boundary\}} \Big\| \big[ \psi_n^\dagger(x+k_i) U_{nm}^\dagger(x,k_i) U_{mn'}(x,k_j) \psi_{n'}(x+k_j) - h.c., \\
&psi_m^\dagger(x+k_i) U_{mn}(x+k_i,k_l) \psi_n(x+k_i+k_l) + h.c \big] \\
&+ \left[ \psi_n^\dagger(x+k_i) U_{nm}^\dagger(x,k_i) U_{mn'}(x,k_j) \psi_{n'}(x+k_j) - h.c., \psi_m^\dagger(x+k_j) U_{mn}(x+k_j,k_l) \psi_n(x+k_j+k_l) + h.c \right] \\
&+ \left[ \psi_m^\dagger(x) U_{mn}(x,k_i) U_{nm'}^\dagger(x+k_i-k_j,k_j) \psi_{m'}(x+k_i-k_j) - h.c., \psi_m^\dagger(x) U_{mn}(x,k_l) \psi_n(x+k_l) + h.c \right] \\
&+ \Big[ \psi_m^\dagger(x) U_{mn}(x,k_i) U_{nm'}^\dagger(x+k_i-k_j,k_j) \psi_{m'}(x+k_i-k_j) - h.c., \\
&\psi_m^\dagger(x+k_i-k_j) U_{mn}(x+k_i-k_j,k_l) \psi_n(x+k_i-k_j+k_l) + h.c \big] \Big\| \\
\leq&\lambda_{GM}^3 \sum_{x/\{boundary\}} \left\| -\psi_n^\dagger(x+k_j) U_{nm}^\dagger(x,k_j) U_{mn'}(x,k_i) U_{n'n''}(x+k_i,k_l) \psi_{n''}(x+k_i+k_l) + h.c. \right\| \\
&+ \left\| \psi_n^\dagger(x+k_i) U_{nm}^\dagger(x,k_i) U_{mn'}(x,k_j) U_{n'n''}(x+k_j,k_l) \psi_{n''}(x+k_j+k_l) + h.c. \right\| \\
&+ \left\| -\psi_n^\dagger(x+k_i-k_j) U_{nm}(x+k_i-k_j,k_j) U_{mn'}^\dagger(x,k_i) U_{n'n''}(x,k_l) \psi_{n''}(x+k_l) + h.c. \right\| \\
&+ \left\| \psi_n^\dagger(x) U_{nm}(x,k_i) U_{mn'}^\dagger(x+k_i-k_j,k_j) U_{n'n''}(x+k_i-k_j,k_l) \psi_{n''}(x+k_i-k_j+k_l) + h.c. \right\| \\
\leq&\lambda_{GM}^3 \sum_{x/\{boundary\}} 4 \left\| U_{W3} U_{W2} U_{W1} H_t U_{W1}^\dagger U_{W2}^\dagger U_{W3}^\dagger \right\| \\
=&\lambda_{GM}^3 \frac{\mathcal{N}_{links}}{2d} 4 d_U
\end{aligned}
\tag{299}
$$

To obtain the nested commutator for the whole gauge matter interactions we need to calculate how many times the commutator calculated above appears. There are $2d$ different gauge-matter Hamiltonians which are implemented separately. Recalling the formula for the total error and taking only the gauge-matter interactions into account, one gets:

$$
\begin{aligned}
\|\mathcal{U}(t) - \mathcal{U}_{2,M}(t)\| &= \|e^{-itH} - (e^{-iH_1\frac{t}{2M}}...e^{-iH_{p-1}\frac{t}{2M}}e^{-iH_p\frac{t}{M}}e^{-iH_{p-1}\frac{t}{2M}}...e^{-iH_1\frac{t}{2M}})^M\| \\
&\leq \frac{t^3}{12M^2}\sum_{k=1}^{p-1}\|[[H_k, H_{k+1}+..+H_p], H_{k+1}+..+H_p]\| + \frac{1}{2}\|[[H_k, H_{k+1}+..+H_p], H_k]\| \\
&= \frac{t^3}{12M^2}\sum_{k=1}^{2d-1}\|[[H_{GM,k}, H_{GM,k+1}+..+H_{GM,2d}], H_{GM,k+1}+..+H_{GM,2d}]\| \\
&+ \frac{1}{2}\|[[H_{GM,k}, H_{GM,k+1}+..+H_{GM,2d}], H_{GM,k}]\|
\end{aligned} \tag{300}
$$

We see that in the first term we can choose two Hamiltonians out of the remaining ones and one Hamiltonian for the second term. This gives rise to partial sums of the natural numbers. The nested commutator for the gauge-matter interactions is therefore:

$$
\begin{aligned}
&\sum_{k=1}^{2d-1}\|[[H_{GM,k}, H_{GM,k+1}+..+H_{GM,2d}], H_{GM,k+1}+..+H_{GM,2d}]\| \\
&+ \frac{1}{2}\|[[H_{GM,k}, H_{GM,k+1}+..+H_{GM,2d}], H_{GM,k}]\| \\
&\leq \lambda_{GM}^3\frac{\mathcal{N}_{links}}{2d}4d_U\sum_{x}^{2d-1}x^2 + \frac{x}{2} \\
&= \lambda_{GM}^3\frac{\mathcal{N}_{links}}{2d}4d_U\left(\frac{1}{6}(2d-1)2d(4d-1) + \frac{1}{4}(2d-1)2d\right) \\
&= \lambda_{GM}^3 d_U\mathcal{N}_{links}(2d-1)\left(\frac{2}{3}(4d-1)+1\right)
\end{aligned} \tag{301}
$$

Putting everything together, we can estimate the trotterization error for the second-order formula.

$$
\begin{aligned}
&\|\mathcal{U}(t)-\mathcal{U}_{2,M}(t)\| \\
=&\left\|e^{-itH}-(e^{-iH_1\frac{t}{2M}}...e^{-iH_{p-1}\frac{t}{2M}}e^{-iH_p\frac{t}{M}}e^{-iH_{p-1}\frac{t}{2M}}...e^{-iH_1\frac{t}{2M}})^M\right\| \\
\leq&\frac{t^3}{12M^2}\sum_{k=1}^{p-1}\|[[H_k,H_{k+1}+..+H_p],H_{k+1}+..+H_p]\|+\frac{1}{2}\|[[H_k,H_{k+1}+..+H_p],H_k]\| \\
=&\frac{t^3}{12M^2}\Bigg(\|[[H_B,H_E],H_E]\|+\frac{1}{2}\|[[H_B,H_E],H_B]\|+\|[[H_E,H_{GM}],H_{GM}]\| \\
&+\frac{1}{2}\|[[H_E,H_{GM}],H_E]\|+\|[[H_M,H_{GM}],H_{GM}]\|+\frac{1}{2}\|[[H_M,H_{GM}],H_M]\| \\
&+\sum_{k=1}^{2d-1}\|[[H_{GM,k},H_{GM,k+1}+..+H_{GM,2d}],H_{GM,k+1}+..+H_{GM,2d}]\| \\
&+\frac{1}{2}\|[[H_{GM,k},H_{GM,k+1}+..+H_{GM,2d}],H_{GM,k}]\|\Bigg) \\
\leq&\frac{t^3}{12M^2}\Bigg(\lambda_E^2\lambda_B\max_j|f(j)|^2\mathcal{N}_{links}64(d-1)d_U+\lambda_E\lambda_B^2\max_j|f(j)|\mathcal{N}_{links}32(d-1)^2d_U^2 \\
&+\lambda_{GM}^2\lambda_E\max_j|f(j)|\mathcal{N}_{links}(2(2d-1)+1)4d_U^2+\lambda_{GM}\lambda_E^2\max_j|f(j)|^2\mathcal{N}_{links}2d_U \\
&+\lambda_{GM}^2M\mathcal{N}_{links}8dd_U+2\lambda_{GM}M^2\mathcal{N}_{links}d_U \\
&+\lambda_{GM}^3d_U\mathcal{N}_{links}(2d-1)\left(\frac{2}{3}(4d-1)+1\right)\Bigg) \\
=&\frac{t^3\mathcal{N}_{links}d_U}{12M^2}\Bigg(\lambda_E^2\lambda_B\max_j|f(j)|^264(d-1)+\lambda_E\lambda_B^2\max_j|f(j)|32(d-1)^2d_U \\
&+\lambda_{GM}^2\lambda_E\max_j|f(j)|(2(2d-1)+1)4d_U+\lambda_{GM}\lambda_E^2\max_j|f(j)|^22 \\
&+\lambda_{GM}^2M8d+2\lambda_{GM}M^2 \\
&+\lambda_{GM}^3(2d-1)\left(\frac{2}{3}(4d-1)+1\right)\Bigg) \\
=&\frac{t^3\mathcal{N}_{links}d_U}{6M^2}\Bigg[16\lambda_E\lambda_B\max_j|f(j)|(d-1)\left(2\lambda_E\max_j|f(j)|+\lambda_Bd_U(d-1)\right) \\
&+\lambda_{GM}\lambda_E\max_j|f(j)|\left(2\lambda_{GM}d_U(2(2d-1)+1)+\lambda_E\max_j|f(j)|\right) \\
&+\lambda_{GM}M\left(4d\lambda_{GM}+M\right)+\lambda_{GM}^3(2d-1)\left(\frac{1}{3}(4d-1)+\frac{1}{2}\right)\Bigg]
\end{aligned}
\tag{302}
$$

# References


[1] Richard P. Feynman. Simulating physics with computers. *International Journal of Theoretical Physics*, 21(6):467–488, Jun 1982.

[2] Iulia Buluta and Franco Nori. Quantum simulators. *Science*, 326(5949):108–111, 2009.

[3] Dieter Jaksch, Ch Bruder, Juan Ignacio Cirac, Crispin W Gardiner, and Peter Zoller. Cold bosonic atoms in optical lattices. *Physical Review Letters*, 81(15):3108, 1998.

[4] Dieter Jaksch and Peter Zoller. The cold atom hubbard toolbox. *Annals of physics*, 315(1):52–79, 2005.

[5] Immanuel Bloch, Jean Dalibard, and Wilhelm Zwerger. Many-body physics with ultracold gases. *Reviews of modern physics*, 80(3):885, 2008.

[6] Juan I Cirac and Peter Zoller. Quantum computations with cold trapped ions. *Physical review letters*, 74(20):4091, 1995.

[7] Dietrich Leibfried, Rainer Blatt, Christopher Monroe, and David Wineland. Quantum dynamics of single trapped ions. *Reviews of Modern Physics*, 75(1):281, 2003.

[8] Daniel Loss and David P DiVincenzo. Quantum computation with quantum dots. *Physical Review A*, 57(1):120, 1998.

[9] Tim Byrnes, Na Young Kim, Kenichiro Kusudo, and Yoshihisa Yamamoto. Quantum simulation of fermi-hubbard models in semiconductor quantum-dot arrays. *Physical Review B*, 78(7):075320, 2008.

[10] JQ You and Franco Nori. Quantum information processing with superconducting qubits in a microwave field. *Physical Review B*, 68(6):064509, 2003.

[11] Alexander van Oudenaarden and JE Mooij. One-dimensional mott insulator formed by quantum vortices in josephson junction arrays. *Physical review letters*, 76(26):4947, 1996.

[12] Hale F Trotter. On the product of semi-groups of operators. *Proceedings of the American Mathematical Society*, 10(4):545–551, 1959.

[13] Michael A Nielsen and Isaac Chuang. Quantum computation and quantum information, 2002.

[14] Markus Greiner, Olaf Mandel, Tilman Esslinger, Theodor W Hänsch, and Immanuel Bloch. Quantum phase transition from a superfluid to a mott insulator in a gas of ultracold atoms. *nature*, 415(6867):39–44, 2002.

[15] Belén Paredes, Artur Widera, Valentin Murg, Olaf Mandel, et al. Tonks-girardeau gas of ultracold atoms in an optical lattice. *Nature*, 429(6989):277, 2004.

[16] Gregor Jotzu, Michael Messer, Rémi Desbuquois, Martin Lebrat, Thomas Uehlinger, Daniel Greif, and Tilman Esslinger. Experimental realisation of the topological haldane model. *arXiv preprint arXiv:1406.7874*, 2014.

[17] Simon Eidelman, KG Hayes, KA ea Olive, M Aguilar-Benitez, C Amsler, D Asner, KS Babu, RM Barnett, J Beringer, PR Burchat, et al. Review of particle physics. *Physics Letters B*, 592(1):1–5, 2004.

[18] Michael Edward Peskin. *An introduction to quantum field theory*. Westview press, 1995.

[19] Kenneth G Wilson. Confinement of quarks. *Physical Review D*, 10(8):2445, 1974.

[20] John B Kogut. An introduction to lattice gauge theory and spin systems. *Reviews of Modern Physics*, 51(4):659, 1979.

[21] Jan Smit. *Introduction to quantum fields on a lattice*. Cambridge University Press, 2002.

[22] Matthias Troyer and Uwe-Jens Wiese. Computational complexity and fundamental limitations to fermionic quantum monte carlo simulations. *Physical review letters*, 94(17):170201, 2005.

[23] Larry McLerran. The physics of the quark-gluon plasma. *Reviews of Modern Physics*, 58(4):1021, 1986.

[24] John B Kogut and Mikhail A Stephanov. *The phases of quantum chromodynamics: from confinement to extreme environments*, volume 21. Cambridge University Press, 2003.

[25] Jürgen Berges. Introduction to nonequilibrium quantum field theory. In *AIP Conference Proceedings*, volume 739, pages 3–62. AIP, 2004.

[26] Erez Zohar, J Ignacio Cirac, and Benni Reznik. Quantum simulations of lattice gauge theories using ultracold atoms in optical lattices. *Reports on Progress in Physics*, 79(1):014401, 2015.

[27] U-J Wiese. Ultracold quantum gases and lattice systems: quantum simulation of lattice gauge theories. *Annalen der Physik*, 525(10-11):777–796, 2013.

[28] John Kogut and Leonard Susskind. Hamiltonian formulation of wilson's lattice gauge theories. *Physical Review D*, 11(2):395, 1975.

[29] Roman Jackiw and Cláudio Rebbi. Solitons with fermion number $1/2$. *Physical Review D*, 13(12):3398, 1976.

[30] Vitor M Pereira and AH Castro Neto. Strain engineering of graphenes electronic structure. *Physical Review Letters*, 103(4):046801, 2009.

[31] Erez Zohar and Benni Reznik. Confinement and lattice quantum-electrodynamic electric flux tubes simulated with ultracold atoms. *Physical review letters*, 107(27):275301, 2011.

[32] Erez Zohar, J Ignacio Cirac, and Benni Reznik. Simulating compact quantum electrodynamics with ultracold atoms: Probing confinement and nonperturbative effects. *Physical review letters*, 109(12):125302, 2012.

[33] Erez Zohar, J Ignacio Cirac, and Benni Reznik. Quantum simulations of gauge theories with ultracold atoms: Local gauge invariance from angular-momentum conservation. *Physical Review A*, 88(2):023617, 2013.

[34] V Kasper, Florian Hebenstreit, MK Oberthaler, and J Berges. Schwinger pair production with ultracold atoms. *Physics Letters B*, 760:742–746, 2016.

[35] Debasish Banerjee, Michael Bögli, M Dalmonte, E Rico, Pascal Stebler, U-J Wiese, and P Zoller. Atomic quantum simulation of u (n) and su (n) non-abelian lattice gauge theories. *Physical review letters*, 110(12):125303, 2013.

[36] Debasish Banerjee, M Dalmonte, M Müller, E Rico, P Stebler, U-J Wiese, and P Zoller. Atomic quantum simulation of dynamical gauge fields coupled to fermionic matter: from string breaking to evolution after a quench. *Physical review letters*, 109(17):175302, 2012.

[37] Erez Zohar, J Ignacio Cirac, and Benni Reznik. Simulating (2+ 1)-dimensional lattice qed with dynamical matter using ultracold atoms. *Physical review letters*, 110(5):055302, 2013.

[38] Daniel González-Cuadra, Erez Zohar, and Juan Cirac. Quantum simulation of the abelian-higgs lattice gauge theory with ultracold atoms. *New Journal of Physics*, 2017.

[39] Simone Notarnicola, Elisa Ercolessi, Paolo Facchi, Giuseppe Marmo, Saverio Pascazio, and Francesco V Pepe. Discrete abelian gauge theories for quantum simulations of qed. *Journal of Physics A: Mathematical and Theoretical*, 48(30):30FT01, 2015.

[40] Erez Zohar, J Ignacio Cirac, and Benni Reznik. Cold-atom quantum simulator for su (2) yang-mills lattice gauge theory. *Physical review letters*, 110(12):125304, 2013.

[41] K Stannigel, P Hauke, D Marcos, M Hafezi, S Diehl, M Dalmonte, and P Zoller. Constrained dynamics via the zeno effect in quantum simulation: Implementing non-abelian lattice gauge theories with cold atoms. *Physical review letters*, 112(12):120406, 2014.

[42] Erez Zohar, Alessandro Farace, Benni Reznik, and J Ignacio Cirac. Digital lattice gauge theories. *Physical Review A*, 95(2):023604, 2017.

[43] Erez Zohar, Alessandro Farace, Benni Reznik, and J Ignacio Cirac. Digital quantum simulation of z 2 lattice gauge theories with dynamical fermionic matter. *Physical Review Letters*, 118(7):070501, 2017.

[44] Philipp Hauke, David Marcos, Marcello Dalmonte, and Peter Zoller. Quantum simulation of a lattice schwinger model in a chain of trapped ions. *Physical Review X*, 3(4):041018, 2013.

[45] Dayou Yang, Gouri Shankar Giri, Michael Johanning, Christof Wunderlich, Peter Zoller, and Philipp Hauke. Analog quantum simulation of (1+ 1)-dimensional lattice qed with trapped ions. *Physical Review A*, 94(5):052321, 2016.

[46] L Tagliacozzo, A Celi, P Orland, MW Mitchell, and M Lewenstein. Simulation of non-abelian gauge theories with optical lattices. *Nature communications*, 4:2615, 2013.

[47] L Tagliacozzo, A Celi, A Zamora, and M Lewenstein. Optical abelian lattice gauge theories. *Annals of Physics*, 330:160–191, 2013.

[48] D Marcos, P Rabl, E Rico, and P Zoller. Superconducting circuits for quantum simulation of dynamical gauge fields. *Physical review letters*, 111(11):110504, 2013.

[49] D Marcos, Philippe Widmer, E Rico, M Hafezi, P Rabl, U-J Wiese, and P Zoller. Two-dimensional lattice gauge theories with superconducting quantum circuits. *Annals of physics*, 351:634–654, 2014.

[50] A Mezzacapo, E Rico, C Sabín, IL Egusquiza, L Lamata, and E Solano. Non-abelian su (2) lattice gauge theories in superconducting circuits. *Physical review letters*, 115(24):240502, 2015.

[51] Omjyoti Dutta, Luca Tagliacozzo, Maciej Lewenstein, and Jakub Zakrzewski. Toolbox for abelian lattice gauge theories with synthetic matter. *Physical Review A*, 95(5):053608, 2017.

[52] Erez Zohar and Benni Reznik. Topological wilson-loop area law manifested using a superposition of loops. *New Journal of Physics*, 15(4):043041, 2013.

[53] Arkadiusz Kosior and Krzysztof Sacha. Simulation of non-abelian lattice gauge fields with a single-component gas. *EPL (Europhysics Letters)*, 107(2):26006, 2014.

[54] Uwe-Jens Wiese. Towards quantum simulating qcd. *Nuclear Physics A*, 931:246–256, 2014.

[55] Stefan Walter and Florian Marquardt. Dynamical gauge fields in optomechanics. *arXiv preprint arXiv:1510.06754*, 2015.

[56] V Kasper, Florian Hebenstreit, F Jendrzejewski, MK Oberthaler, and J Berges. Implementing quantum electrodynamics with ultracold atomic systems. *New journal of physics*, 19(2):023030, 2017.

[57] Esteban A Martinez, Christine A Muschik, Philipp Schindler, Daniel Nigg, Alexander Erhard, Markus Heyl, Philipp Hauke, Marcello Dalmonte, Thomas Monz, Peter Zoller, et al. Real-time dynamics of lattice gauge theories with a few-qubit quantum computer. *Nature*, 534(7608):516–519, 2016.

[58] Pascual Jordan and Eugene Paul Wigner. über das paulische äquivalenzverbot. In *The Collected Works of Eugene Paul Wigner*, pages 109–129. Springer, 1993.

[59] Frank Verstraete and J Ignacio Cirac. Mapping local hamiltonians of fermions to local hamiltonians of spins. *Journal of Statistical Mechanics: Theory and Experiment*, 2005(09):P09012, 2005.

[60] Erez Zohar. Half a state, half an operator: a general formulation of stators. *Journal of Physics A: Mathematical and Theoretical*, 50(8):085301, 2017.

[61] Maciej Lewenstein, Anna Sanpera, Veronica Ahufinger, Bogdan Damski, Aditi Sen, and Ujjwal Sen. Ultracold atomic gases in optical lattices: mimicking condensed matter physics and beyond. *Advances in Physics*, 56(2):243–379, 2007.

[62] Kendall B Davis, M-O Mewes, Michael R Andrews, NJ Van Druten, DS Durfee, DM Kurn, and Wolfgang Ketterle. Bose-einstein condensation in a gas of sodium atoms. *Physical review letters*, 75(22):3969, 1995.

[63] Neil W Ashcroft and N David Mermin. Solid state physics (saunders college, philadelphia, 1976). *Google Scholar*, page 29, 2010.

[64] William D Phillips. Nobel lecture: Laser cooling and trapping of neutral atoms. *Reviews of Modern Physics*, 70(3):721, 1998.

[65] Lev Davidovich Landau and Evgenii Mikhailovich Lifshitz. Quantum mechanics: non-relativistic theory. 1958.

[66] Maciej Lewenstein, Anna Sanpera, and Verònica Ahufinger. *Ultracold Atoms in Optical Lattices: Simulating quantum many-body systems*. Oxford University Press, 2012.

[67] Dan M Stamper-Kurn and Wolfgang Ketterle. Spinor condensates and light scattering from bose-einstein condensates. In *Coherent atomic matter waves*, pages 139–217. Springer, 2001.

[68] Christopher J Pethick and Henrik Smith. *Bose-Einstein condensation in dilute gases*. Cambridge university press, 2002.

[69] Cheng Chin, Rudolf Grimm, Paul Julienne, and Eite Tiesinga. Feshbach resonances in ultracold gases. *Reviews of Modern Physics*, 82(2):1225, 2010.

[70] PO Fedichev, Yu Kagan, GV Shlyapnikov, and JTM Walraven. Influence of nearly resonant light on the scattering length in low-temperature atomic gases. *Physical review letters*, 77(14):2913, 1996.

[71] John B Kogut. The lattice gauge theory approach to quantum chromodynamics. *Reviews of Modern Physics*, 55(3):775, 1983.

[72] Heinz J Rothe. *Lattice gauge theories: an introduction*, volume 82. World Scientific Publishing Co Inc, 2012.

[73] Kenneth G Wilson et al. New phenomena in subnuclear physics. 1977.

[74] Paul H Ginsparg and Kenneth G Wilson. A remnant of chiral symmetry on the lattice. *Physical Review D*, 25(10):2649, 1982.

[75] David B Kaplan. A method for simulating chiral fermions on the lattice. *Physics Letters B*, 288(3-4):342–347, 1992.

[76] Leonard Susskind. Lattice fermions. *Physical Review D*, 16(10):3031, 1977.

[77] Masuo Suzuki. Decomposition formulas of exponential operators and lie exponentials with some applications to quantum mechanics and statistical physics. *Journal of mathematical physics*, 26(4):601–612, 1985.

[78] Masuo Suzuki. General theory of fractal path integrals with applications to many-body theories and statistical physics. *Journal of Mathematical Physics*, 32(2):400–407, 1991.

[79] M Zielonkowski, I Manek, U Moslener, P Rosenbusch, and R Grimm. Manipulation of spin-polarized atoms in an optical dipole-force trap. *EPL (Europhysics Letters)*, 44(6):700, 1998.

[80] SE Hamann, DL Haycock, G Klose, PH Pax, IH Deutsch, and PS Jessen. Resolved-sideband raman cooling to the ground state of an optical lattice. *Physical Review Letters*, 80(19):4149, 1998.

[81] S Friebel, C Dandrea, J Walz, M Weitz, and TW Hänsch. Co 2-laser optical lattice with cold rubidium atoms. *Physical Review A*, 57(1):R20, 1998.

[82] Miguel Aguado, GK Brennen, F Verstraete, and J Ignacio Cirac. Creation, manipulation, and detection of abelian and non-abelian anyons in optical lattices. *Physical review letters*, 101(26):260501, 2008.

# Acknowledgements

First and foremost I would like to thank Prof. Dr. Ignacio Cirac for giving me the opportunity to carry out my master thesis in his research group, where I had the chance to work in a very friendly and fruitful atmosphere among very gifted people, as well as for his supervision throughout the whole project. I also would like to express my deep gratitude to Dr. Erez Zohar for all his support during the last year. His guidance and patience were a major factor for the success of this work.

# Declaration of Authorship

I hereby declare that this thesis has been composed by myself and is based entirely on my own work unless where clearly stated otherwise.

Munich, 11 October 2017

. . . . . .

Julian Bender